NERC Scientific Facilities and Technology
Ion Microprobe Facility

University of Edinburgh
NERC Ion Microprobe Facility

2014 Annual Science Report

Ion Microprobe Facility
School of Geosciences
Kings Buildings
James Hutton Road
Edinburgh
EH9 3FE

http://www.geos.ed.ac.uk/facilities/

Contents

Ion Microprobe Projects

Accurate climate reconstruction from fossil corals: The impact of seawater carbonate chemistry on the $\delta^{11}B$ of coral aragonite

N. Allison[1], C. Cole[1], A.A. Finch[1] & C. Hintz[2]

[1]Department of Earth and Environmental Sciences, University of St. Andrews, St. Andrews KY16 9AL, UK.
[2] Faculty of Marine Sciences, Savannah State University, Savannah, Georgia, USA.

Introduction

Marine carbonate $\delta^{11}B$ is a potential proxy of seawater pH [1]. The skeletal $\delta^{11}B$ of tropical coral skeletons is influenced by seawater pCO_2 [2] and analysis of fossil corals may yield estimates of past sea surface pH. The aragonite skeleton precipitates from an extracellular calcification fluid (ECF) enclosed in a semi-isolated space between the skeleton and the overlying coral tissue. The ECF is derived from seawater but corals actively elevate the fluid pH, a process termed pH upregulation [3]. pH upregulation shifts the dissolved inorganic carbon (DIC) equilibrium in favour of CO_3^{2-}, inducing high carbonate saturation states (Ω), favourable to the precipitation of calcium carbonate. Two observations indicate that the relationship between seawater pH and coral skeletal $\delta^{11}B$ is not simple. pH upregulation demonstrates significant temporal variation over periods of weeks-months within single coral heads [4] and corals cultured under high pCO_2 conditions appear to upregulate ECF pH more than their counterparts cultured at ambient pCO_2 [3].

To investigate the relationship between seawater pH and skeletal $\delta^{11}B$ we cultured a series of *Porites* spp. corals (Figure 1) over a range of seawater pCO_2 ranging from the last glacial maximum (180 ppm) to levels projected by the end of this century (750 ppm). *Porites* is the coral genus most commonly used in palaeoclimate reconstructions. Four different coral genotypes were cultured in each treatment. Following an acclimation period of > 5 months, corals were stained with alizarin red to mark the start of skeletal material for subsequent analysis. Corals were grown for a further 5 weeks and then restained and sampled for skeleton. Chips of skeleton were mounted in epoxy resin and polished to a flat surface. Skeletal $\delta^{11}B$ and B/Ca were determined in each coral by multiple SIMS analyses which were evenly spaced between the two stain lines.

Results

The pH of the calcification fluid used to precipitate the skeleton was estimated from skeletal $\delta^{11}B$ using the empirically-determined αB (=1.0272) [5] and assuming that the $\delta^{11}B$ ECF is the same as culture seawater. Our data show that the pH of the extracellular calcification fluid (ECF) varies significantly between individual coral heads cultured at the same seawater pCO_2 in all treatments (Figure 2). ECF pH was significantly higher in corals cultured at 180 ppm than in corals cultured at the other 2 treatments ($p<0.013$, 2 tailed test). There was no significant difference in ECF pH between the datasets for corals cultured at 400 and 750 ppm ($p=0.84$) but this reflected the performance of two coral genotypes which maintained a high ECF pH even at high seawater pCO_2. pH upregulation varied significantly between all pCO2 treatments (Figure 3).

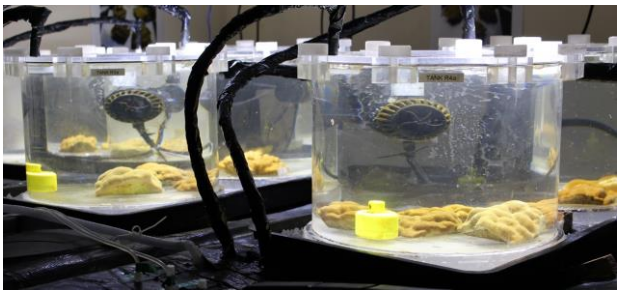

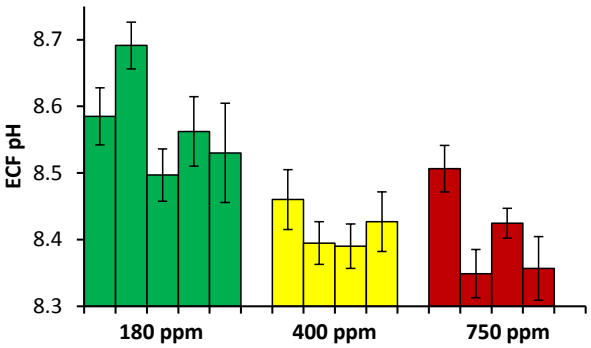

Figure 1 (left). *Porites* spp. corals in the pCO_2 controlled coral culturing system at St. Andrews. Corals are maintained in small perspex tanks fed with seawater from the large 1000 l reservoir tanks beneath. **Figure 2**

(right). Estimated ECF pH in *Porites* spp. corals cultured over a range of seawater pCO_2. Bars represent mean ECF pH in single coral heads. Errors indicate 95% confidence limits.

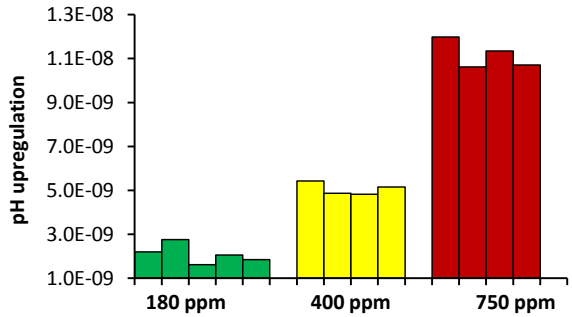

Figure 3. pH upregulation in *Porites* spp. corals cultured over a range of seawater pCO_2. pH upregulation is calculated as the decrease in $[H^+]$ between the culture seawater and the coral calcification fluid (ECF). Bars represent mean pH upregulation in single coral heads.

Our data confirm that the magnitude of pH upregulation in coral is dependent on seawater pH. Some coral genotypes cultured at high seawater pCO_2 were capable of maintaining the high ECF pH observed in control corals cultured under ambient CO_2. We are currently working to explore the relationships between coral metabolic processes (photosynthetic, respiration and calcification rates) and ECF pH. The high skeletal $\delta^{11}B$ (ECF pH) variability between corals cultured at the same pH is likely to hamper the estimate of past seawater pH from fossil coral $\delta^{11}B$.

References

[1] A. Sanyal et al. (2000) Geochim. Cosmochim. Acta, **64** 1551-1555
[2] S. Reynaud, N.G. Hemming, A. Juillet-Leclerc, J.P. Gattuso (2004) Coral Reefs **23**, 539-546
[3] A.A. Venn et al. (2012) Proc. Natl. Acad. Sci., **110** 1634-1639
[4] N. Allison, A.A. Finch, et al., (2010) Geochim. Cosmochim. Acta, **74** 1790-1800
[5] K. Klochko et al. (2006) Earth Planet. Sci. Lett., **248** 276-285

Appendix

Skeletal $\delta^{11}B$ and B/Ca were determined by SIMS using the Cameca 1270. The high spatial resolution of SIMS (primary beam diameters = 25-40 µm) allows the selective analysis of both the primary coral aragonite, avoiding contamination from secondary cements or microboring organisms, and the small skeletal volumes deposited in the culture experiment. Analyses were normalized to multiple daily analyses of a Desmophyllum spp. cold water coral chip. Multiple analyses were completed each day to yield a 95% confidence limit of the standard mean $\delta^{11}B$ concentration which was typically ~0.9‰ and was always better than ±1.2‰. 95% confidence limit of the standard mean B/Ca concentration was always better than ±2.6%.

Reconstructing the aragonite saturation state in coral calcification fluid

N. Allison & A.A. Finch

Department of Earth and Environmental Sciences, University of St. Andrews, St. Andrews KY16 9AL, UK

Introduction

Coral skeletal Sr/Ca is a commonly used palaeothermometer. However the interpretation of coral Sr/Ca is complicated by unresolved influences on skeletal Sr/Ca which may result in significant errors in reconstructed sea surface temperatures (SSTs). In particular, skeletal Sr/Ca is usually higher in slow growing corals [1]. Skeletal Sr/Ca may be significantly affected by Rayleigh fractionation which occurs when varying proportions of the calcification fluid are precipitated.

Coral aragonite precipitates from an extracellular calcifying fluid (ECF), enclosed in a semi-isolated space between the skeleton and the overlying coral tissue. The precipitation rate of synthetic aragonite is governed by the aragonite saturation state (Ω) of the fluid from which it forms [2]. We have pioneered an approach using skeletal boron geochemistry to reconstruct coral ECF Ω [3]. There are no known active transport mechanisms for boron in coral and it is likely that dissolved boron is transported to the calcification site in seawater and that this transport rate is constant. Dissolved boron in seawater occurs primarily as boric acid, $B(OH)_3$, and borate, $B(OH)_4$, and speciation is controlled by ambient pH [4]. $B(OH)_4$ is selectively incorporated into the carbonate substituting for CO_3^{2-} in the aragonite lattice. We used skeletal $\delta^{11}B$ to estimate the pH of the ECF at the time of skeletal deposition. We used skeletal B/Ca to estimate the concentration of the DIC species which co-precipitates with $B(OH)_4$ in the carbonate lattice. Our previous data suggest that coral aragonite precipitates from HCO_3^- only or from both CO_3^{2-} and HCO_3^- and we observe a strong positive correlation between ECF Ω and coral calcification rate in a suite of cultured corals [3].

To test if variations in coral skeletal Sr/Ca reflect Rayleigh fractionation we applied this technique to estimate ECF Ω in 2 *Porites lobata* field corals from Hawaii. We reconstructed ECF Ω along the maximum growth axes of the two corals and along a slow growing axis in one of the corals. We used SIMS to make multiple analyses of $\delta^{11}B$ and B/Ca along each transect. The high resolution of SIMS allows us to target sections of each transect which are high or low in Sr/Ca to test the Rayleigh fractionation hypothesis.

Results

Our reconstruction demonstrates that the aragonite saturation state of the calcification fluid is higher in the slow growing axis of coral 1 compared to the fast growing axis (Figure 1). This is counterintuitive and suggests that calcification rate along the slow growing axis is not predominantly controlled by calcification fluid dissolved inorganic chemistry. Calcification may be controlled by some other process e.g. production of the organic template used during calcification. Our data suggest that ECF Ω (derived from skeletal B geochemistry) can not be used to infer Rayleigh fractionation between slow and fast growing axes of *Porites* spp. corals.

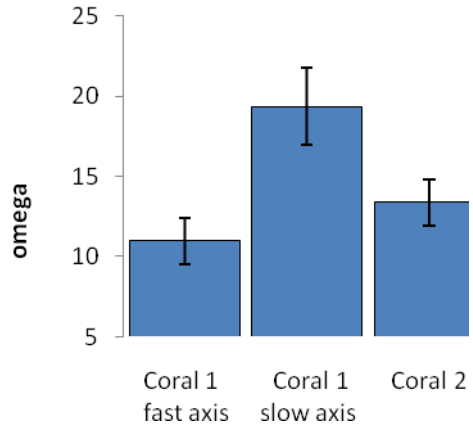

Figure 1. Reconstructed aragonite saturation state (omega) along 3 axes of 2 *Porites lobata* corals from Hawaii. Bars represent mean omega of multiple SIMS measurements in each coral. Error bars indicate 95 confidence limits. Errors were calculated by propagating 95% confidence limits in B/Ca and δ11B analyses onto omega estimates.

References

[1] S. de Villiers et al, (1995) Science, **269** 1247-1249.

[2] E.A. Burton amd L.M. Walter (1987) Geology **15** 111-114.

[3] N. Allison et al. (2014), Nature Communications**5**:5471, DOI:10.1038/ncomms6741.

[4] N.G. Hemming and G.N.Hanson (1992) Geochim. Cosmochim. Acta **56**, 537-543.

Appendix

Skeletal $\delta^{11}B$ and B/Ca were determined by SIMS using the Cameca 1270. The high spatial resolution of SIMS (primary beam diameters = 25-40 μm) allows the selective analysis of both the primary coral aragonite, avoiding contamination from secondary cements or microboring organisms. Analyses were normalized to multiple daily analyses of a Desmophyllum spp. cold water coral chip. Multiple analyses were completed each day to yield a 95% confidence limit of the standard mean $\delta^{11}B$ concentration which was typically ~0.9‰ and was always better than ±1.2‰. 95% confidence limit of the standard mean B/Ca concentration was always better than ±1.5%.

Constraining volcanic hazard on Dominica (Interim Report)

J. Blundy[1], R. Brooker[1], H. Balcone-Boissard[2] & C. Martel[3]

[1]School of Earth Sciences, University of Bristol, Bristol BS8 1RJ, UK
[2]ISTEP, Université Pierre et Marie Curie, 75005, Paris, France
[3]ISTO, Université d'Orléans, 45071, Orléans, France

Rationale

Dominica sits in the centre of the Lesser Antilles volcanic arc and like many of the neighbouring islands, represents a major challenge in evaluating volcanic hazards and development of strategies for mitigation. Although evidence of unrest, such as seismic swarms and changes to fumarolic activity, are common, they rarely lead to an eruption. But when they do, as on Montserrat, the consequences are catastrophic. The problem is to link signs of unrest to eruption probability. The key to this is to use past eruptions as a key to likely precursor events. The situation is perhaps most egregious on Dominica. Whilst all the other volcanic islands in the Lesser Antilles have only one known active volcano, Dominica has nine (Fig 1C). Many of these are associated with large, pyroclastic eruptions sourced from volcanic centres in the south of the island. However, recent evidence of unrest beneath the Morne Aux Diables (MAD) dacite dome complex at the north of the island (Fig 1B) has focussed attention on a potentially imminent volcanic hazard and this is the main reason for this study. Samples from the southern volcanoes are included to provide useful context and comparison.

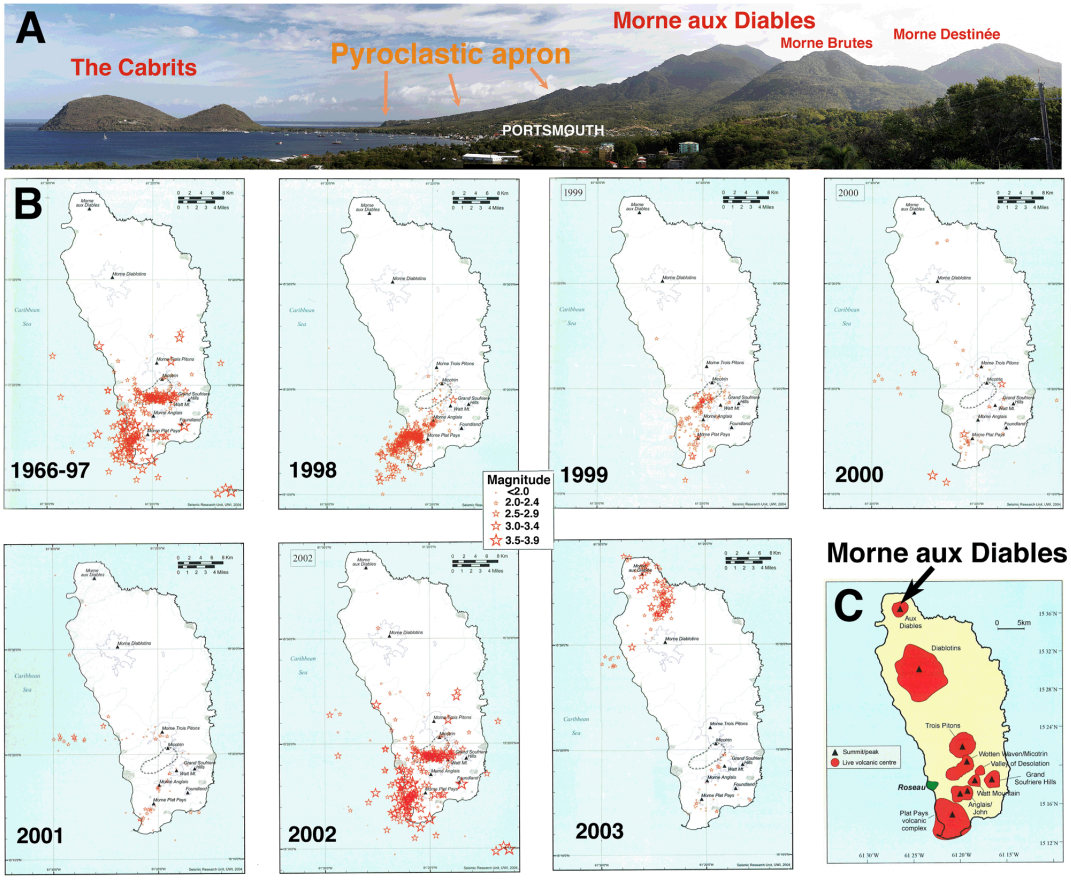

Figure 1. A. Panorama of Morne aux Diables and related domes viewed from the south; note proximity of domes to town of Portsmouth. B. Changing location of earthquake swarms with time beneath Dominica. Note sudden transition of activity to north of island in 2003. C. Map showing locations of Dominica's nine volcanoes.

Objectives.

The main project objectives are; i) to measure the dissolved volatiles (H_2O and CO_2) in melt inclusions and use pressure dependant solubility models to establish whether these snap shots of pre-eruptive magma storage conditions for MAD match the locations of recent earthquakes (1-3 km depth). If so, then the seismic events can plausibly be attributed to recharge of the magma storage region; ii) compare the storage depths with the southern volcanoes; iii) relate this to different geochemical trends we have identified using bulk rock data and confirm the trends using the same trapped melt inclusions.

Results and Preliminary Interpretation

The first of two visits to the ion probe facility has allowed us to measure the H_2O and CO_2 contents of melt inclusions in a few selected rocks and start to constrain the depths of magma storage for previous eruptions of MAD as well some pyroclastic rocks from the southern volcanoes. It is already clear that two distinct magma systems operate beneath the island and both are feeding the MAD complex. Preliminary volatile data suggests the lower K_2O system (blue in Fig 2), which is dominant at MAD (Fig 2B) comes from a considerable depth (>450 MPa or 15km) that is similar to the southern samples examined, suggesting a high explosive potential. In contrast, the higher K_2O series at MAD (in red) may come from only ~100MPa or 3km consistent with the recent seismic activity. This represents a lower risk, but perhaps a higher probability of imminent activity.

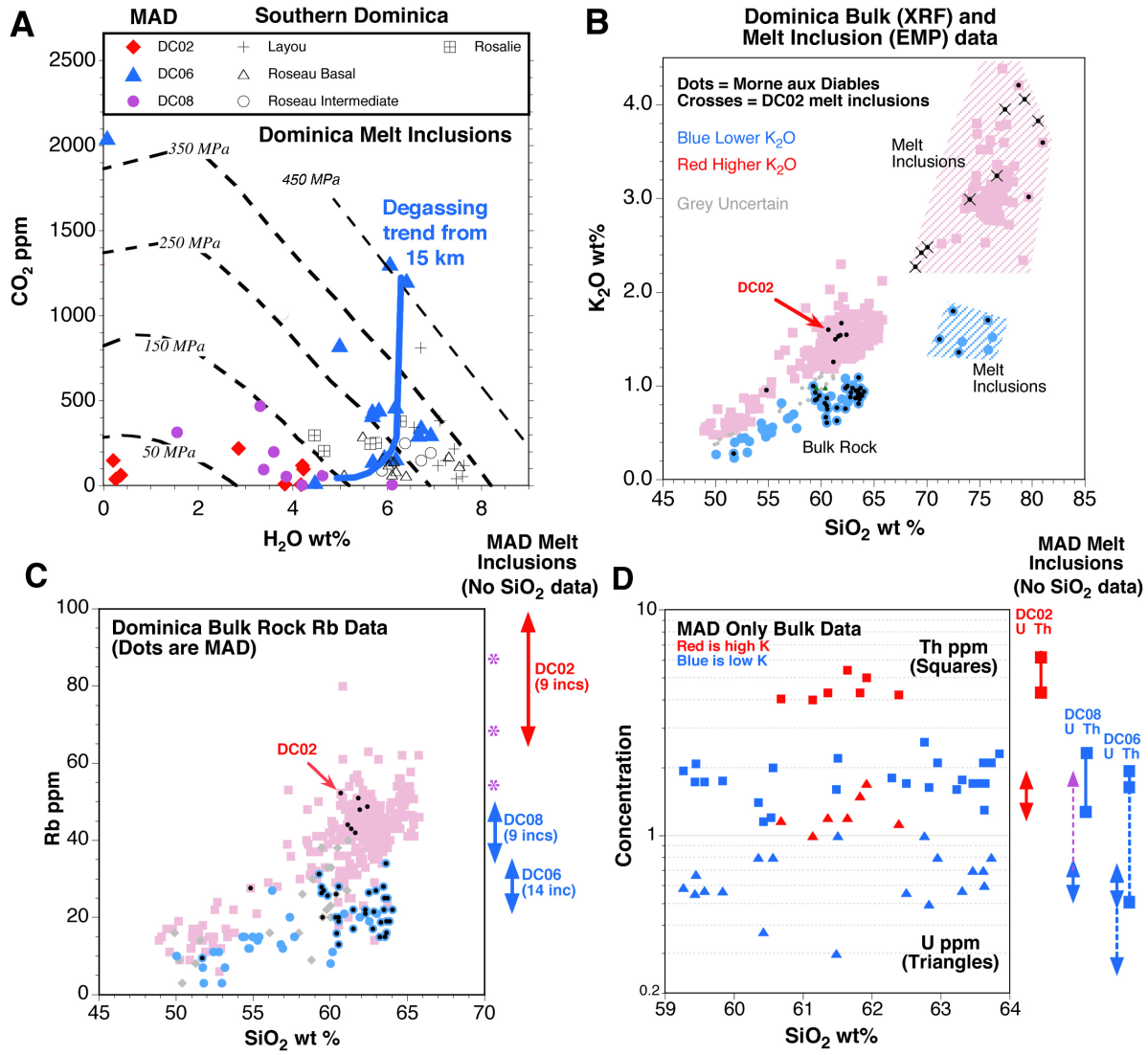

Figure 2. In A the H_2O and CO_2 content of Dominica melt inclusions are plotted along with dashed lines showing the minimum pressure required to dissolve these volatile concentrations. MAD sample DC06 require a minimum pressure of 450MPa which is >15km, but follows a trend typical of degassing as the magma rises. The Southern Dominica samples may have also degassed, but require at least 200-350 MPa. The MAD sample DC02 requires lower pressures of 50-100MPa. DC08 (in purple) has inclusion that seem to fall on both trends. B illustrates the two K_2O trends on Dominica. In C and D these geochemical trends are also be defined by the Rb, U and Th contents of the whole rocks and the melt inclusion measured by ion probe (awaiting SiO_2 data). DC02 inclusions clearly have the high K_2O character, whilst DC06 is clearly low. DC08 is mainly low K_2O in character, but also has a few inclusions that are extend to the higher K_2O trend (in purple) suggesting it contains some crystals that have seen both systems. Dominica bulk rock data combines our new and other published data.

Hydrogen mobility in olivine under mantle conditions

J. Brooke & G. Bromiley

School of GeoSciences, University of Edinburgh, Edinburgh EH9 3JW, UK

A considerable amount of water may be stored in the Earth's mantle as structurally incorporated hydrogen in minerals whose chemical formulae indicated that they are nominally anhydrous. As a result, there may be a significant volume of water stored in the interior of our planet (estimates range from almost none to several ocean volumes) and this water could play a key role in the geodynamics of the Earth. However, the deep Earth is clearly not an accessible area of study and models of the interior structure of the planet are primarily based on geochemical and geophysical considerations, as well as analysis of what samples are available. The water content of the mantle can be estimated through the analysis of shallow samples and xenolith material but these estimates may not be representative of the whole mantle and there is significant potential for modification of water content during xenolith ascent. Quantifying the amount of water in mantle minerals is, therefore, an important step in understanding many deep-Earth processes.

Due to its sensitivity to small amounts of water, electrical conductivity should be a very useful parameter in mapping out changes in water content and subsequently quantifying the total water content of the Earth. It is possible to use geophysical techniques such as magnetotellurics (MT) to 'map-out' the water content of the mantle, although accurate interpretation of such data relies on good quality conductivity data from mineral physics studies. Difficulties in measuring conductivity in wet (hydrogen-bearing) samples, coupled with the fact that traditional diffusion experiments do not provide thermodynamic data on hydrogen mobility, mean that the influence of hydrogen on conductivity remains poorly constrained.

In this study, electrical conductivity in synthetic hydrous olivine was considered using a novel technique measuring hydrogen-deuterium exchange in single crystals. Hydrogen-saturated crystals synthesised under mantle conditions are sealed in a silver palladium or gold piston-cylinder capsule with deuterium oxide, allowing deuterium to exchange with hydrogen under controlled pressure and temperature conditions for a specified time period. The resulting H-D exchange profiles can be characterised using SIMS and fitted to diffusion laws; extrapolated data for hydrogen self mobility can then be directly related to electrical conductivity through the Nernst-Einstein equation [1].

A pilot study was carried out in September 2013 to determine the viability of the method and successfully showed that measurable deuterium diffusion profiles could be obtained by SIMS in the synthetic forsterite crystals. Additionally, the pilot identified the need for better quality analysis surfaces and thus polishing of the crystal faces prior to D-H exchange experiments was incorporated. This step greatly improved the quality of the data obtained from SIMS but unfortunately some surfaces were still too poor for good quality analysis (as a result of the need to polish prior to experimental runs and therefore difficulties in retrieving the crystals, identifying the polished face and successfully mounting with the polished face in the correct orientation). Additionally, once mounted, the majority of the forsterite surfaces that were suitable for analysis were not large enough to carry out full depth profiling [2] (in order to minimise surface effects, a significant area is rastered but collection is gated so that only that from the centre of the pit is counted). Single pit analysis was carried out on these grains for comparison of the effect, and to obtain an approximate estimate of the total deuterium/hydrogen content of each grain.

Of the grains suitable for full depth profiling, sufficient deuterium was measured in two; E6-A and E8-A. A trend of decreasing deuterium concentration with depth was identified in both grains (see Fig. 1.), indicating the diffusion of deuterium into the crystal structure, exchanging with hydrogen. In order to accurately determine diffusion coefficients we are currently measuring depth of the analysis pits using white light interferometry (in collaboration with the School of Engineering, University of Edinburgh). Once the depths of the pits have been accurately measured, diffusion coefficients for the two full depth profiles will be calculated. Results to date indicate that our experimental approach can

be used to determine, for the first time, hydrogen self mobility directly under mantle conditions. The main challenge of this technique is ensuring samples are larger than a minimum crystal size needed for accurate depth analysis by SIMS.

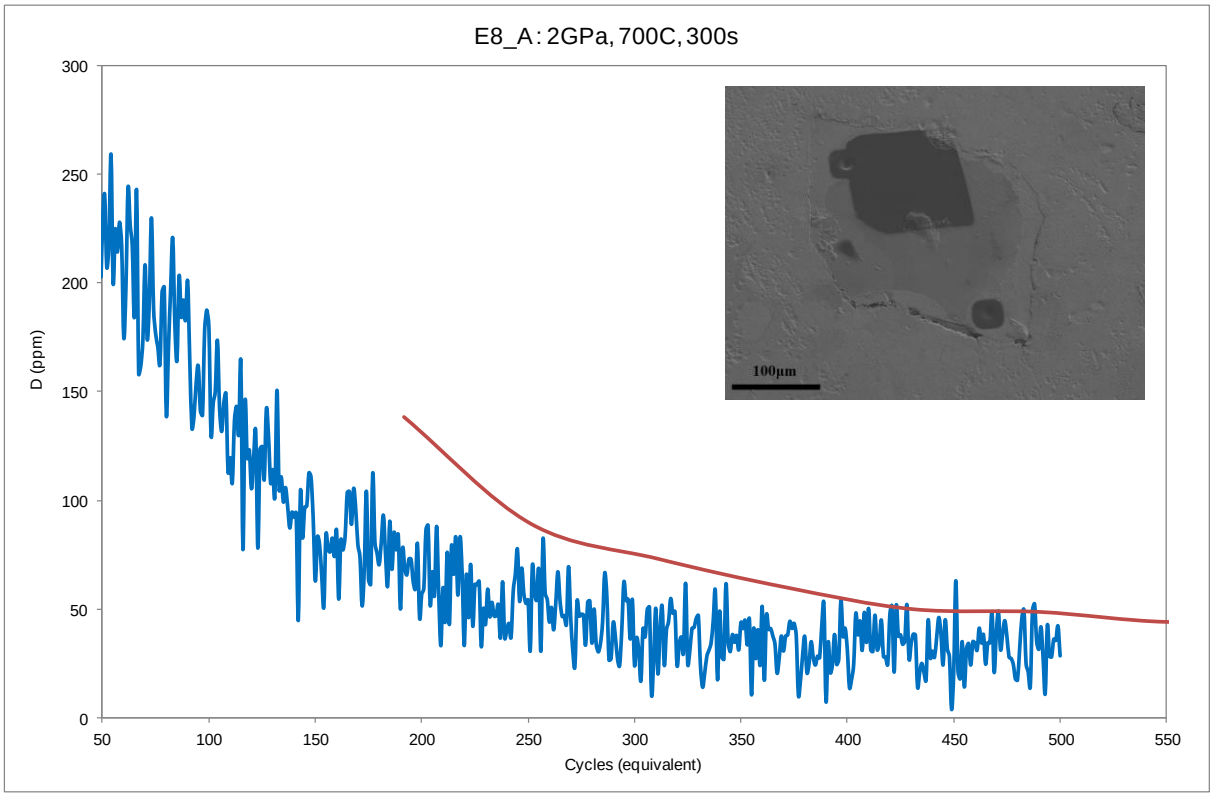

Figure 1. Depth analysis showing deuterium concentration profile for forsterite grain E8-A. Blue line represents full depth analysis collected using a large raster area and gated beam and the red line is the data collected from a single pit analysis carried out in the bottom right of the grain. As discussed in text, the true depth of the pits has not yet been measured. *(insert)* SEM image showing analysis on E8-A: the large dark area represents the main gated raster analysis; two smaller marks where single pit analysis was carried out can also be seen. The mark in the middle of the grain is trace of the mounting material which was unfortunately not entirely removed, limiting the selection of pit placement.

Preliminary data from the study were presented by J. Brooke at the Deep Earth Processes meeting in October 2014.

References

[1] DuFrane & Tyburczy (2012) Geochemistry, Geophysics, Geosystems **13**
[2] J. L. Hunter (2009) Mineralogical Association of Canada Short Course **41**, 132-148

Coupled C and O isotopes of superdeep diamonds and their inclusions

A.D. Burnham[1,2], S.C. Kohn[1], A. R. Thomson[1], M.J. Walter[1], G.P. Bulanova[1] and C.B. Smith[1]

[1]School of Earth Sciences, University of Bristol, BS8 1RJ, UK
[2](present address) Research School of Earth Sciences, Australian National University, Acton ACT 2601, Australia

Background

Diamonds are of considerable importance because they often contain mineral inclusions that are pristine samples of the deep Earth, uncontaminated by the chemistry of the magma that brought them to the surface (in contrast to the alteration experienced by xenoliths and xenocrysts in the same host rocks). Diamonds from the Juina region, Brazil, contain inclusions that are consistent in composition with the mineralogy that peridotite and basalt would assume at the pressures and temperatures of the deep upper mantle and lower mantle[1]. To reflect their likely origin at such great depths within the Earth these diamonds are termed "superdeep", in contrast to lithospheric diamonds. The C isotopic compositions of many of these diamonds extend as low as -26 ‰ relative to PDB, in contrast to the normal mantle value of -5.5 ± 1 ‰. These variations in the carbon isotopic compositions of diamonds have been attributed by various authors to either primordial heterogeneity of the Earth, fractionation processes or subduction of crustal C, which can range from –45 ‰ to > +5 ‰ relative to PDB.

At other localities an anticorrelation between $\delta^{13}C_{diamond}$ and $\delta^{18}O$ of inclusions within diamond has been observed[2,3]. High values of $\delta^{18}O$ can only be generated at low temperatures, i.e. near the Earth's surface. Therefore, this covariation cannot be explained by isotope fractionation but is consistent with a subduction origin for diamonds with eclogitic inclusions. The diamonds displaying this anticorrelation are all lithospheric diamonds: what relationship might occur in superdeep samples? One possibility is that the modification of the slab during its descent erases the crustal O isotope signature, in which case the inclusions would have normal mantle $\delta^{18}O$ values.

In order to assess the coupling/decoupling of C and O isotopes during deep subduction of crustal material, isotopic measurements were made on superdeep diamonds and their mineral inclusions.

Methods

Diamonds containing inclusions of coesite (often after stishovite), garnet and $CaSiO_3$-walstromite (after $CaSiO_3$ perovskite) were selected for study by Raman spectroscopy and polished to expose the inclusions. The major element compositions of the inclusions were measured by EPMA at Bristol. C and O isotopes were measured using the Cameca ims-1270 at Edinburgh using standard procedures. Cathodoluminescence images enabled the C isotopic measurement to be made in the same growth zone as the inclusion. Some inclusions were large enough to make replicate analyses.

Results

The samples show an anticorrelation of C and O isotope compositions (Fig. 1). The C isotopic compositions are consistent with those previously observed for these suites of diamonds. The $\delta^{18}O$ values are among the highest observed for diamond inclusions (Fig. 2) and clearly indicate a crustal origin for the protolith of these samples. The C isotopic compositions range from very light (-26 ‰) to near mantle values; in contrast the range for O isotopes is small and the values are consistently elevated above typical mantle values ($\delta^{18}O = 5.7 \pm 1$ ‰).

Discussion

Formation of diamond in the deep upper mantle occurs as a result of a reaction between the oxidised carbonate melt released from the subducted slab and the reduced ambient mantle. This process is known as redox freezing. The relationship observed in the isotopic data can be explained by reaction of a carbonate melt with a mantle phase that is rich in C but poor in O, i.e. the C isotopes mix efficiently while the crustal O isotope signature is preserved.

Cohenite, Fe_3C, is an expected mantle phase at deep upper mantle depths and is an effective reductant for carbonate melt:

$$(Ca,Mg)CO_3 + Fe_3C = 3\,(Fe,Ca,Mg)O + 2\,C$$
in melt *carbide* *in silicates* *diamond*

The solid silicate component generated by this reaction will further react with the surrounding silicates in the mantle. The data obtained can be fit using a mixing relationship in which the isotopic composition of the mantle endmember is fixed at canonical values, and that of the crustal endmember and proportion of mantle silicate (expressed as Fe_3C/Mg_2SiO_4) involved in the reaction are fit by eye. This is illustrated in Fig. 1. The scatter about this fit reflects the heterogeneous isotopic composition of the subducted crust and also the variable proportions of mantle silicate that are involved in the reaction.

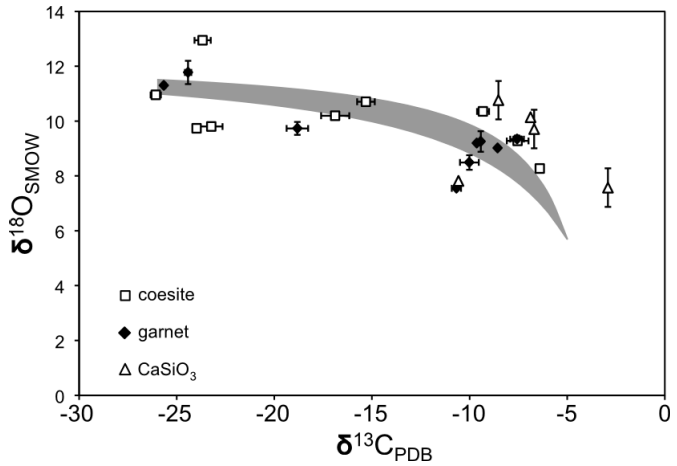

Figure 1 (left). Covariation of $\delta^{18}O$ and $\delta^{13}C$ in the samples studied. Error bars indicate the standard deviation of replicate analyses. Two possible fits to the data are demonstrated by the shaded field: the upper bound is fit using $\delta^{18}O^{melt}$ = 11.5 ‰ and Fe_3C/Mg_2SiO_4 = 3.5; the lower bound has $\delta^{18}O^{melt}$ = 11 ‰ and Fe_3C/Mg_2SiO_4 = 2.

Figure 2 (right). Comparison of the $\delta^{18}O$ of the inclusions analysed in this study and previously reported inclusions in diamonds.

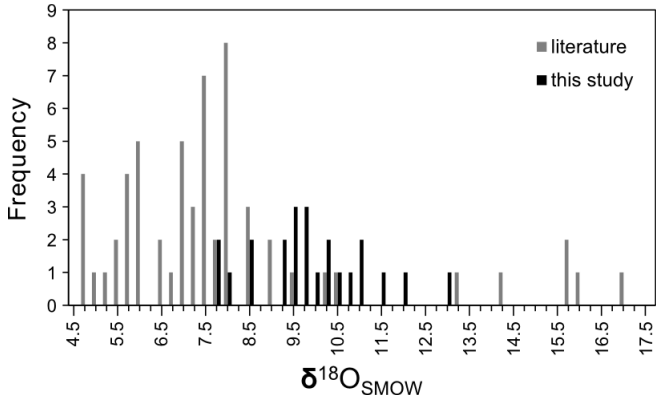

References

[1] M.J. Walter et al. (2011). Science 334, 54-57.
[2] R.B. Ickert et al. (2013). Earth and Planetary Science Letters 364, 85-97.
[3] D.J. Schulze et al. (2013). Geology 41, 455-458.

Accurate climate reconstruction from fossil corals

C. Cole[1], N. Allison[1] & A. Finch[1]

[1]Department of Earth and Environmental Sciences, University of St. Andrews, St. Andrews KY16 9AL, UK

The geochemistry of skeletal aragonite deposited by massive tropical corals preserves a valuable record of past climate. In particular, coral skeletal Sr/Ca records sea surface temperature (SST) at the time of deposition and is a widely used palaeothermometer. Good correlations have been observed between SST and skeletal Sr/Ca in modern corals [1], however SSTs estimated from many fossil corals are significantly cooler than those predicted from other proxies and climate models [2]. This discrepancy may reflect changes in the processes affecting trace metal uptake into skeletal aragonite between past and present day. Seawater Sr/Ca is unlikely to have varied significantly on glacial-interglacial timescales, but surface ocean pH is estimated to have varied by 0.2 units across glacial cycles [3], associated with changes in atmospheric CO_2 [4]. Corals precipitate aragonite from an extracellular fluid (ECF) by actively increasing the fluid pH, which raises the saturation state of $CaCO_3$. We hypothesised that past variations in seawater pH significantly influenced the pH of the ECF, and consequently the incorporation of trace elements in the skeleton.

We used SIMS to determine the Sr/Ca composition of skeletal aragonite deposited by massive *Porites* corals, the coral genus most commonly used in palaeoclimate reconstructions, cultured in our purpose-built aquarium system at pCO_2 levels ranging from the last glacial maximum (180 ppm) to levels projected by the end of this century (750 ppm). Following an acclimation period of > 5 months, SIMS analyses were made at a 1-2 day resolution along skeletal units deposited over a five-week period, defined by alizarin red stain lines (Figure 1). We explore the relationship between seawater pH and skeletal Sr/Ca, and we investigate how Sr/Ca varies between different genotypes within the same treatment. Additionally, the high spatial resolution of SIMS enables examination of geochemical heterogeneity within an individual coral. We aim to develop a methodology for correcting for the effects of seawater pH, and changes in calcification, photosynthesis and respiration rates, on skeletal Sr/Ca, enabling more accurate reconstruction of SST from fossil coral skeletons.

Results

Trace elements (Sr, Ca, B, Ba, Mg) were measured by SIMS along 2-3 skeletal units, each spanning the 5-week experimental period, in 4-5 coral heads from each treatment. Representative Sr/Ca data is shown in Figure 1 from individual coral heads grown at 180 and 750 ppm pCO_2.

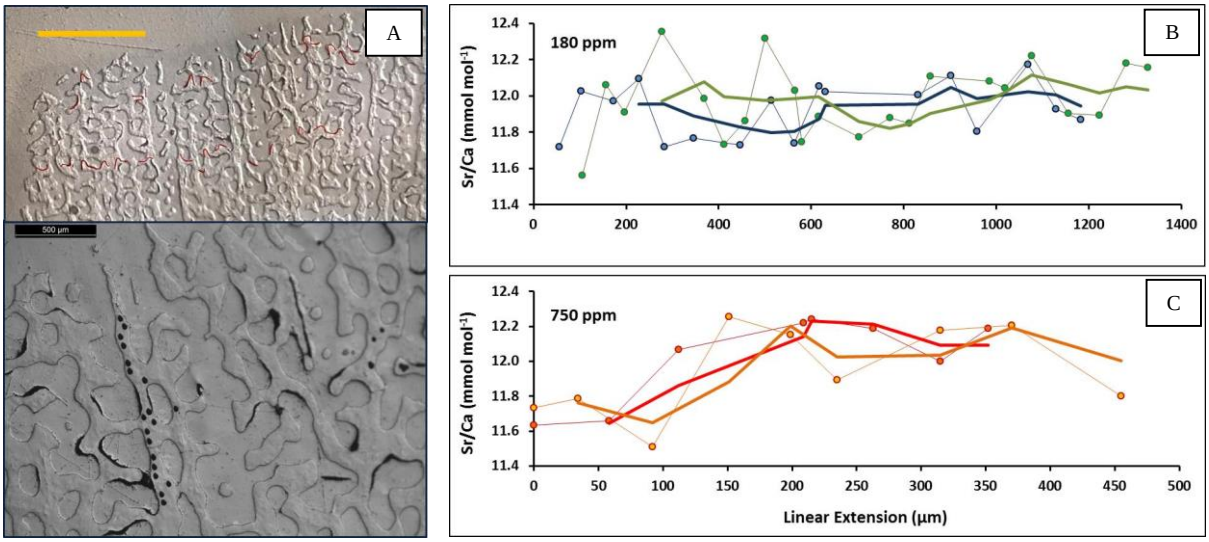

Figure 1. (A) Polished cross-section through a coral skeleton, showing material deposited during the 5-week experimental period within the outermost two red stain lines. Orange scale bar is 2 mm. Inset shows sputter pits along a single skeletal unit following SIMS. (B, C) SIMS Sr/Ca measurements across two individual skeletal units spanning 5 weeks of growth at 180ppm (B) and 750ppm (C). Thick lines show ~5 day running mean.

We observe significant heterogeneity in Sr/Ca across single skeletal units within cultured *Porites* corals (~2% variation), indicating high frequency biological noise in aragonite deposited in constant controlled aquarium conditions. Corals were maintained at constant temperature (25 ± 0.1°C) throughout the acclimation and experimental period, yet variations in Sr/Ca suggest temperature fluctuations of ~2 °C. Applying a smoothed running mean to all data suggests a regular oscillation in Sr/Ca on scale of 1-2 weeks, which may reflect cyclical changes in calcification, photosynthesis and respiration rate, independent of the external environment. We will compare this data with metabolic rates measured over the time period of skeletal deposition, and assess whether a correction can be applied to Sr/Ca to resolve the temperature component more accurately.

Mean skeletal Sr/Ca values, normalised to seawater Sr/Ca, for each coral head cultured at 180, 400 and 750 ppm pCO_2 are presented in Figure 2. We find that the influence of seawater pH on skeletal Sr/Ca varies between genotypes, and we also observe significant variability in Sr/Ca between corals cultured within the same treatment. Corals from genotype 1 show an increase in skeletal Sr/Ca of 3.5% at 750 ppm pCO_2 compared with both 180 and 400 ppm pCO_2. In contrast, skeletal Sr/Ca is reduced by 3.8% at 400ppm pCO_2 compared with 180ppm in corals from genotype 3, whilst no significant change is observed at 750ppm. Genotype 2 corals show no significant effect of seawater pH on skeletal Sr/Ca. Further, skeletal Sr/Ca between corals cultured under the same conditions was found to vary by up to 2.3% at 180ppm, 2.7% at 400ppm, and 4.1% at 750ppm. The magnitude of these biological variations is likely to account for a portion of the error reported in sea surface temperature estimates from fossil corals, as a difference of 1% in Sr/Ca typically represents a 1°C temperature increment [5].

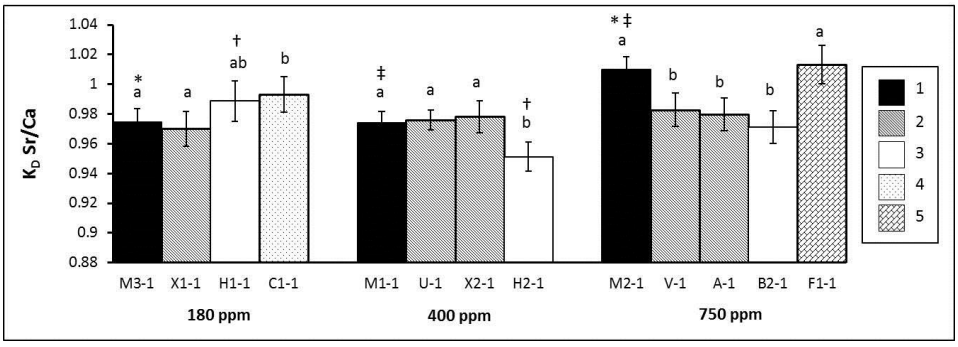

Figure 2. Mean Sr/Ca of skeletal aragonite, normalised to seawater Sr/Ca, for individual coral heads sampled from each pCO_2 treatment. Bars represent Sr/Ca averaged across 2+ skeletal units. Five different genotypes (3-4 per treatment) are indicated in the legend. Paired symbols (*, †, ‡) indicate significant differences ($p < 0.05$; ANOVA) between treatments. Within treatments, different letters indicate significant differences between corals. Error bars show 95% confidence limits.

This study demonstrates that there is significant variability in skeletal Sr/Ca in massive *Porites* corals, independent of SST and pH, highlighting the need for large sample sets in fossil coral SST reconstructions. We are currently working towards a method for correcting for some of this biological variation in Sr/Ca using both metabolic rate measurements and ECF pH estimates from skeletal $\delta^{11}B$.

References

[1] M.T. McCulloch and T. Esat (2000) Chem. Geol. **169**, 107-129
[2] K.L. DeLong et al. (2010) Geochem. Geophys. Geosys. **11**, Q06005, doi: 10.1029/2009GC002758
[3] B. Hönisch and N.G. Hemming (2005) Earth Planet. Sci. Lett. **236**, 305-314
[4] J.R. Petit et al. (1999) Nature **399**, 429-436
[5] S. Reynaud et al. (2007) Geochim. Cosmochim. Acta **71**, 354-362

Appendix

Analyses were made on the Cameca 4f. Positive secondary ions were produced by an 8nA, 10.8 kV, $^{16}O^-$ primary beam. Primary aperture = 2, field aperture =1, contrast aperture = 2. The primary beam was ~20 x 30 µm. Secondary ions were measured by electron multiplier by sequential stepping of the magnetic field through a cycle of relative atomic mass. Singly-charged cations were collected at masses ^{11}B (15 seconds), ^{26}Mg (3s), ^{44}Ca (2s), ^{88}Sr (4s) and ^{138}Ba (15s). A pre-analysis sputter time of 60 s in spot mode was used to remove surface contamination. External Sr/Ca reproducibility was calculated from the relative standard deviation ($\sigma/\bar{x}$) of 90 replicate analyses on the carbonate standard Haxby and was <0.04 mmol mol^{-1}.

Neodymium in cold water corals

K.C. Crocket[1] & E.C. Hathorne[2]
[1]Scottish Association for Marine Science, Scottish Marine Institute, Oban, Argyll PA37 1QA, UK
[2]GEOMAR Helmholtz Centre for Ocean Research Kiel, Wischhofstrasse 1-3, Kiel 24148, Germany

Background

Fossil cold water scleractinian corals are a promising archive for investigating changes in ocean circulation through reconstruction of seawater Nd isotope compositions and concentrations. Cold water corals have the potential to provide high resolution records with absolute (U-Th) age constraints and from depths in the ocean where sedimentary archives are typically absent. To exploit this archive with confidence, investigation is required to establish both archive integrity (influence of secondary precipitates and contaminant phases) and the distribution of Nd within the aragonitic skeleton (e.g. fibrous aragonite crystals, early mineralisation zones, and organic phases). A one-day pilot SIMS study was undertaken firstly to determine if SIMS measurements of coral Nd were feasible despite low concentrations (<few 10s ppb), and secondly to measure selected rare earth elements (La, Nd) and trace elements (Al, Si, P, Fe, Sr, Y) in two species of cold water coral to investigate variation in chemical composition (i) across different skeletal components, and (ii) between coralline aragonite and non-coralline phases.

A fossil *D. dianthus* and two *L. pertusa* samples were selected and prepared for analysis by the Cameca IMS4f ion microprobe in May 2014. The *D. dianthus* sample originated from the New England Seamounts (1176 mbsl, NW Atlantic), with a U-Th age of 315 years [1]. The *L. pertusa* was sourced from the Scottish Mingulay coral reef, and then placed in aquarium culture tanks for 12 months under controlled conditions of temperature (9 °C) and partial pressure of atmospheric CO_2 (1000 ppm). One sample was grown live, while the other was a dead fragment kept in the tank under the same conditions (both provided by S. Hennige, Heriot-Watt University). Sectioning and polishing of the dead fragment revealed a rim of secondary precipitate acquired during the year spent in culture.

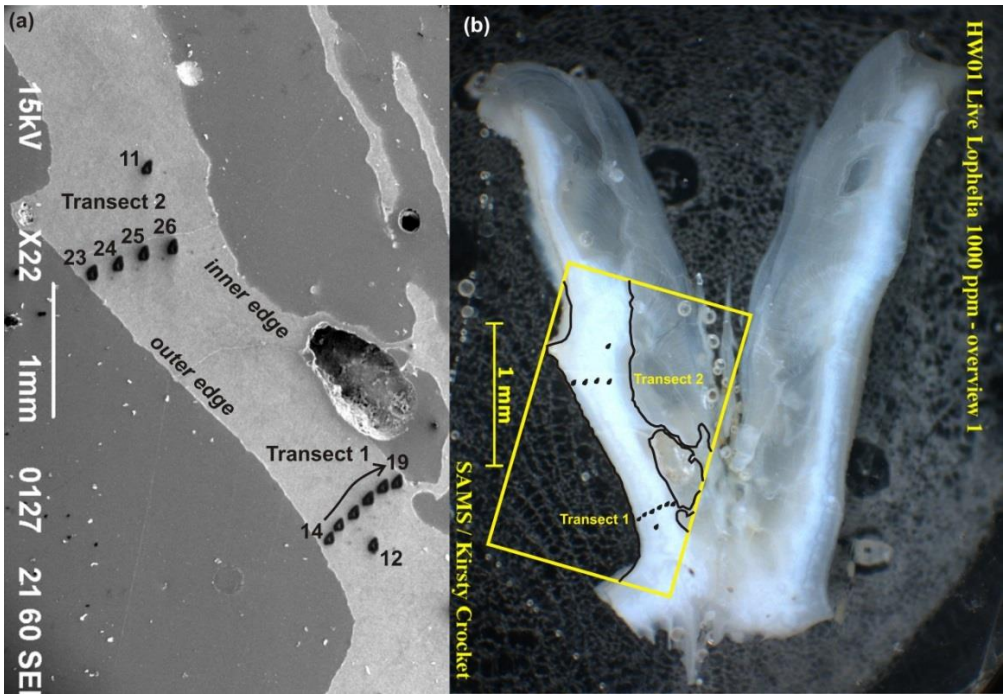

Figure 1: (a) Post-SIMS SEM image of the live cultured *L. pertusa* sample, and (b) the corresponding location of Transects 1 and 2 in a pre-SIMS, light reflected image.

Results

The rim of secondary precipitate observed in the dead fragment of *L. pertusa* showed consistently higher concentration factors, relative to coralline aragonite, of La (11), Nd (2), Al (4), Si (3), P (3), Fe (6), and Y (2). This could be due to either higher partition coefficients associated with the secondary phase, and/or aquarium water with a different composition to seawater at the Mingulay Reef.

Comparison of aragonite Nd concentrations in the dead fragment and live coral reveal overlap, suggesting that the elevated Nd in the secondary phase is not the result of higher aquarium water Nd concentrations. In the live cultured *L. pertusa*, two spot transects were made perpendicular to the growth direction in one polyp (Figs. 1 and 2). The Nd concentrations across each transect show variation corresponding to internal structure of the sample, and both transects show similar trends in variation (Fig. 3).

Spot measurements in *D. dianthus* were carried out perpendicular to the growth direction. Target areas were: (i) the external wall, where numerous unidentified filaments (<2 μm diameter) permeated the coralline aragonite, and (ii) obvious internal skeletal structural components. The external wall spots (n=3) had higher concentrations, compared to internal spots (n=14), of La (25), Nd (7), Al (6), Si (4), and Fe (3). The internal spots showed variation corresponding to structural features, with marginally lower concentrations in early mineralisation zones.

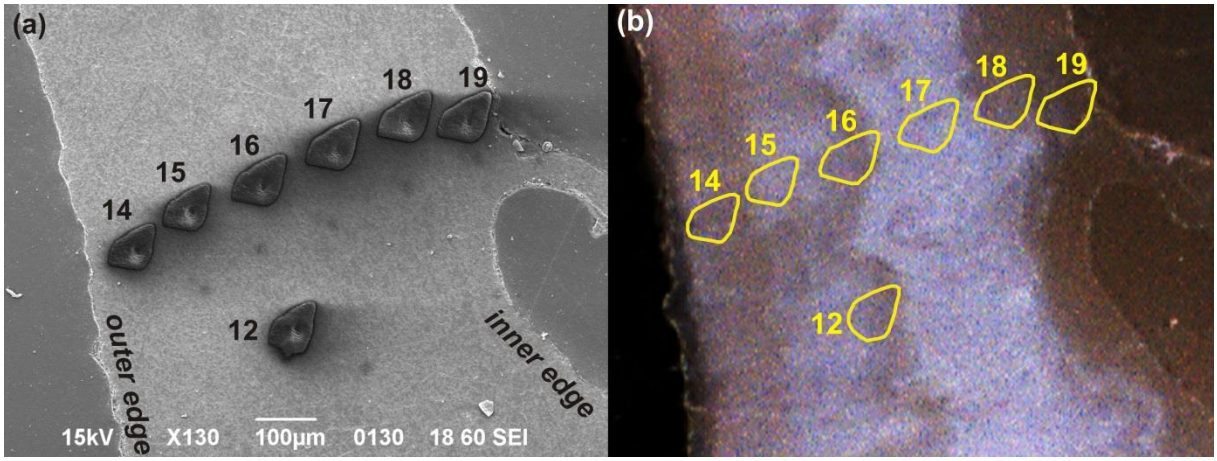

Figure 2: (a) Post-SIMS SEM image of Transect 1, and (b) a pre-SIMS, light reflected image showing the internal structure of the live cultured *L. pertusa* sample and spot locations.

Conclusion

Secondary phases only conspicuous at high magnification in both samples show higher Nd concentrations than the primary coralline aragonite. Consistent variation in Nd concentration is observed across different structural features in both *D. dianthus* and *L. pertusa*, although this is more pronounced in *L. pertusa*. Our interpretation of the data is limited by two caveats. The SIMS Nd concentrations in both *D. dianthus* and *L. pertusa* are higher than expected when compared to results obtained by bulk sample digestion and laser ablation of the same sample material. This could be due to molecular interferences on Nd during SIMS measurements by the Cameca IMS4f, potentially resolvable by using the greater mass resolution of the Cameca 1270. Secondly, the chemical composition of seawater in which the corals grew is not available for comparison to distinguish, for example, effects due to phase partitioning or different seawater Nd concentrations.

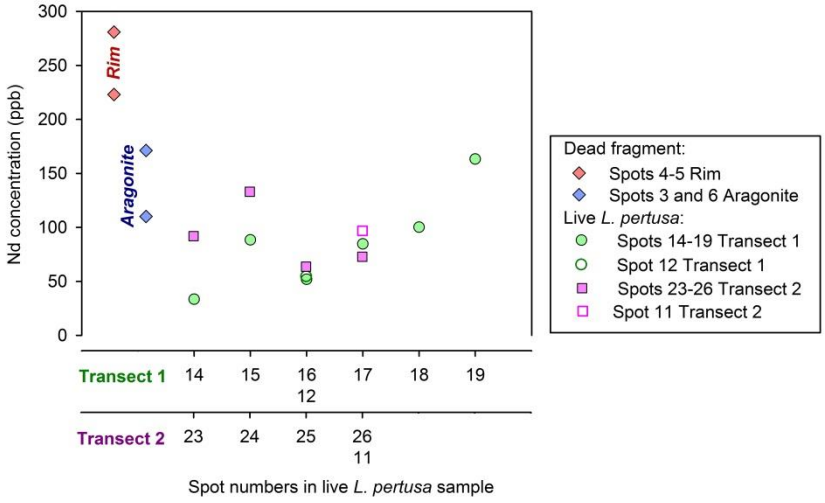

Figure 3: Nd concentration in the rim and coralline aragonite of the dead fragment, and in the two transects of the live cultured *L. pertusa* sample (Figs. 1 and 2).

Reference

[1] Robinson, L.F., et al. (2007) Bulletin of Marine Science **81**, 371-391

Insights into volcanic processes from water in the structure of pyroxenes

M. Edmonds[1], S. Kohn[2] & EIMF[3]

[1]Earth Sciences, University of Cambridge, CB2 3EQ, UK
[2]Earth Sciences, University of Bristol, Bristol BS8 1RJ, UK
[3] Edinburgh Ion Microprobe Facility, University of Edinburgh, Edinburgh EH9 3JW, UK

Introduction

Water in arc magmas influences profoundly petrogenesis, crustal assimilation, magma buoyancy, compressibility, rheology, eruption style, and the availability of fluids for metal transport and deposition. Records of magma water content are elusive and poorly constrained. Melt inclusions are subject to re-equilibration, post-entrapment processes and are in themselves a biased record, only forming during conditions of rapid crystal growth. In this study we seek to establish whether useful records of magma water content are stored in volcanic phenocrysts of pyroxene.

Strategy

Phenocrysts of augite and enstatite were picked from crushed fractions of samples from Soufriere Hills Volcano, Montserrat. The samples were all scoria or pumice, chosen to minimise the effect of water loss from the phenocrysts. Crystals were polished, or double polished, then mounted in indium for H_2O analysis using Secondary Ion Mass Spectrometry (SIMS) at the University of Edinburgh. Backgrounds for H_2O in pyroxene were ~ 5-8 ppm. Crystals were then analysed for major elements using electron microprobe at Cambridge. Double polished crystals were analysed for their H_2O content by Fourier Transform Infra red Spectroscopy. Melt inclusions hosted within the crystals were also analysed for H_2O (using SIMS) and major elements (using electron microprobe).

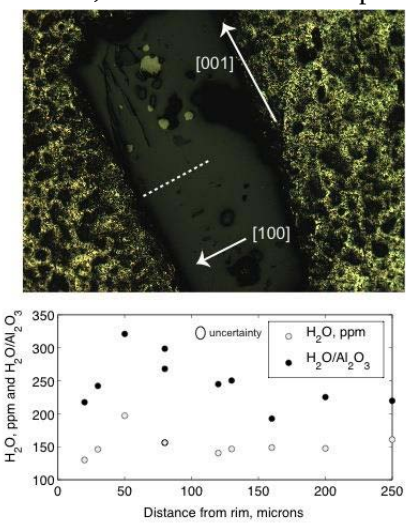

Figure 1. Top, reflected light image of a pyroxene crystal (approximately 2 mm long) mounted in indium for analysis, with crystallographic directions and the location of the analytical traverse marked. Bottom, H_2O concentration and H_2O/Al_2O_3 along a traverse through the crystal.

Results and discussion

The H_2O content of pyroxenes ranges from 50-300 ppm (**Figures 1, 2, 3**) and is correlated with Al and Mg number (**Figure 2**). In a small subset of grains there is a decrease in H_2O content towards the rim of the crystal (**Figure 1**), but on the whole the there is little relationship between distance from the rim and H_2O content (**Figure 2, left**).

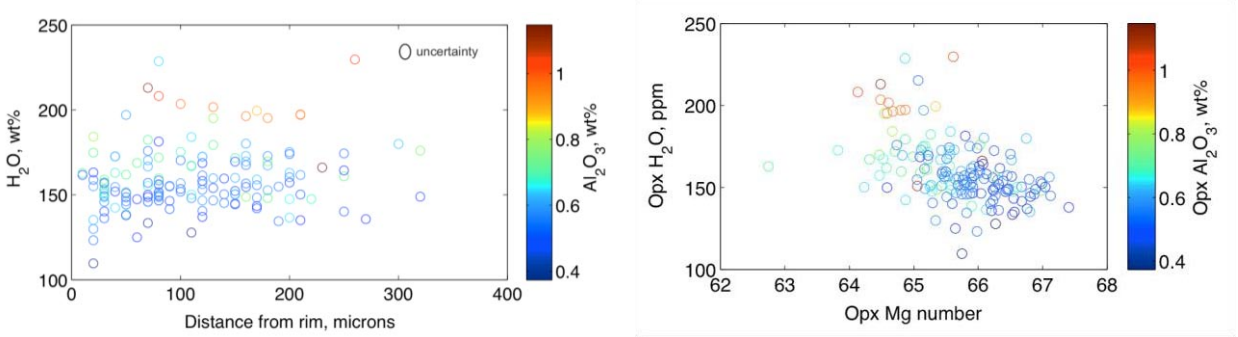

Figure 2. H_2O content of orthopyroxenes from Soufriere Hills Volcano pumice (from SIMS) plotted against left, distance from crystal rim and right, the Mg number of the orthopyroxene. In both plots the data points are colour-coded for orthopyroxene Al_2O_3 content.

These data show that most of the grains have not lost H_2O by diffusion during magma ascent to lower pressures, when the surrounding melt would have outgassed H_2O.

The H_2O content of the melt in which the pyroxenes grew may be estimated using the relationship between the Al_2O_3 content of the pyroxene and the pyroxene-melt partition coefficient [1] and the results are shown in **figure 3**. It can be seen that for most crystals the H_2O content of the melt ranged from 6 to 8 wt%, typical of vapor-saturated melts in the mid-crust (10-15 km depth). Some crystals show a large range, with core H_2O contents suggesting carrier liquids containing up to 10 wt% and rims 4 wt% H_2O.

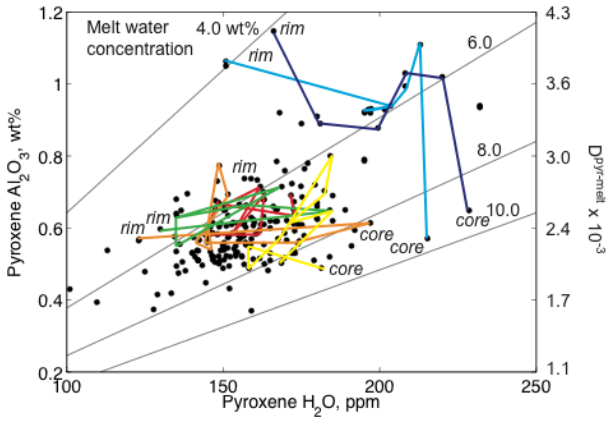

Figure 3. Plot of enstatite Al_2O_3 content against H_2O content, contoured for melt H_2O content. Melt water contents were calculated by assuming that the melt-enstatite partition coefficient for water is proportional to Al_2O_3. Individual crystal zoning pathways are marked on with a single color, and the core and rim concentrations are labelled.

The pyroxenes in general record higher melt H_2O contents than have been preserved as melt inclusions. Plagioclase-hosted melt inclusions contain up to 6.3 wt% H_2O (**figure 4**). Scarce melt inclusions in enstatite have H_2O contents that agrees well with that inferred from the H_2O in the enstatite structure. The two datasets might be fundamentally reflecting different parts of the system: the enstatites deep magma storage; the melt inclusions magma transport.

Figure 4. Melt water contents plotted against enstatite Mg#, color-coded for enstatite Al_2O_3 content. Melt inclusion data are also shown: the range in H_2O contents recorded by plagioclase-hosted melt inclusions are shown as the grey shaded box (encompassing the entire range of Mg# as the composition of plagioclase in equilibrium with the enstatite is not constrained). The water content of the melt inclusions hosted by enstatite are shown by the smaller grey rectangles, plotted at the Mg# of the host enstatite adjacent to the melt inclusion. Uncertainties are indicated by the ellipse.

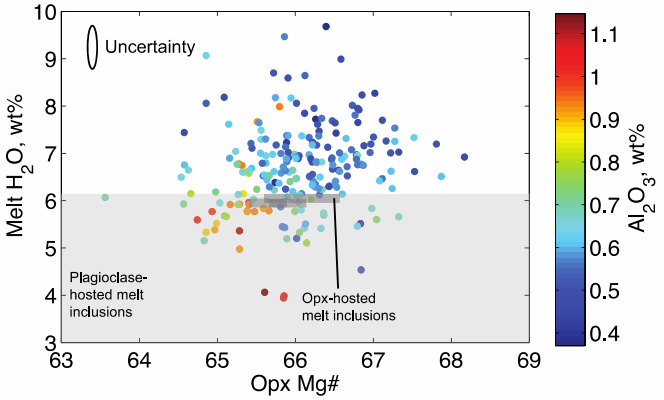

References

[1] S.C. Kohn and K.J. Grant (2006) Reviews in Mineralogy and Geochemistry **62**, 231-241.
[2] K.J. Grant, S.C. Kohn, R.A. Brooker (2006). Contributions to Mineralogy and Petrology **151**, 651-664.

Zircon and its isotopic systems during intracrustal differentiation

S. Fischer[1], P. Cawood[1] & C. Hawkesworth[2]

[1]Dept of Earth Sciences, University of St Andrews, Irvine Building, North Street, St Andrews KY16 9AL, UK
[2]School of Earth Sciences, University of Bristol, Wills Memorial Building, Queens Road, Bristol BS8 1RJ, UK

Zircon is widely regarded as a robust record keeper of information on crustal evolution. Uranium-lead dating provides an age of crystallisation, hafnium isotopes can be used to calculate model ages for mantle extraction of the rock zircons crystallised from and oxygen isotopes allow the distinction of zircons crystallised from a mantle-derived melt from those which interacted with (supra-)crustal material. Furthermore, zircon trace element composition can be used as a petrogenetic indicator (i.e. crystallisation in the presence or absence of garnet) and geothermometer (Ti-in-zircon).
The purpose of this project is to present a detailed study on zircon throughout a section of continental crust, investigating the behaviour of the key isotopic systems (U-Pb, Hf, O) and trace elements in zircons from lower crustal mafic rocks, and how metamorphic grade and partial melting influence the information that zircon records. For this, we have sampled the Kapuskasing uplift in the southern Superior province in Canada, where crustal tilting along a major fault zone has exposed a more or less complete section through Archaean continental crust, as well as the Lewisian complex in NW Scotland, which provides examples of partial melting in mafic Archaean granulites. Zircons from high-grade terrains can have a highly complex internal structure, including inherited cores and multiple overgrowths. The use of cathodoluminescence (CL) and back-scatter electron (BSE) image guided, *in situ* analysis with high spatial resolution is therefore critical – aspects at which the ion microprobe excels. In this report we present the results of $\delta^{18}O$ analyses of zircons from the Kapuskasing uplift. The project is ongoing and results will be complemented with U-Pb dating and trace element analysis at the Edinburgh Ion Microprobe facility (as well as Hf isotopes at NIGL).

Samples
From the *amphibolite facies region* of the Kapuskasing uplift, two mafic samples were collected from the same outcrop. They have very different orientation in foliation, one (13-Kap-01A) clearly overprinting the other (13-Kap-01B). Associated with the amphibolites is a pegmatite (13-Kap-01C) which cross-cuts both foliations, but is deformed by the second foliation. From the *granulite facies region*, an outcrop of mafic gneiss that shows compositional banding provided two samples (13-Kap-07A: g+cpx+plag+amph+tit, 13-Kap-07B: amph+plag). A different outcrop supplied a sample of mafic gneiss with thin (< 1 cm) quartzofeldspathic leucosome (13-Kap-08A and $08A_{pure}$, the latter with all visible leucosome cut away) and a sample of leucosome (13-Kap-08C) that contains peritectic minerals implying local derivation. The pegmatite as well as the leucosome contain zircons of quite variable grain size, ranging from about 50 µm to over 500 µm, and were subdivided into a large grain and a small grain fraction.

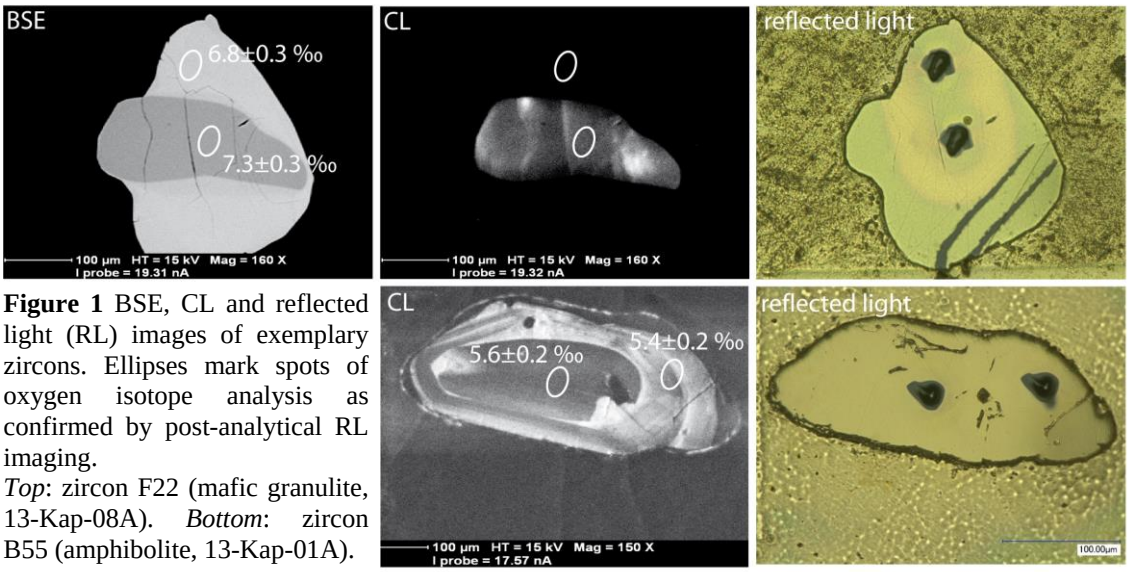

Figure 1 BSE, CL and reflected light (RL) images of exemplary zircons. Ellipses mark spots of oxygen isotope analysis as confirmed by post-analytical RL imaging.
Top: zircon F22 (mafic granulite, 13-Kap-08A). *Bottom*: zircon B55 (amphibolite, 13-Kap-01A).

Results and comparison with regional detrital data

Despite zonation patterns observed in BSE and/or CL imaging, revealing cores with one or two overgrowths (Figure 1), the $\delta^{18}O$ values of cores and rims are indistinguishable within samples (Figure 2a-d). Amphibolite facies mafic gneisses 13-Kap-01A and -01B show very uniform values of 5.7 ± 0.2 ‰ and 6.0 ± 0.3 ‰, respectively, both in cores and rims (Fig. 2a). These values are close to those from mantle-derived melts and overlap with values for igneous zircons from the upper crust of the Superior province (~5.7 ± 0.6 ‰, [1]). They also overlap with the lower end of the range of detrital cores in zircons from a Kapuskasing paragneiss nearby (< 10 km, $\delta^{18}O_{cores}$ 5.1 – 7.1 ‰, [2]).

Granulite facies gneisses 13-Kap-07B and -08A have values of 7.5 ± 0.5 ‰ and 7.2 ± 0.3‰, respectively. These elevated values overlap or are slightly higher than the upper end of the range of detrital cores, but are significantly lower than any metamorphic overgrowth in the paragneiss zircons [8.4 – 10.4 ‰, [2]). Whether these slightly heavier values are a primary feature of the host rock (i.e. incorporation of sedimentary rock in the magma forming the basaltic protolith) or a result of metamorphic fluids is currently unknown – upcoming U-Pb dating and trace element analyses on the Kapuskasing samples might help to answer this open question.

The large leucosome zircons (150–500 µm) of 13-Kap-08C have the same values (7.2 ± 0.3 ‰) for cores and one (sometimes two) overgrowths (Fig. 2c) and are identical to those of the hosting mafic granulite. The small leucosome-hosted grains (< 150 µm) show much greater variability in $\delta^{18}O$ (mainly 6.1 – 9 ‰, two grains above 9 ‰), but cores and rims are still indistinguishable (Fig 2d).

The large pegmatite grains are variable, with values of 5.1 – 8.5 ‰ they cover almost the entire spectrum of mafic and leucosome hosted zircons. Notably, they are the only population to show a difference between core and rim analyses, the range for the rims being smaller (5.1 – 6.8 ‰). Rims (as observed in BSE/CL) are usually lower than the core of the same grain. The smaller pegmatite grains range from as low as - 4.1 ‰ to 5.3 ‰ and therefore overlap with the lower end of the large grain spectrum. The negative values only found in this population could reflect a higher vulnerability of small grains to be affected by the fluid-rich pegmatitic melt.

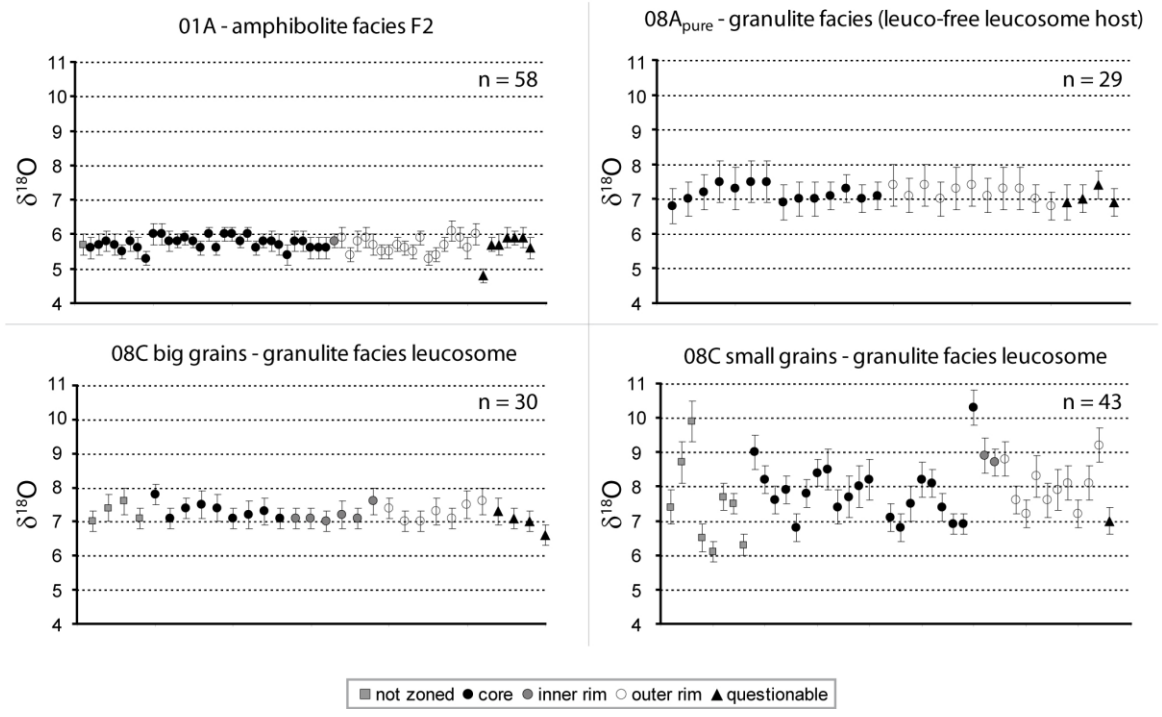

Figure 2. Examples of variation of O isotope compositions within individual samples. Note similarity of of $\delta^{18}O$ values for cores and rims within most samples. Uncertainties indicated in figures are at 2σ, whereas values for entire samples as mentioned in text are the mean of all zircon analyses of a sample with one standard deviation of the mean used as uncertainty.

References

[1] King et al. (1998) Precambrian Research **92**, 365–387; [2] Moser et al. (2008) Geology **36**, 239–242

Distinguishing between sediment melting and crustal assimilation in the Lesser Antilles using Molybdenum

H. Freymuth[1], T. Elliott[1], S. Skora[2] & J. Blundy[1]

[1]School of Earth Sciences, University of Bristol, Bristol BS8 1RJ, UK
[2]Institute of Geochemistry and Petrology, ETH Zürich, 8092 Zürich, Switzerland

The aim of this study was to examine the partitioning of molybdenum (Mo) and the rare earth element neodymium (Nd) into melts and residual crystals, respectively, during melting of black shales under pressure and temperature conditions relevant for subduction zones. We are currently exploring the transport of Mo from subducted slabs into arc magma sources in subduction zones. Our data for Mo concentrations and Mo isotope ratios in the Mariana arc indicate that Mo enrichment in the arc lavas and Mo istotope ratios are sensitive tracers of fluids derived from the subducted oceanic crust. Molybdenum does not appear to be mobilized in significant quantities during sediment melting beneath the Mariana arc.

The case is apparently different for the Lesser Antilles arc where a sequence of black shales is subducting. The black shales have exceptionally high concentrations of Mo and heavy Mo isotope ratios. We found Mo isotope ratios in Lesser Antilles arc magmas that are consistent with a derivation from black shales. This is an important observation because it can potentially be used to distinguish between generation of 'crustal' isotope signatures in the Lesser Antilles arc magmas via assimilation during the magma's ascent or addition of subducted sediment melts to the mantle wedge, respectively. These two end-member scenarios are hotly debated in the literature (e.g. [1,2]).

In order to establish whether Mo is mobilized during melting of black shales, and thus to test the models outlined above, we conducted melting experiments on black shales at 800-900°C (Fig. 1). We used two different starting compositions that reflect the potential variability in the FeS_2 content of the black shales. Molybdenum and Nd are similar in their degree of incompatibility during mantle melting and are thus not fractionated during partial mantle melting and magma differentiation. Their ratio is therefore highly diagnostic for addition of components derived from the subducted slab. In addition to Mo and Nd we measured concentrations of a small set of other trace elements commonly used in the interpreation of magma sources (Ba, La, Ce, Sm, Dy, Hf, Sr, Y, Zr, Nb, Th and U) in the experimentally-derived melts at the NERC Ion Microprobe Facility.

Figure 1: Example of a black shale melting experiment performed at 850°C consisting of approximately 50 % melt (dark area in thetop half of the experimental charge).

Results show approximate partition coefficients for Mo of $Kd_{min/melt}$ = 4 for an FeS_2 rich starting material and $Kd_{min/melt}$ = 0.5 for an FeS_2 poor starting material. Thus, while the amount of Mo partitioning into the melt is strongly dependent on the composition of the black shales, the data show that even in high FeS_2 compositions (with residual sulfides) a substantial fraction of Mo will be mobilized in black shale melts.

The data also indicate high partition coefficients for Nd on the order of $Kd_{min/melt}$ = 10-50 which we interpret to reflect Nd retention in residual epidote. We originally predicted the black shale melts to have high Nd/Mo ratios, because the Lesser Antilles arc lavas for which Mo isotope ratios indicated the largest contribution of black shale melts tend to have high Nd/Mo (Fig. 2a). However, the trace

element partitioning data for black shale melts do not support such a model. Our results predict significant Mo transport from the sediment but a sediment component with even lower Nd/Mo than the starting sediment. Thus we have significantly modified our model for the processes leading to Mo enrichment in the Lesser Antilles arc magmas.

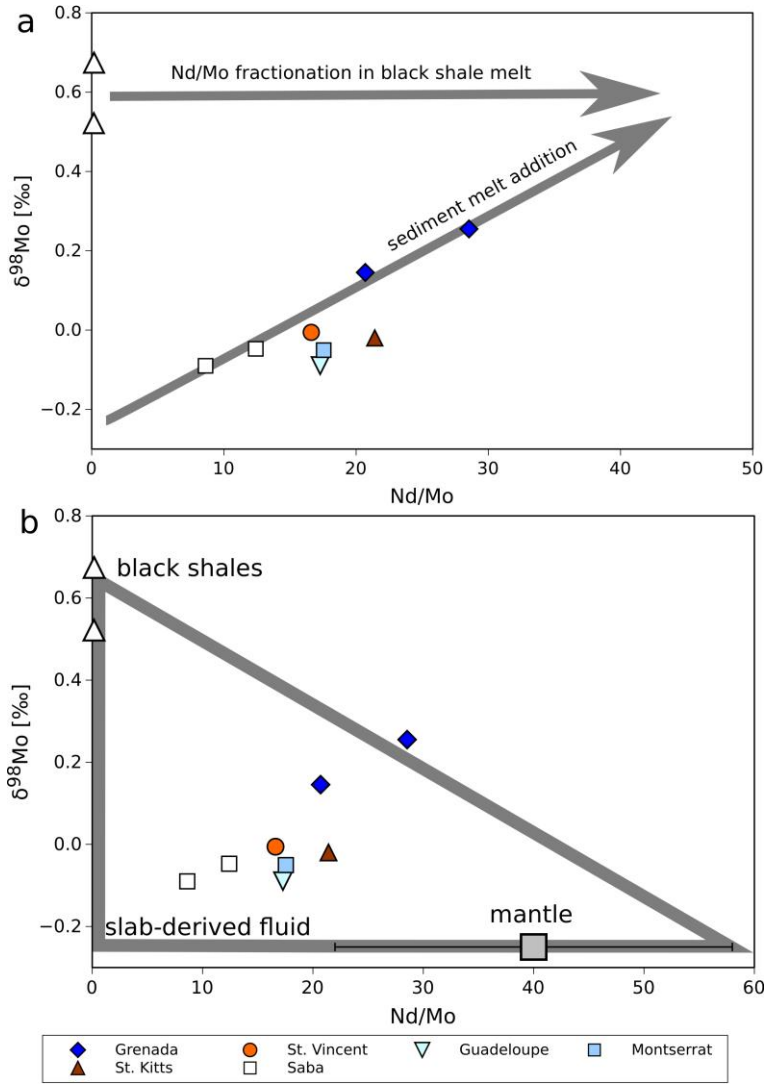

Figure 2: Mo isotope ratios vs. Nd/Mo of Lesser Antilles arc lavas and black shales from ODP site 144. a) in our initial model we interpreted the Mo budget of the Lesser Antilles arc lavas to be dominated by slab derived fluids and high Nd/Mo melt of black shales. b) in our current model we envisage a larger contribution of the sub-arc mantle to the Mo budget of the Lesser Antilles arc lavas.

Our revised interpretation of the Mo systematics in the Lesser Antilles arc lavas is illustrated in Fig. 2b. Heavy Mo isotope ratios indicate the largest fraction of black shale melts in lavas from Granada. In addition to the black shale melts we now envisage a larger contribution of the sub-arc mantle to the Mo budget of the Lesser Antilles arc lavas in order to explain the high Nd/Mo ratios of the Granada samples compared to the other islands. There are thus three major sources for Mo in the Lesser Antilles arc: the sub-arc mantle, slab-derived fluids, and subducted black shales. These form a mixing triangle in Fig. 2b. We are in the process of further refining our model but the critical constraint – the observed partitioning of Mo into the black shale melts – supports our prediction that Mo isotope ratios trace a component derived from black shale melts in the manle source of the Lesser Antilles arc lavas.

References:

[1] Carpentier et al. (2008) Earth and Planetary Science Letters **272**, 199 – 211

U-Pb dating of deep-crustal xenoliths in a Tertiary dyke on Mull

G. Fitton[1] & R. Gooday[1]

[1]School of GeoSciences, University of Edinburgh, Edinburgh EH9 3FE, UK

Background

A remarkable assemblage of xenoliths has been discovered in a Tertiary tholeiitic dyke south of Grass Point on the SE coast of Mull. These comprise anorthosites, gabbros and quartzo-feldspathic metasediments. The occurrence of deep-crustal xenoliths in a Tertiary tholeiitic dyke is unique in the UK, although similar xenoliths have been reported from Permo-Carboniferous alkaline dykes in Mull [1]. The xenoliths formed the subject of an MEarthSci project carried out by Robert Gooday, who studied the mineral composition of the xenoliths and the chemical composition of the xenoliths and their host rock. He showed that the dyke almost certainly originated in the Tertiary central complex and must therefore have propagated south-eastwards across the Great Glen Fault (GGF), which cuts the south-east part of Mull 4 km to the north-west of Grass Point. A source for the xenoliths within the GGF could account for their presence in a dyke whose magma evolved in a shallow magma reservoir. If the xenoliths originated in the fault melange then they would represent the deep crust across a large area of Scotland. The quartzo-feldspathic xenoliths contain zircon crystals and an application for one day of ion-probe time was submitted in order to date these zircons.

Results

Zircon ages were obtained on several *in situ* grains in polished thin sections and also in separated grains. The results are shown below.

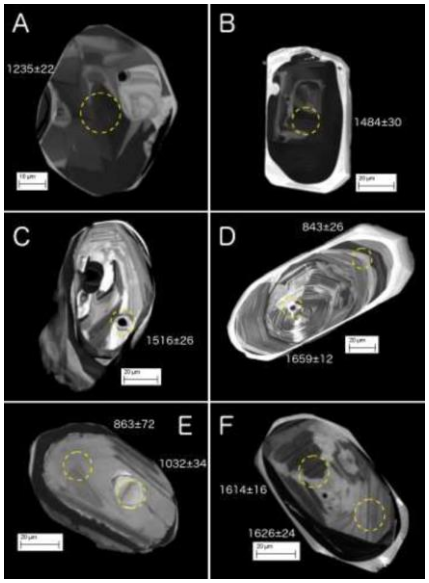

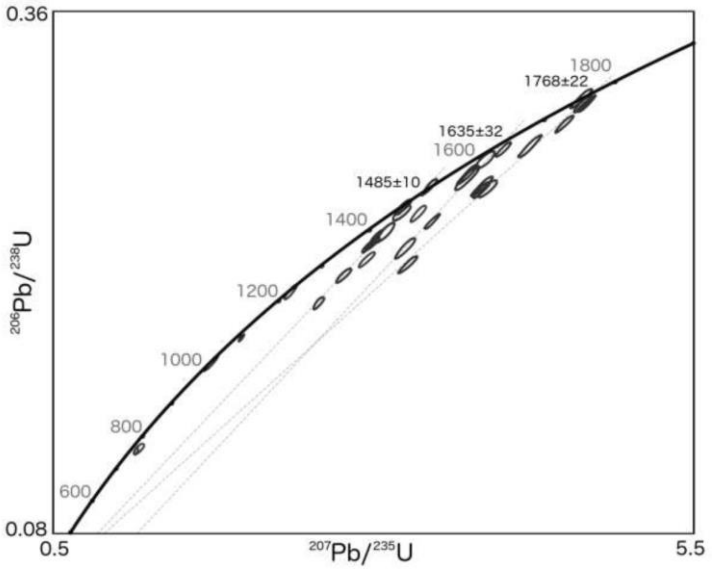

The detrital zircon population shows age peaks identical to those from the Morar gneisses in Ardnamurchan [2,3]. The Laxfordian granites may have supplied a large number of detrital zircons to the sandstone protolith of the Morar Group, as could orogenic belts in both Laurentia and Baltica. There is no evidence that any of the xenoliths originated in the Dalradian basement that underlies the SE part of Mull.

References

[1] B.G.J. Upton, P. Aspen, D.C. Rex, F. Melcher & P. Kinny (1998). J. Geol. Soc. Lond. **155**, 813–828.
[2] C.L. Kirkland, R.A. Strachan & A.R. Prave (2008). Precambrian Research, **163**, 332-350.
[3] K.M. Goodenough, Q.G. Crowley, M. Krabbendam & S.F. Parry (2013). Precambrian Research, **233**, 1-19.

(PAGE INTENTIONALLY LEFT BLANK)

The influence of hydrothermally altered crust on boron and oxygen isotope systematics in melt inclusions from the Askja volcanic system, North Iceland

M. Hartley[1,2]

[1]Department of Earth Sciences, University of Cambridge, Cambridge B2 3EQ
[2]School of Earth, Environmental and Atmospheric Sciences, University of Manchester, Manchester M13 9PL

Objectives

The aim of this project was to determine the origin of low $\delta^{18}O$ values in olivine- and plagioclase-hosted melt inclusions and glasses from a series of eruptions on the Askja volcanic system, and the c. AD 1860 Holuhrauun fissure lava (which was previously linked to the 1875-76 volcano-tectonic episode on the Askja volcanic system). Trace element abundances and ratios in these melt inclusions preclude the possibility that the observed O-isotopic variability (+2.1‰ to +5.2‰) is the result mixing with andesitic or rhyolitic contaminants in the crust [1]. If ascending primary magmas with mantle-like $\delta^{18}O$ mix with variable amounts of hydrated, low-$\delta^{18}O$ basaltic magma bodies in the upper crust, the melt inclusions could acquire low $\delta^{18}O$ signatures with minimal modification to the magma's bulk composition. Alternatively, the melt inclusions may reflect a low-$\delta^{18}O$ component in the mantle.

Boron isotopic ratios in Icelandic basalts can be used to determine the extent to which a melt has been contaminated by low-$\delta^{11}B$, hydrothermally altered crustal material. In this project I analysed CO_2, H_2O and light element concentrations (B, Li, F, Cl), and boron isotopes, in melt inclusions and glasses from Askja and Holuhraun, to determine the extent of interaction with hydrothermally altered crust, and the likely depth of any such interactions.

Results

Boron correlates positively with incompatible minor and trace elements (K_2O, Ce). Boron concentrations and boron isotopic ratios in the melt inclusions are negatively correlated (Fig. 1). A similar relationship found in melt inclusions from Laki [2] was interpreted as a signature of assimilation of hydrothermally altered crustal minerals.

Melt inclusion trapping pressures, calculated using the VolatileCalc CO_2-H_2O solubility model, indicate that most inclusions were trapped in the shallow crust at pressures between 1 and 2 kbar. These pressures are likely to provide only a minimum entrapment pressure, since the inclusions may have been trapped during the crystallisation of vapour-undersaturated melts. However the calculated pressures are consistent with models of hydrothermal circulation in the Icelandic upper crust.

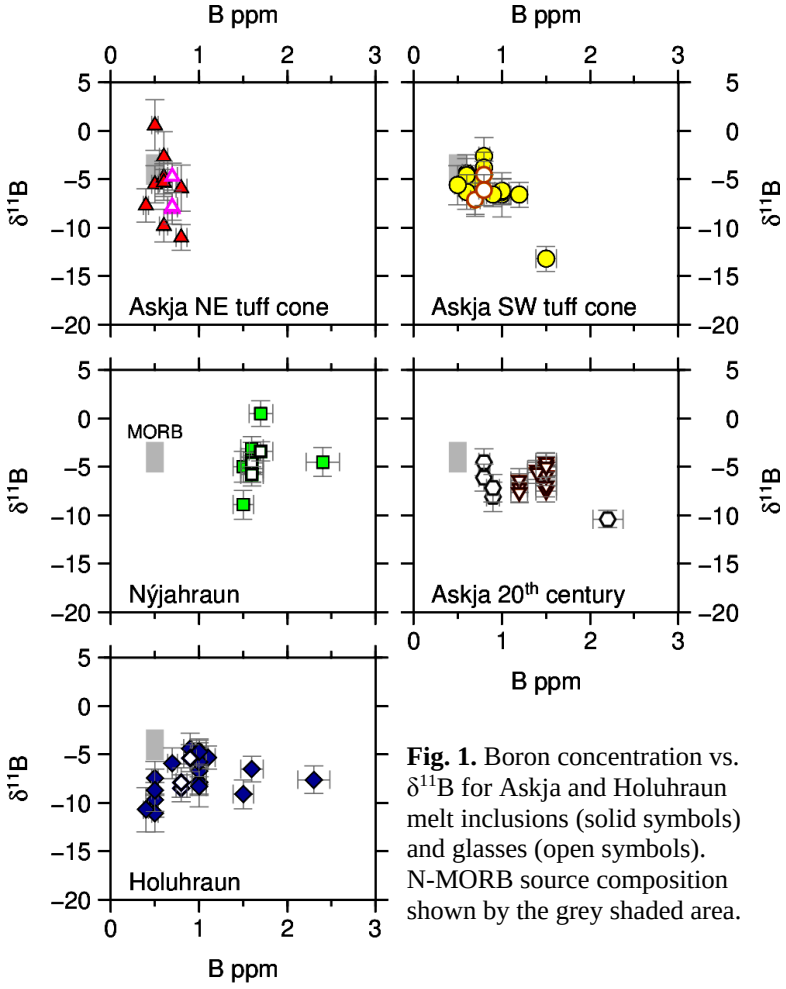

Fig. 1. Boron concentration vs. $\delta^{11}B$ for Askja and Holuhraun melt inclusions (solid symbols) and glasses (open symbols). N-MORB source composition shown by the grey shaded area.

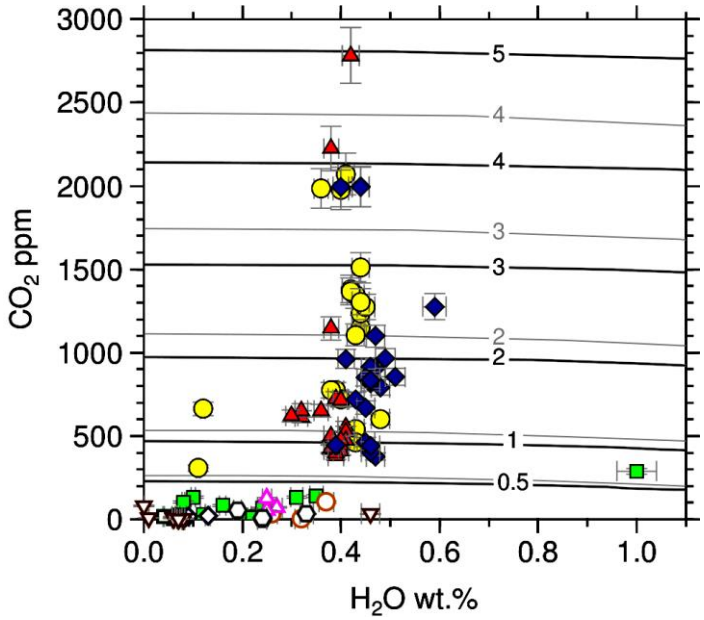

Fig. 2. CO_2 and H_2O concentrations for Askja melt inclusions and glasses (same symbols as Fig. 1). Black lines show isobars calculated using VolatileCalc; grey lines are isobars calculated using SolEx.

There appears to be little systematic variability between oxygen and boron isotopic ratios for the Askja melt inclusions and glasses (Fig. 3). However, Holuhraun melt inclusions do show a robust negative correlation between $\delta^{18}O$ and $\delta^{11}B$. This may reflect an assimilation-fractional crystallisation (AFC) trend between high $\delta^{18}O$, low $\delta^{11}B$ primary melts and hydrothermally altered crust with low $\delta^{18}O$ and high $\delta^{11}B$.

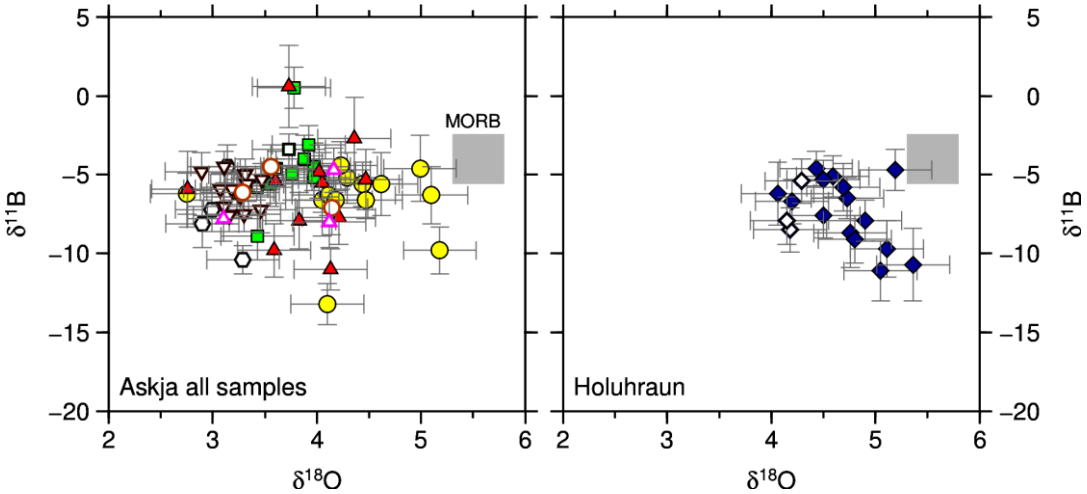

Fig. 3. Oxygen and boron isotopic variation in Askja and Holuhraun melt inclusions (solid symbols) and glasses (open symbols). N-MORB source composition shown by the grey shaded area.

Further work

The relationship between $\delta^{18}O$ and $\delta^{11}B$ and melt inclusion trapping pressure needs to be investigated further, particularly for the Askja melt inclusions. AFC and mixing trends between the Askja and Holuhraun parental melts and suitable contaminant compositions will be calculated to assess the contribution of hydrothermally altered material to the isotopic signatures of Askja and Holuhraun magmas.

References

[1] M.E. Hartley et al. (2012) Geochim. Cosmochim. Acta **123**, 55-73.
[2] M. Brounce et al. (2012) Geochim. Cosmochim. Acta **94**, 164-180.

Intra-spicule silicon isotope variation in deep sea sponges

K.R. Hendry

School of Earth Sciences, University of Bristol, Bristol BS8 1RJ, UK

Background

($Si(OH)_4$) provide insight into the operation of the global marine silicon cycle and the role played by the oceans in nutrient supply and carbon drawdown, both in the modern and in the past. Silicon isotope (denoted by $\delta^{30}Si$) studies of diatoms have provided insight into the history of silica production in surface waters [1], while the analysis of spicules from deep sea sponges has defined both the spatial and the temporal variability of silicic acid concentrations in the water column.

Sponges are simple filter feeding benthic animals, without tissue grade of organisation. Skeletal support is provided by spicules, formed in many sponges by amorphous silica or opal. Sponge spicule $\delta^{30}Si$, which has a greater range and is isotopically light compared to diatoms, shows a relationship between fractionation factor (under equilibrium conditions $\varepsilon \sim \Delta^{30}Si$, ranging from -1 to -5 ‰, where $\Delta^{30}Si$ is the difference in $\delta^{30}Si$ between seawater and the sponge spicules) and $Si(OH)_4$ [2,3]. The lack of an apparent relationship between $\delta^{30}Si$ in spicules and species or temperature, pH, salinity, etc., suggests that spicules, from different ocean basins, may provide a robust proxy for past bottom water $Si(OH)_4$ concentrations [3]. The non-linear relationship between $\Delta^{30}Si$ and $Si(OH)_4$ concentration is likely a result of a uptake rate effect, whereby fractionation involved with uptake processes also becomes enhanced as Si uptake rates increase with concentration, suggesting that spicule $\delta^{30}Si$ may also be used as an indicator of growth conditions in modern sponges.

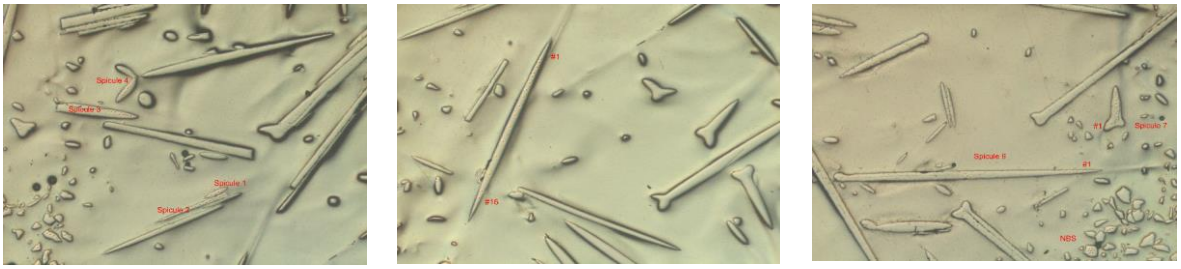

Figure 1. Light microscope images of the spicules mounted for ion microprobe analysis

Aim

The existing modern calibration studies have relied on bulk analyses of many spicules, and the possibility of variations within and between spicules has not been explored. The aim of this project is to establish whether variations in the $\delta^{30}Si$ composition of individual spicules can be detected by ion microprobe.

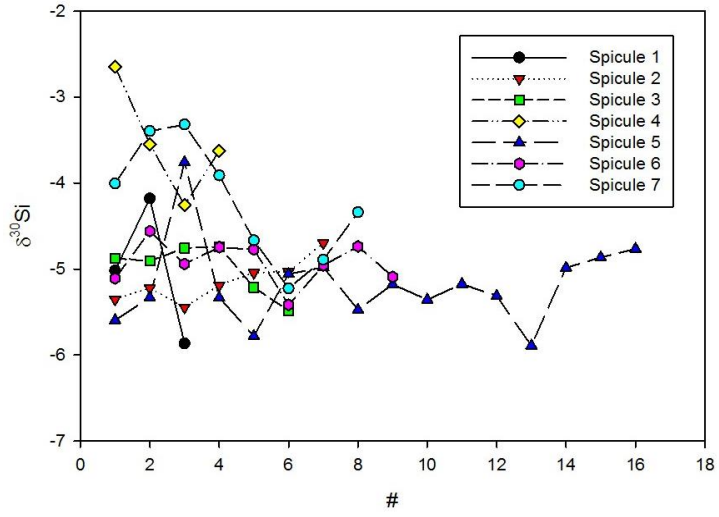

Figure 2. Results of the spicule analyses, with silicon isotopes reported relative to standard NBS28.

Methods

To do this, spicules from a sponge specimen collected in the Southern Ocean on Nathaniel B Palmer cruise NBP0805 (specimen TO3-100) was mounted with NBS28 reference standard and analysed by ion microprobe. Scanning Electron Microscope images showed that this specimen has sufficiently robust spicules for such analysis. This specimen has already been analysed for $\delta^{30}Si$ using two different methods in two different laboratories [4], and this bulk measurement was compared to the ion microprobe results.

Results

Seven spicules from TO3-100 were analysed (Figures 1) and showed significant variability in $\delta^{30}Si$ (-2.5 to -6 ‰, Figure 2). However, there was also a significant offset between ion microprobe spicule $\delta^{30}Si$ and bulk $\delta^{30}Si$ values (-3.06 ‰, [2]). Elemental analysis indicated high levels water within the spicule structure and variable trace metal content (Figure 3), which could be responsible for the variability and the offset. Further work would be required to develop suitable bracketing standards – with variable water content - for future analysis.

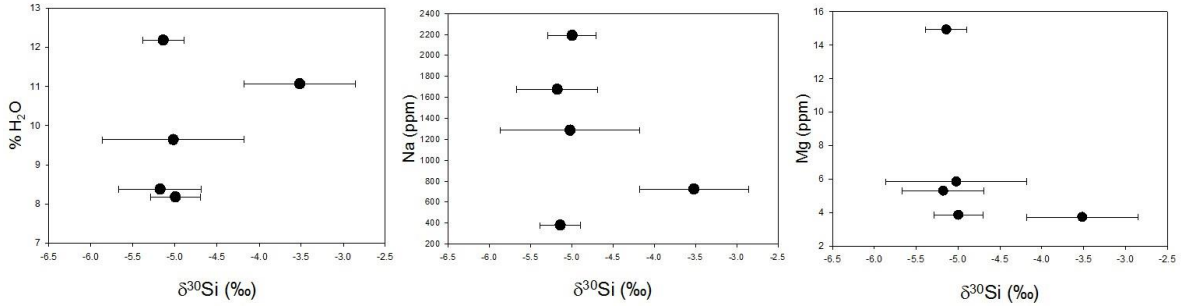

Figure 3. Trace metal results for five spicules, plotted against mean $\delta^{30}Si$ (error bars 1SD)

References

[1] De La Rocha, C., et al. (1997) Geochim. Cosmochim. Acta **61**, 5051-5056.
[2] Hendry, K. R., et al. (2010) Earth Planet. Sci. Lett. **292**, 290-300.
[3] Hendry, K. R., Robinson, L. F. (2012) Geochim. Cosmochim. Acta **81**, 1-12.
[4] Hendry, K. R., et al. (2011) Antarctic Science **23**, 34-42.

Temporal variations in the influence of the subducting slab on Central Andean arc magmas: Evidence from boron isotope systematics

R.E. Jones

Department of Earth Sciences, University of Oxford, OX1 3AN

Abstract

The Pampean flat-slab segment in the southern Central Andes represents an ideal setting at which to investigate how changes in the tectonic configuration of a subduction zone affects the recycling of subducted components to arc magmas. To constrain sources, particularly of slab-derived fluids and their contribution to arc magmatism, boron isotope and select major and trace element compositions were determined for pyroxene- and zircon-hosted melt inclusions obtained from a suite of Palaeocene to Miocene arc magmatic rocks, from the southern Central Andes.

Considerable changes in $\delta^{11}B$ values and boron concentrations are observed with time. Significantly lower $\delta^{11}B$ values (average = −1.9±2.2‰ (1σ)) were obtained for melt inclusions from Oligocene arc rocks (~24 Ma) compared to those from the Palaeocene (~61 Ma) (averages = +1.6±0.8‰ and 17.8±1.4 (1σ), respectively) and the Miocene (~18 Ma) (averages = +4.7±1.9‰ and 11.9±5.5 (1σ), respectively).

Boron isotope analysis

Boron isotope analyses were conducted on 70 glassy and re-homogenised melt inclusions and selected host phenocrysts, using the Cameca ims 1270 secondary ion mass spectrometer (SIMS) at the NERC Edinburgh Ion Microprobe Facility (EIMF), University of Edinburgh.

Positive secondary ions of $^{10}B^+$ and $^{11}B^+$ were produced by sputtering the sample with a 5nA, $^{16}O_2^-$ primary beam with a net impact energy of 22keV, focused using Kohler illumination to a ~25µm spot size. The secondary ions were analysed using a mass resolution (ΔM) of ~2400 (sufficient to resolve mass interferences of $^9Be^1H^+$ (ΔM = 1400) and $^{10}B^1H^+$ (ΔM = 900)) using a 100 eV energy window, a 400 µm contrast aperture and a field aperture suitable for the beam diameter. The beam was manually centred by adjusting lens 4, X/Y deflectors before each analysis. Prior to each analysis the samples were pre-sputtered for 30 seconds to remove surface contamination. B isotope ratios were measured for 60 cycles, with each cycle consisting of 8 seconds of counting on $^{10}B^+$, 3 seconds counting on $^{11}B^+$ and 1 second counting on $^{28}Si^{2+}$. Ion counts were measured using a single electron multiplier (AF133H) in magnetic peak switching mode. Counts were dead time corrected using a value of 51 ns.

In order to correct for instrumental mass fractionation (IMF) the boron isotope ratios of the melt inclusions and host phenocrysts were determined relative to the reference material GSD-1G (10.1 $‰_{NIST951}$ ±1.0 (2σ) [1]), which was analysed throughout the analytical session. Boron isotope ratios are expressed in the conventional $\delta^{11}B$ (‰) notation relative to the reference material NIST SRM 951, and calculated using the following equation:

$$\delta^{11}B_{(sample)} = ((\delta^{11}B_{(GSD\text{-}1G\ literature)} + 1000) \times (^{11}B/^{10}B_{(sample\ measured)} / {}^{11}B/^{10}B_{(GSD\text{-}1G\ measured)})) - 1000$$

Where $^{11}B/^{10}B_{(GSD\text{-}1G\ measured)}$ is the average $^{11}B/^{10}B$ ratio of GSD-1G measured during the same analytical session. Analyses of 3-5 unknowns were bracketed by 2-3 analyses of standard GSD-1G. It is well documented that the ion yields obtained during SIMS analysis can be affected by the chemical and structural matrices of the sample (e.g., [2] [3] [4]). However, it has been shown that boron isotope determinations of basaltic to rhyolitic glasses by SIMS are not significantly affected by these matrix effects (e.g., [5] [6]). The analysis of readily available glass standards with an SiO_2 contents ranging between 46.1 and 63.7 wt.%, which are routinely analysed at the Edinburgh Ion Microprobe Facility, show no apparent matrix-dependent fractionations at the precision of the analysis (Fig. 1).

An average deviation of +0.9 ±1.6‰ (2σ) was obtained for basaltic glass GSD-1G (relative to StHs6/80) from the published value of 10.1 ±1.0 $‰_{NIST951}$ [1]; an average deviation of -0.3 ±1.8‰ (2σ) was obtained for komatiite glass GOR128-G (relative to StHs6/80) from the published value of +13.6 ±0.2 $‰_{NIST951}$ [7]. The analysis of these additional glass standards, with SiO_2 contents both lower and higher than GSD-1G, confirms the findings of other studies that matrix-dependent fractionations are minor for basaltic to rhyolitic glasses ([5] [6]) and that the accuracy of the presented $\delta^{11}B$ values is <±1.0‰.

Data correction

During SIMS analysis the count rate of isotopes varies during the sputtering process. A correction was made for the varying count rates with time using a linear interpolation approach [8].

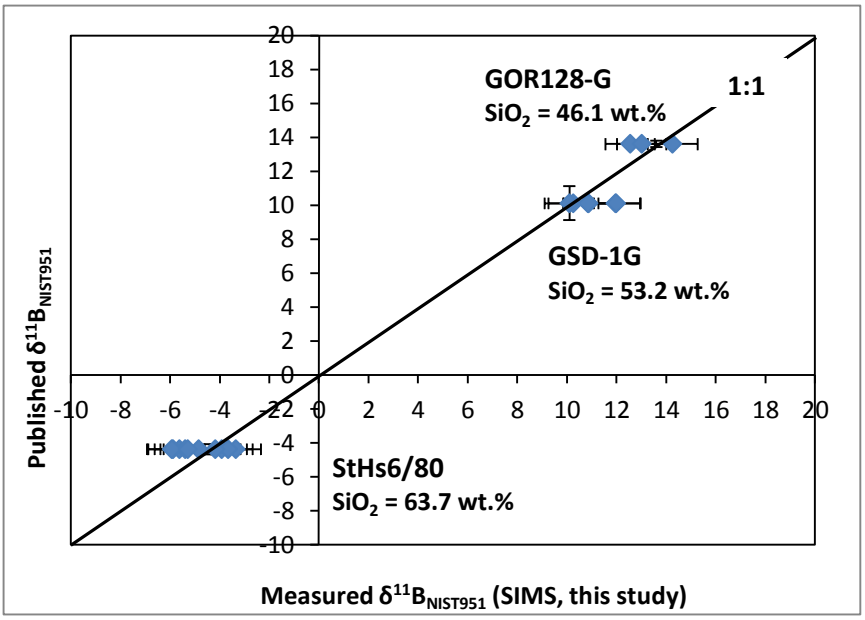

Figure 1. Comparison of $\delta^{11}B$ values measured by SIMS versus published values for glass standards GSD-1G (basaltic glass, $\delta^{11}B$ = +10.1 ±1.0 ‰$_{NIST951}$ [1], GOR128-G (komatiite glass, $\delta^{11}B$ = +13.6 ±0.2 ‰$_{NIST951}$ [7], and StHs6/80 (dacitic glass, $\delta^{11}B$ = -4.4 ±0.3 ‰$_{NIST951}$ [5]. The errors on the measured and published $\delta^{11}B$ values are at the 2σ level.

Data processing

A total of 16 boron isotope analyses of melt inclusions were ruled out due to low or variable boron count rates, or analytical issues (e.g., loss of primary beam). Individual analysis cycles which produced $^{11}B/^{10}B$ which were greater than 4σ away from the average $^{11}B/^{10}B$ (spikes) were rejected and an average was taken of the count rates before and after. This data processing was applied to only 20 analyses out of 189 in total.

A total of 70 successful boron isotope analyses were made on melt inclusions (55 hosted in pyroxene and 15 hosted in zircon), from 8 samples. The internal precision of individual standard analyses, based on the standard error of the mean, ranged from 0.55 – 0.68 ‰ (1σ). The internal precision of the unknowns is dependent on boron content (i.e., count rate) and ranged from 0.29 – 1.33 ‰ (1σ) for melt inclusion analyses. The external precision of the analyses is estimated from the external reproducibility of the standard GSD-1G, and is typically 0.23‰ (n=13) (quoted as the standard error of the mean at the 1σ level).

The uncertainties quoted on the individual unknowns are propagated analytical uncertainties, which take into account both the uncertainty on the individual analysis (internal precision) and the reproducibility of the standard in each analytical session (external precision). The analytical uncertainty (A.U.) on the individual unknowns are quoted at the 2σ level and calculated using the following equation:

$$A.U. = \sqrt{\left(\frac{SEM_{(GSD-1G\ measurements)}}{\overline{x}^{11}B/^{10}B_{(GSD-1G\ measurements)}}\right)^2 + \left(\frac{SEM_{(sample\ measurement)}}{^{11}B/^{10}B_{(sample\ measurement)}}\right)^2}$$

where SEM represents the standard error of the mean, GSD-1G measurements represents the $^{11}B/^{10}B$ ratio of GSD-1G measured during the same analytical session.

References:

[1] Jochum, K.P., et al. (2011). Geostandards and Geoanalytical Research **35**, 193-226.
[2] Deline, V.R., et al. (1978). Applied Physics Letters **33**, 832-835.
[3] Eiler, J.M., et al. (1997). **138**, 221-244.
[4] Shimizu, N., Hart, S., (1982). Journal of Applied Physics **53**, 1303-1311.
[5] Chaussidon, M., et al. (1997). Geostandards Newsletter **21**, 7-17.
[6] Rosner, M., et al. (2008). Geostandards and Geoanalytical Research **32**, 27-38.
[7] Rosner, M., Meixner, A., (2004). Geostandards and Geoanalytical Research **28,** 431-441.
[8] Coakley, K.J., et al. (2005). International Journal of Mass Spectrometry **240**, 107-120.

Rare earth element variability in coloured fluorite from the Pennine ore fields – the role of fluid migration

L. Kirstein, G. Fitton & C. Herron

School of GeoSciences, University of Edinburgh, Edinburgh EH9 3FE, UK

Fluorite, rare-earth elements and colour

Fluorite is a common gangue mineral in Pb and Zn ore deposits as well as being an important source of fluorine for industrial processing. Fluorite-quartz-galena mineralisation occurs throughout the North Pennine orefield. Mineralisation occurs in fracture veins and in metasomatised strat bound flats (Smith, 1974). The associated fluorite occurs in a wide range of colours (purple, green, yellow, colourless) that may be related to fluid-rock interaction during transport. Trace elements and specifically rare earth elements in fluorite can provide information on the source of the transporting fluids, in addition to the environment of ore formation. REE may also be the cause of the colour variability of fluorite. Understanding how trace element concentrations vary across zoned phenocrysts of different coloured fluorite from the same region, should indicate whether variations in the composition of the hydrothermal fluid occurred during growth and whether there is a link to fluorite colour.

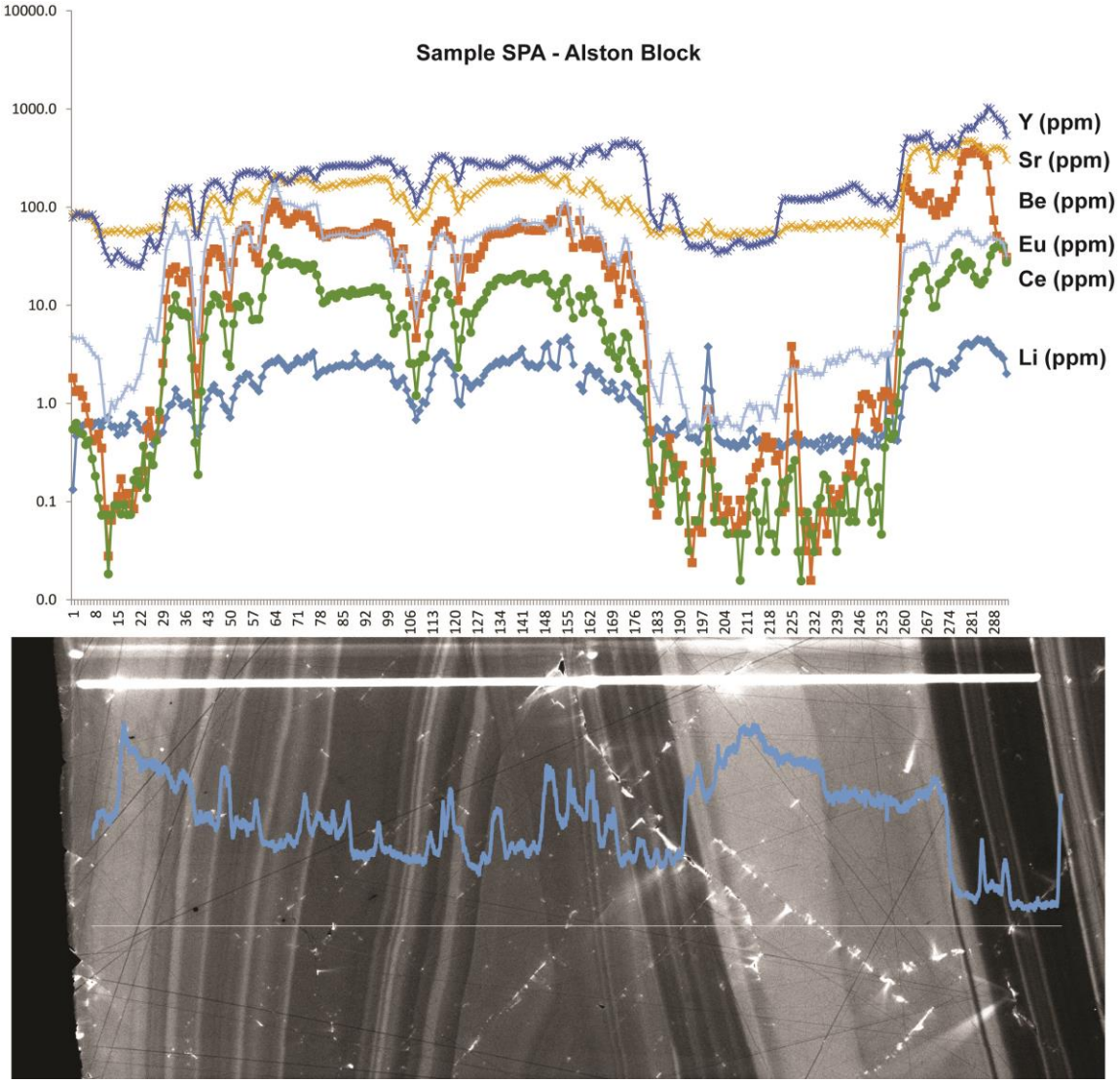

Figure 1. SIMS step scan across zoned, colourless fluorite crystal for selected trace elements. Note the steps in the Y and Eu data consistently mirror the cathodoluminescence image greyscale analysis (inset blue line on photo) of the scanned section. White line on photo is area scanned during data acquisition.

During a one day scoping study we documented the trace element variability across three fluorite samples of different colour from the Alston Block, northern Pennines including a purple fluorite (BP-W), a green fluorite (BC-G) and a colourless fluorite (SP-A). This allowed us to investigate (i) the relationship between CL zoning and elemental concentration; and (ii) potential change in fluid chemistry during crystal growth.

Two types of data were collected spot data and continuous scan data. The spot data focussed on the full spectrum of rare earth elements as well as Be, Sr, Y, Ba. The scan data were focussed on a smaller subset of trace elements specifically Li, Be, Sr, Y, Ce and Eu. The data confirmed that the colourless fluorite has the lowest concentrations of trace elements compared to the green and purple fluorite. In addition there is a clear correlation between CL greyscale intensity and elemental concentration with lighter, more luminescent regions correlating with low concentrations of all elements scanned (Figure 1). Eu and Y concentrations appear to be more sensitive to luminescence even at low concentrations (Figure 1).

Within the zoned colourless fluorite there is large trace element variability for example Sr varies from 51 (bright region) to 207 ppm (dark region) and Y from 25 (bright) to 1039 ppm (dark). Sr and Li co-vary and are not as variable as Be, Eu, Ce and Y. All samples have positive Eu anomalies. The most luminescent zones are LREE depleted, HREE enriched.

Simple bivariate plots particularly of Ce versus Eu indicates the composition of the different coloured fluorites are substantially different and that at least during the formation of the colourless fluorites that the composition of the fluorite changed substantially and indicates a change to a potentially more oxidising environment.

References

[1] Smith F.W. (1974) Transactions of the Institution of Mining and Metallurgy **25**, 95-96.

Trace element compositions of zoned dolomite cements in reservoir rocks from the naturally leaking Green River CO_2 accumulation

A. Maskell[1], M. J. Bickle[1], N. Kampman[2] & A. Busch[2]

[1]Department of Earth Sciences, University of Cambridge, Cambridge, CB2 3EQ, UK
[2]Shell Global Solutions International, Kessler Park 1, 2288 GS Rijswijk, The Netherlands

Understanding the geochemical behaviour of anthropogenic carbon dioxide stored in geological reservoirs, over a range of time-scales, is crucial for understanding the fate of the stored CO_2 through the life of an individual storage site and thus quantifying the risk of leakage. Reactions between CO_2-charged brines and reservoir minerals might either enhance the long-term storage of CO_2 in geological reservoirs or facilitate leakage by corroding caprocks and fault seals. Investigation of natural accumulations of CO_2 will provide insight into the long-term consequences of CO_2 exposure on geological materials that are typical of those proposed as geological repositories for anthropogenic CO_2.

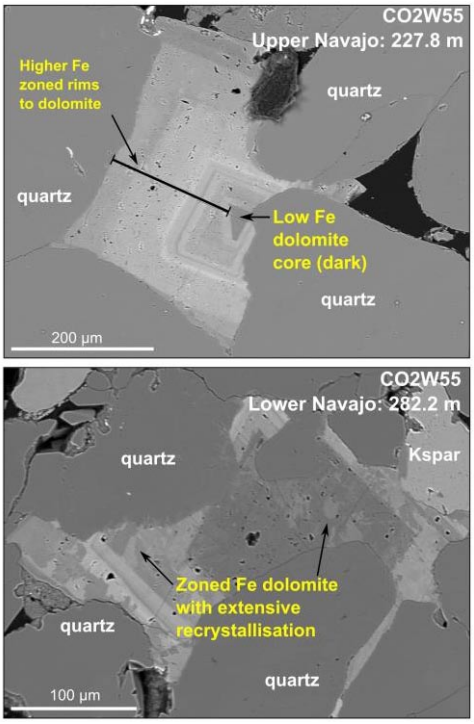

Figure 1. Backscatter images of representative carbonates that were analysed in this study.

To understand and quantify CO_2 promoted fluid-mineral reactions and their reaction kinetics within a CO_2 reservoir, a number of geochemical and petrophysical properties must be accurately determined. This project aimed to do this by characterising reservoir cements in a leaking natural CO_2-charged reservoir near Green River, Utah. The coarse Fe-dolomite cements in the reservoir rocks exhibit spectacular zoning and high-resolution analyses of these zones have enabled a more detailed interpretation of their formation environment and fluids. Backscatter electron images of the zoned carbonates are shown in Figure 1.
Using the trace element data collected in this study we aim to investigate whether the:

1) Zoned Fe-bearing dolomite cements are the result of CO_2-charged fluid–rock interactions (Fe is derived from the dissolution of haematite).
2) Zoning relates to the episodic recharging of the reservoir by CO_2 documented by the U-Th dated travertines sampled at surface.

Initial results

The early, Fe-poor cores of the dolomites show a variable enrichment in Sr and a high La/Ce ratio, as Fe concentrations increase in the concentric zones both Sr and La/Ce values decrease (Figure 2). Ba, which is enriched in the modern day reservoir fluid, has a low concentration in the carbonate cements with what appears to be a very small increase on the outer rim.
Shale-normalized rare earth elements and yttrium (REY_{SN}) patterns display pronounced Ce anomalies in the early Fe-poor cores of dolomite cements (Figure 3A). A plot of Ce/Ce* vs Pr/Pr* confirms that they are true Ce anomalies (Figure 4). The later Fe-rich rims of the dolomites are slightly depleted in LREE showing more of a concave down shape (Figure 3B).

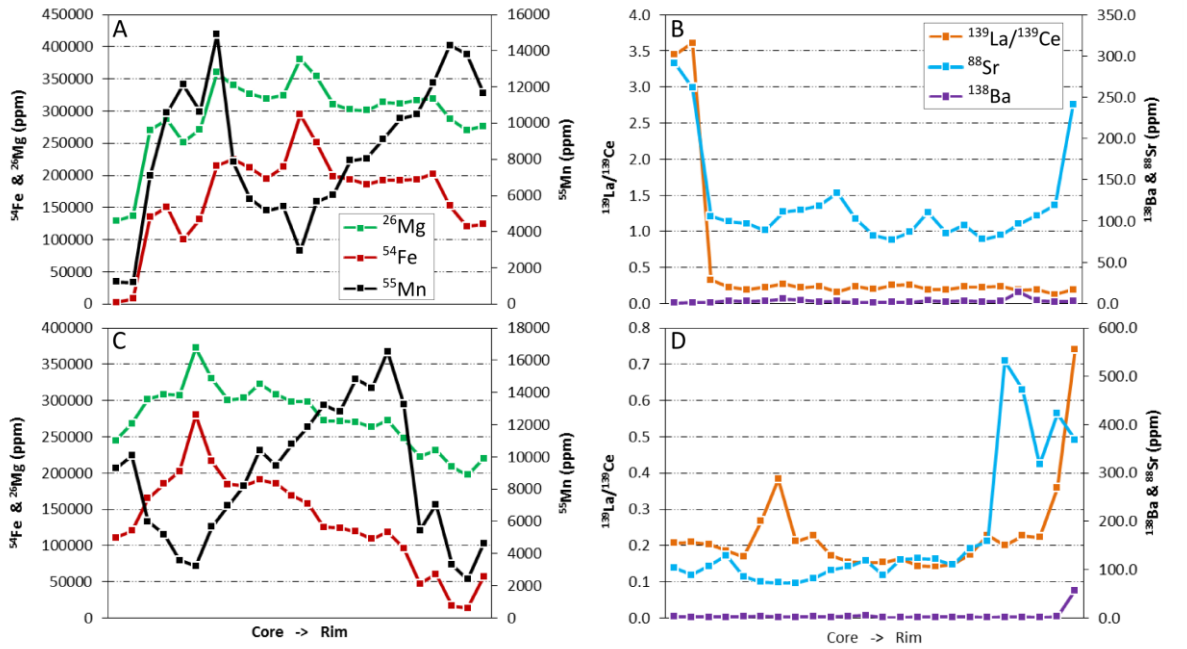

Figure 2. Plots of trace element data of two step scans across the upper carbonate in Figure 1. A and C show Fe, Mn, Mg concentrations and B and D show La/Ce, Ba and Sr concentrations from the core to rim, left to right respectively.

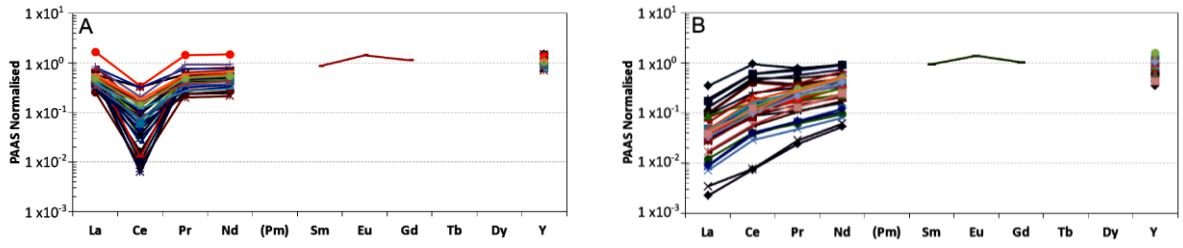

Figure 3. PAAS normalised REY patterns of; A) the Fe-poor cores and B) the Fe-rich rims of the dolomite cements. Moderately Fe-enriched rims show a mixture of these patterns.

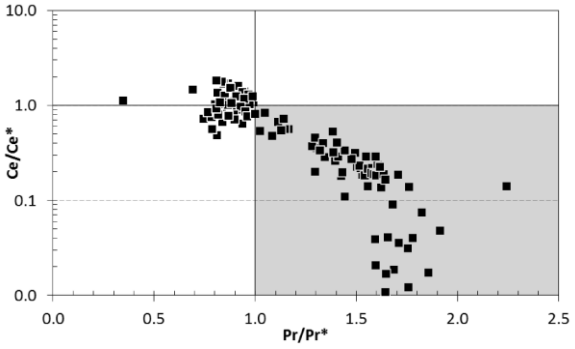

Figure 4. Graph of $(Ce/Ce^*)_{SN}$ against $(Pr/Pr^*)_{SN}$ for all carbonate measurements. The shaded area represents negative Ce_{SN} anomalies, $(Pr/Pr^*)_{SN} > 1$. A positive Ce_{SN} anomaly results in $(Pr/ Pr^*)_{SN} < 1$ while a positive La_{SN} anomaly results from a combination of $(Ce/Ce^*)_{SN} < 1$ and $(Pr/Pr^*)_{SN} \sim 1$[1].

Implications

The negative Ce anomaly in the Fe-poor cores indicates they were precipitated in an oxidising environment or fluid, whereas the Fe-rich rims were precipitated in a reducing environment or fluid. Critically this data supports our hypothesis that the Fe-rich carbonate rims were deposited in a reducing environment when the sandstone was being bleached by SO_4 with minor H_2S bearing, CO_2-charged fluids [2]. Comparison of the reservoir carbonate trace element data with existing surface travertine data has proven difficult and as a result we are carrying out further analyses and modelling of the travertines to determine their relationships to the reservoir cements.

References

[1] M. Bau and P. Dulski (1996) Precambrian Research **79**, 37-55; [2] Kampman, N. et *al.* (2014) Chemical Geology **369**, 51–82

Volatile evolution of St Kitts magmas

E. Melekhova & J. Blundy

School of Earth Sciences, University of Bristol, Wills Memorial Building, Queen's Road, BS8 3EG, UK

Introduction

Island arc volcanism is the key to understanding of magma generation, formation of continents and the recycling of the material into the mantle. The Lesser Antilles Arc have been attracting the scientist for decades due to the unusually broad geochemical variation of erupted rocks along the arc, presents of primitive basalts, mantle and crustal xenolith. This makes Lesser Antilles a unique natural laboratory for understanding magma differentiation processes. The island of St. Kitts was chosen for the study, because it has erupted basalts during Pleistocene, and contains crustal cumulate materials erupted as xenolith. The island is situated in the north of the arc and the mafic erupted rocks are tholeites.

The aim of the study was to constrain the P-T-H_2O-CO_2 conditions under which the range of erupted magmas and cumulate xenolith formed.

One component of the project was to perform high pressure-temperature petrological experiments. Another component was to find glassy melt inclusions in olivine from scoria and in minerals from cumulate xenoliths, which help place constraints on parental magma volatile contents and on the liquidus assemblages for comparison to the experiments. There are no analyses of volatile content of St Kitts lavas in the literature.

The phase equilibrium experiments on a basaltic andesite from St. Kitts were curried out under a variety of volatile (H_2O, CO_2) contents at 0.24 GPa, which we believe approximates the depth of the cumulates. The basaltic andesite starting composition is a natural lava, with added CO_2 and H_2O. The H_2O activities in the experiments were 0.33, 0.66 and 1.0. Experiments were performed in internally heated pressure vessels in Orleans, France at controlled fO_2 (~NNO).

Unfortunately, all the melt inclusions in olivine from scoria were devitrified and not suitable for the estimation of H_2O-CO_2 content of lavas. Still, we were fortunate to find 12 glassy melt inclusions and interstitial melts in cumulate xenolith. The melt inclusions are in 5 different minerals; orthopyroxene, amphibole, plagioclase, ilmenite and magnetite. Melt inclusions in oxides are particularly valuable as they do not effected significantly by post-entrapment modification caused by crystallisation on the walls of the host mineral. On figure 1 a, b the analysed melt inclusions hosted in ilmenite and plagioclase are shown.

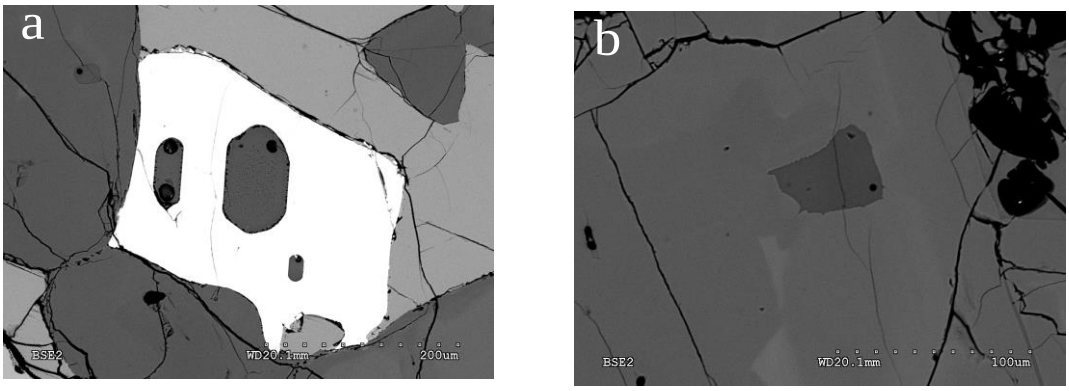

Figure 1. Melt inclusions in a) ilmenite and b) plagioclase.

Results

The H_2O and CO_2 concentration in glasses were analysed by SIMS in four experiments and the results are in a good agreement with estimates of measured volatiles added during preparation of experiments. The H_2O content of experimental glasses with water activities of 1 and 0.66 are 6 and 3.8 wt%, respectively. In the experiments with activity of 0.33 the volatile concentration in the glasses were not analysed because of very small glass pools. However, our calculations show that it should be around

1.5 wt%. The CO_2 concentration of glasses in experiments with H_2O activity 1 and 0.66 are 20 and 800 ppm, respectively.
On Figure 2 the H_2O content of melt inclusions from cumulate xenolith vs CO_2 and SiO_2 is presented. The majority of melt inclusions are degaussed. The high CO_2 concentrations in melt inclusion hosted by magnetite are easily explained by flax of CO_2 through the melt inclusion as it has several cracks, which are connected to interstitial melt. The interstitial melt analysed in the same sample support this. It is remarkable that andesitic melts have consistently between 4.5 and 6 wt% of H_2O. Assuming, that cumulates where trapped in the low crust for some time one would expect to loose all the H_2O because of H diffusion through the host mineral rather than keep it at such a high level. These high concentrations in andesitic melts suggest that primitive magmas in St Kitts have between 1 to 2 wt% of H_2O. Further constrains are required to support this evaluation. For the last 6 years we produced extensive set of data for several Lesser Antilles islands including estimation of water content of primitive melts. The melt inclusions from St Kitts and run products were also analysed for trace elements. This and our set of data on other studied islands should help us to support the calculated values of 1 to 2 wt% (the work is in progress).
Our work on melt inclusions hosted in minerals from cumulate xenolith show that they could be valuable in evaluating the H_2O concentration in magmas prior an eruption when the fast quenched scoria samples are not available or melt inclusions in them are devitrified.

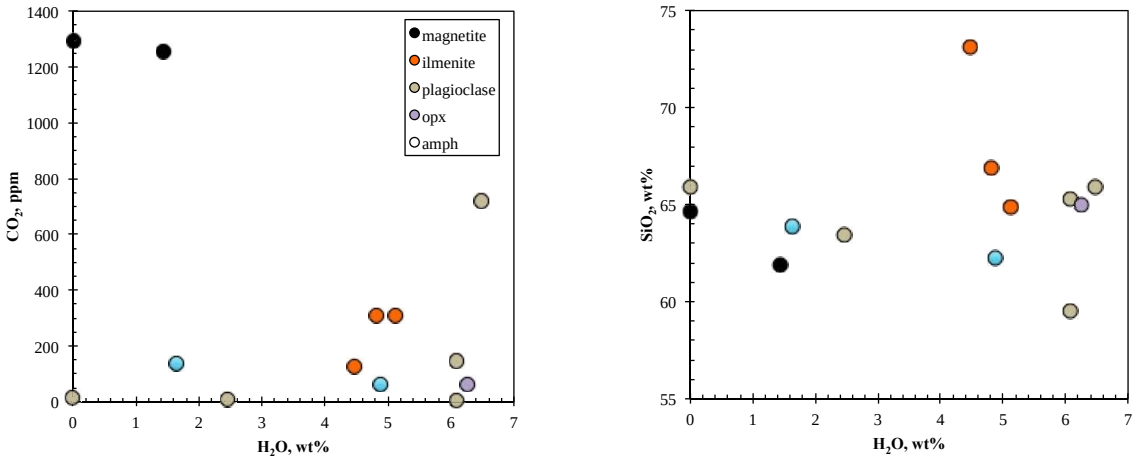

Figure 2. Volatile content of melt inclusions from cumulate xenolith.

Estimating the CO_2 content of the Icelandic mantle plume from Kistufell olivine-hosted melt inclusions

W. Miller[1], J. Maclennan[1] & T. Thordarson[2]

[1]Department of Earth Sciences, University of Cambridge, Cambridge CB2 3EQ, UK
[2]Faculty of Earth Sciences, University of Iceland, Reykjavik, Iceland

Introduction

Understanding the CO_2 fluxes and reservoirs of the Earth's system is a major scientific target at present. The volcanic/magmatic flux of CO_2 from the mantle reservoir to the atmosphere is one of the major fluxes, modulating the Earth's climate on short to long timescales. Very few direct observational constraints on magmatic CO_2 flux or CO_2 content of the deep Earth are available. The majority of magmas are degassed at the surface; therefore the parental melt CO_2 content cannot be quantified from basaltic samples. A handful of studies have been able to estimate the undegassed CO_2 contents of primary mantle melts at mid-ocean ridges (MORs), and these values have proved to be key in estimating the CO_2 content of the mantle and the global CO_2 flux. It is well know that the Sr-Nd-Pb-He isotopic compositions of the mantle sampled by spreading ridges is variable, but it has not been established whether this variability is linked to variability in CO_2 content and other volatile elements.

Strategy

Highly forsteritic olivines are in equilibrium with primary mantle melts, therefore they have the potential to trap primitive mantle melts before they evolve and degas. We have analysed over 120 olivine-hosted melt inclusions from Kistufell, Iceland – a monogenetic, subglacial eruption situated above the inferred locus of the Icelandic mantle plume[1]. Using Secondary Ion Mass Spectrometry (SIMS) we have been able to measure the volatile (including CO_2) and trace element contents of these melt inclusions. This technique has provided estimates of volatile/trace element ratios that ultimately tell us about the volatile content of the mantle beneath Iceland, which from Helium isotope analysis is thought to have a plume component. We aimed to produce the first CO_2/Nb estimate of the mantle beneath central Iceland, providing a comparison with unpublished data from Borgarhraun, Theistareykir, Northern Volcanic Zone, Iceland[2].

Results

CO_2 contents of the measured melt inclusions are quite variable, ranging from 0-1200 ppm, with the carrier glass containing <30 ppm CO_2 (Figure 1.). Measured water concentrations are low for the melt inclusions and carrier glass, with both averaging 0.15 wt%. Trace element concentrations show limited variability across the suite of melt inclusions and carrier glass; showing depleted trace element ratios of La/Yb<1.5 and Ce/Y~0.36 (Figure 2.). The concentrations produce a relatively flat trace element spider plot, showing a slight depletion in Rare Earth Elements (REEs) with respect to normal mid-ocean ridge basalt (N-MORB). Forsterite contents of host olivines, measured using electron microprobe analysis range from $Fo_{89.1}$-$Fo_{87.8}$.

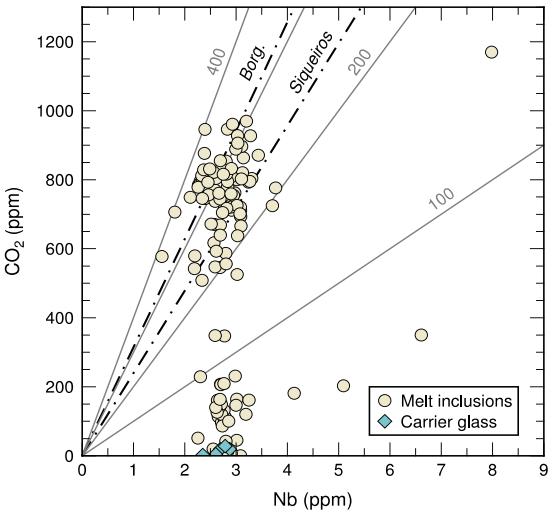

Figure 1. CO_2 versus Nb concentrations for melt inclusions (circles) and carrier glass (diamonds). Solid lines show constant CO_2/Nb ratio, dot-dash lines show average CO_2/Nb ratios for Borgarhraun[2], Iceland; and Siqueiros[3], East Pacific Rise (EPR).

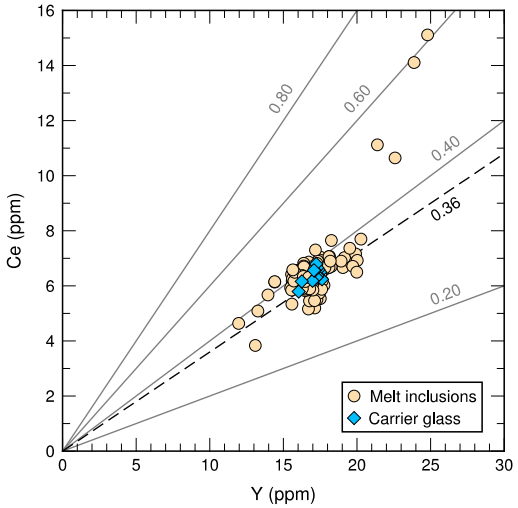

Figure 2. Ce versus Y concentrations for melt inclusions (circles) and carrier glass (diamonds). Solid lines show constant Ce/Y ratio, dashed line shows average ratio.

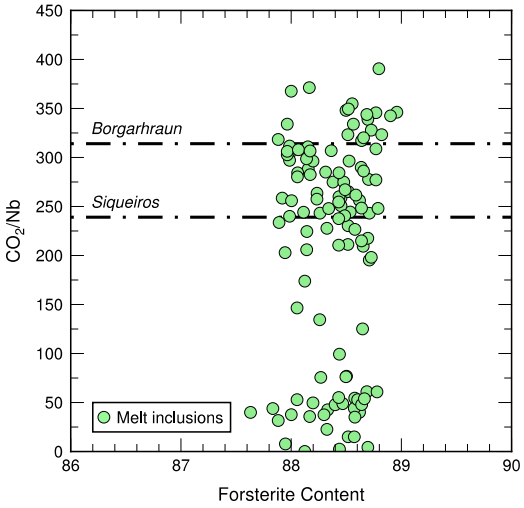

Figure 3. CO_2/Nb ratio of melt inclusions versus forsterite content of host olivine. Dot-dash lines show average CO_2/Nb ratios for Borgarhraun[2], Iceland; and Siqueiros[3], EPR.

Discussion

The variability in CO_2 content at constant Nb concentrations (Figure 1.) is mainly due to degassing of the melt before/during melt inclusion entrapment, with the highest CO_2 contents likely to represent undegassed melt inclusions. From these inclusions we can constrain a lower bound for the CO_2/Nb ratio of primitive mantle melts of ~350. Water concentrations are fairly constant across the melt inclusions and carrier glass (~0.15 wt%), suggesting re-equilibrium of the melt inclusions with the carrier glass by the diffusion of H^+ through the host olivine upon eruption.

Trace element variability is not as great as anticipated due to the lack of melt inclusions trapped within hightly forsteritic ($Fo_{>90}$) olivines. If there initially was measureable heterogeneity amongst primary mantle melts, mixing processes prior to melt inclusion entrapment have homogenised their chemistry, which is also shown by the carrier liquid. Rare Earth elements (REEs) show a depleted signature with low Ce/Y (~0.36, Figure 2.) and low La/Yb (~1.3). The lack of variability has come as a surprise and might indicate that the processing of mantle heterogeneity by melting/melt transport/storage is different under central Iceland and Theistareykir.

Comparison of melt inclusion CO_2/Nb ratios from Kistufell with the averages of Borgarhraun (Figure 3.) shows that Kistufell has a similar CO_2/Nb average ratio as the northern end of the NVZ. Iceland as a whole shows a higher ratio than Siqueiros, EPR. This suggests that the depleted melt source beneath the NVZ has a constant CO_2/Nb ratio; however when considering the MOR system there is clear CO_2/Rb heterogeneity within the mantle source.

Future Work

We are going to look at fluid inclusions within the Kistufell olivines to see if we can better constrain the depths of entrapment and the possibility of CO_2 loss from the melt inclusions. We are in the process of analysing volatiles and trace elements within olivine-hosted melt inclusions from Miðfell, western volcanic zone, Iceland. The Miðfell eruption is known to contain highly forsteritic olivines with melt inclusions, allowing us to constrain the chemistry of primitive mantle melts from beneath Miðfell.

References

[1] K. Breddam (2002) Journal of Petrology **43**, 345-373; [2] E. Hauri (2002) Goldschmidt Abstract ; [3] A. Saal et al. (2002) Nature **419**, 451-455.

Driving large explosive basaltic eruptions in Iceland: Records of magmatic evolution and degassing from the widespread 10ka Saksunarvatn tephra

D.A. Neave[1], J. Maclennan[1], Th. Thordarson[2] & M.E. Hartley[3]

[1]Department of Earth Sciences, University of Cambridge, Downing St., Cambridge, CB2 3EQ, UK
[2]Faculty of Earth Sciences, University of Iceland, Askja, Sturlugata 7, 101 Reykjavik, Iceland
[3]School of Earth, Atmospheric and Environmental Sciences, Univ. Manchester, M13 9PL, UK

Objectives

Volcanic activity in Iceland is particularly focussed along the Eastern Volcanic Zone (EVZ), which has contributed ~60% of the total mass erupted in Iceland since the end of glaciation at ~11 ka. Although the recent summit eruptions of Grímsvötn have generated locally-damaging melt water floods, (e.g. 1996 Gjálp eruption), and interfered with aviation, (e.g. 2004 and 2011 eruptions), they have been generally small in volume (≤0.1 km^3 DRE), and with few far reaching effects. However, much larger Laki-sized, explosive eruptions are known from the early Holocene that would have been widely environmentally-impacting. The >>15km^3 Saksunarvatn tephra has been dated to ~10.3 ka and is an important tephrochronological marker across the North Atlantic, being found in a broad swathe from ice cores in Greenland to lake deposits in Germany. While recent studies suggest that the Saksunarvatn tephra may have been deposited cumulatively during a number of eruptions, each eruptive phase is likely to have been at least comparable in size to the largest explosive basaltic eruptions known from Iceland (5–8 km^3). Despite the huge volume of the Saksunarvatn tephra, and its formation at a time of major climatic change, the tephra has yet to be characterised petrologically.

This project uses glassy tephra samples cored from Lake Hvítárvatn in central Iceland, in order to constrain magmatic evolution and degassing processes in the melts that supplied the Saksunarvatn eruption. Project objectives include: (1) How was the Saksunarvatn magma assembled? (2) At what depth was the magma stored and processed? (3) How did the volatile elements degas both before and during the eruption?

Approach

A total of 134 plagioclase- and olivine-hosted melt inclusions were analysed for major, trace and volatile elements. Macrocrysts containing large, naturally-quenched melt inclusions were picked from glassy tephra in order to minimise the effects of post-entrapment processes (**Figure 1**). Inclusions and glasses were analysed for CO_2, H_2O, Li, B F, Cl and selected trace elements (REEs, Nb, Zr, Sr) using a Cameca IMS-4f ion microprobe at the University of Edinburgh. Major elements, F and S were measured using a Cameca SX-100 electron microprobe at the University of Cambridge. A total of 22 clinopyroxene macrocrysts were also analysed for major and trace elements by electron and ion microprobe, respectively.

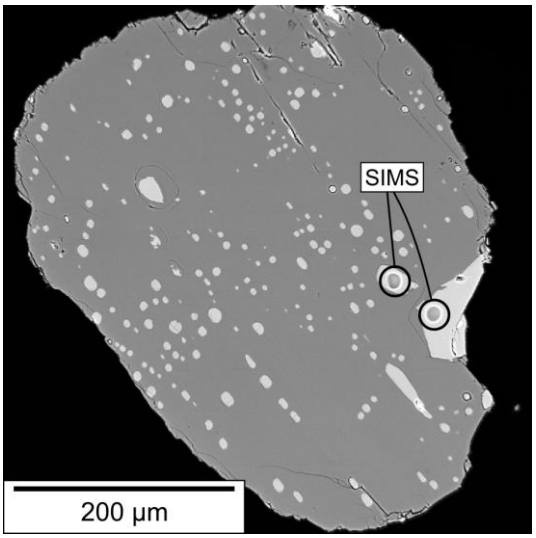

Figure 1. Backscattered scanning electron image of typical plagioclase-hosted melt inclusions from the Saksunarvatn tephra.

Results

Macrocrysts from the Saksunarvatn tephra can be divided into a primitive assemblage of zoned macrocryst cores (An_{78}–An_{92}, $Mg\#_{cpx}$ = 82–87, $Fo_{79.5}$–Fo_{87}), and an evolved assemblage consisting of unzoned macrocrysts and zoned macrocryst rims (An_{60}–An_{68}, $Mg\#_{cpx}$ = 71–78, Fo_{70}–Fo_{76}). The evolved assemblage is close to being in equilibrium with the matrix glass.

Trace element disequilibrium between primitive and evolved components of the magma indicates that they were derived from different distributions of mantle melts (**Figure 2**). These distinct mantle melts may have become juxtaposed during disaggregation of incompatible trace element-depleted mushes (mean La/Yb_{melt} = 2.1) into incompatible trace element-enriched melts (La/Yb_{melt} = 3.6) during melt

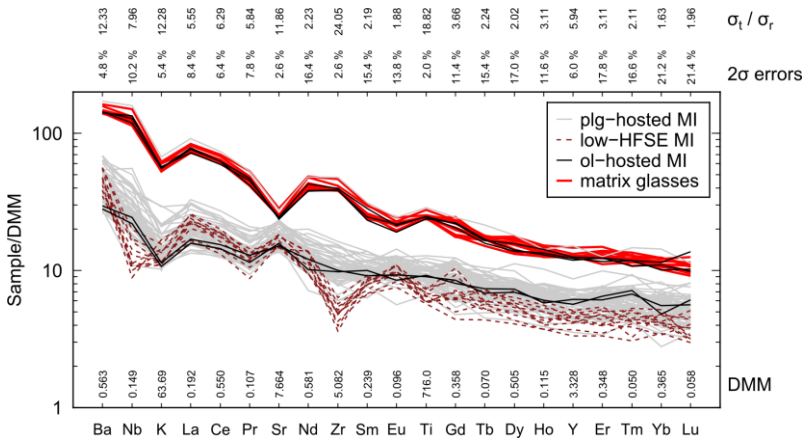

Figure 2 Depleted MORB Mantle (DMM) normalised trace element spider diagram of Saksunarvatn melt inclusions (MI) and matrix glasses. Signal to noise ratios (σ_t/ σ_r) and 2σ % relative errors are shown along the top of the plot, with normalisation values shown along the bottom.

transport and magma assembly. The major and trace element contents of plagioclase-hosted inclusions have not experienced significant post-entrapment modification, and record crystallisation and mixing of compositionally variable mantle melts that are amongst the most primitive liquids known from the EVZ. Coupled high field strength element (HFSE) depletions and incompatible trace element enrichments in a subset of primitive plagioclase-hosted melt inclusions is best accounted for by inclusion formation during mixing-induced crystal dissolution. Extrapolating a mean liquid line of descent to compositions in equilibrium with $Mg\#_{melt}$ = 70 suggests the near-primary melts recorded in primitive inclusions from the Saksunarvatn tephra are compositionally similar to high-Mg# melts erupted elsewhere in Iceland.

Thermobarometric calculations indicate that the evolved assemblage last equilibrated at ~1140°C and 1±1 kbar (**Figure 3**). However, given the large volume of the Saksunarvatn eruptions, 1±1 kbar is unlikely to represent a depth of long-term magma accumulation and storage. Although multiple thermometers indicate that the primitive assemblage crystallised at high temperatures of 1240–1300°C, barometric calculations are initially equivocal on the depth at which crystallisation took place. Raw clinopyroxene-melt pressures of 5.5–7.5 kbar conflict with apparent inclusion entrapment pressures of ~1.4 kbar (**Figure 3**). After applying corrections derived from comparisons with experimental data, clinopyroxene-melt equilibria return mid-crustal pressures of 2.5–5.5 kbar that are consistent with pressures calculated from primitive melt inclusion compositions. Long term storage of primitive magmas thus probably occurred within the mid crust, implying that primitive melt inclusions have lost substantial quantities of CO_2 prior to eruption.

This research will be presented in manuscript to be submitted in early 2015. A detailed investigation of Li, B, F, Cl and S systematics is currently underway, and will be presented in a second contribution.

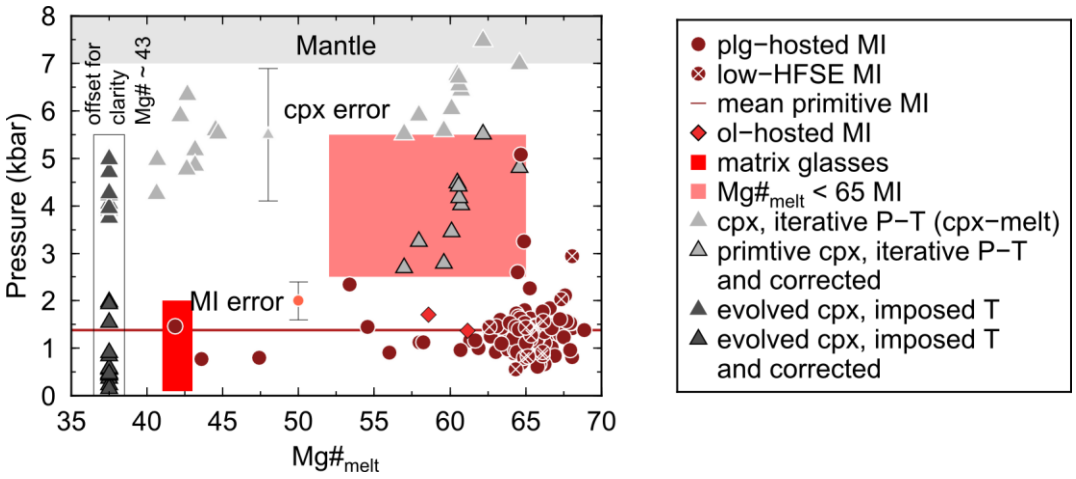

Figure 2 Summary of barometric calculations applied to the Saksunarvatn tephra showing the poor correspondence between different techniques. Although melt and clinopyroxene-melt pressures can be reconciled in the mid crust after the applying a correction, melt inclusion (MI) entrapment pressures are almost uniformly low, implying that significant quantities of CO_2 were lost prior to quenching.

Volatile and trace elements variability of Siberian Traps melts

S. Sibik (née Novikova) [1], M. Edmonds[1], J. Maclennan[1], H. Svensen[2]

[1]Department of Earth Sciences, University of Cambridge, Cambridge, CB2 3EQ, UK
[2]Center for Earth Evoluton and Dynamics, University of Oslo, Oslo, 1048 Blindern, Norway

Introduction

The Siberian Traps Large Igneous Province (Figure 1) is thought to have formed over 1 Ma at the end of the Permian, synchronous with the largest mass extinction in Earth's history, when >96% of all marine species disappeared. There remains much controversy as to the exact mechanism of the mass extinction. The source of volatiles is a crucial question as it determines the speciation of some volatile components, which then can lead to climate perturbation and ozone depletion to a different extent. Being the country rocks for the huge volumes of sills (about 800 000 km^3) evaporites and beds with organic-rich accumulations must have had a significant influence on the amount and composition of released gases. In order to assess the relative importance of volatile sources (with the exception of the metamorphic outgassing source, which cannot be tested via a study of melt inclusions), we have conducted a geochemical study of melt inclusions hosted by clinopyroxene in Siberian Traps tholeiitic lavas and sills. The magmas were not emplaced in or erupted on evaporite deposits, in contrast to previous studies (Figure 1).

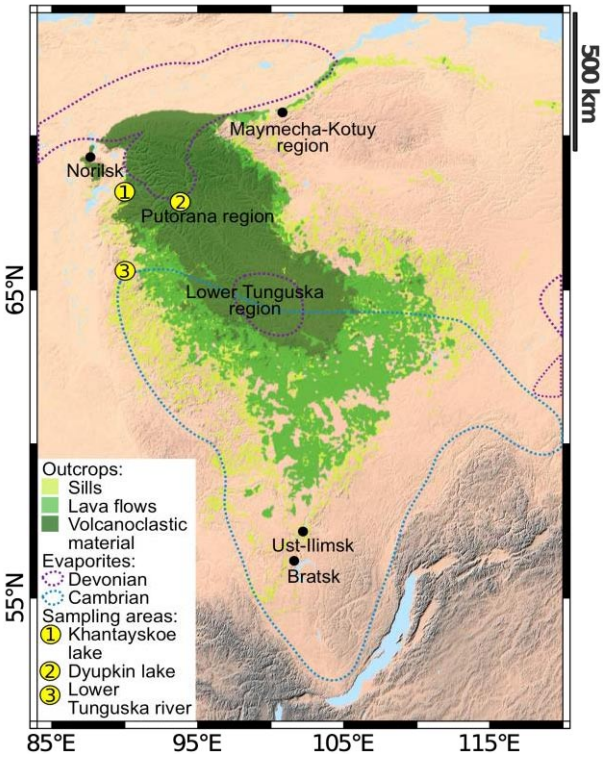

Figure 1. Schematic geological map of Tunguska Basin, Eastern Siberia (modified from [1]).

Results and Discussion

The session in the past year was performed in order to complete the analyses started in 2013. Trace elements and volatiles in melt inclusions hosted by clinopyroxenes and olivines were measured by SIMS and then the same pits were analysed for major elements as well as for sulfur, chlorine and fluorine by EPMA in Cambridge. The first data set was corrected and combined with the second one,that had better accuracy and precision.

It has been shown that sills and lava flows erupted south-east from Norilsk are formed from evolved melts that were subject to fractionation, crustal contamination, interaction with crustal fluids and possibly degassing. As expected, the melt analysis revealed the contamination by siliceous crustal material (Nb minimum , Figure 2b), whereas the evidence of volatile-rich evaporite contamination has not been identified. The resuslts of current investigation show that despite all of these overlain processes, peridotite and pyroxenite mixing in the source is indeed preserved. Moreover, it is the second important parameter controlling the compositional variability (variable La/Yb ratio, Figure 2a) of the melts after fractional crystallisation. In conjunction with oceanic sediment addition, pyroxenite and peridotite mixing in the source can explain most of geochemical features of generated melts.

Overall, the melts are more volatile-poor than those presented from the Gudchikhinsky formation [2] and from Bratsk and Ust-Ilimsk sills [3]. In the former case it is the result of both an increased proportion of peridotite in the source and a significant amount of dilution by assimilation of volatile-poor continental crust, whereas in the latter it is due to a lack of contamination by evaporite. We suggest that these volatile-poor magmas may have been widespread during across the Platform and the volatile budget of the eruptions may have been previously overestimated by as much as an order of magnitude.

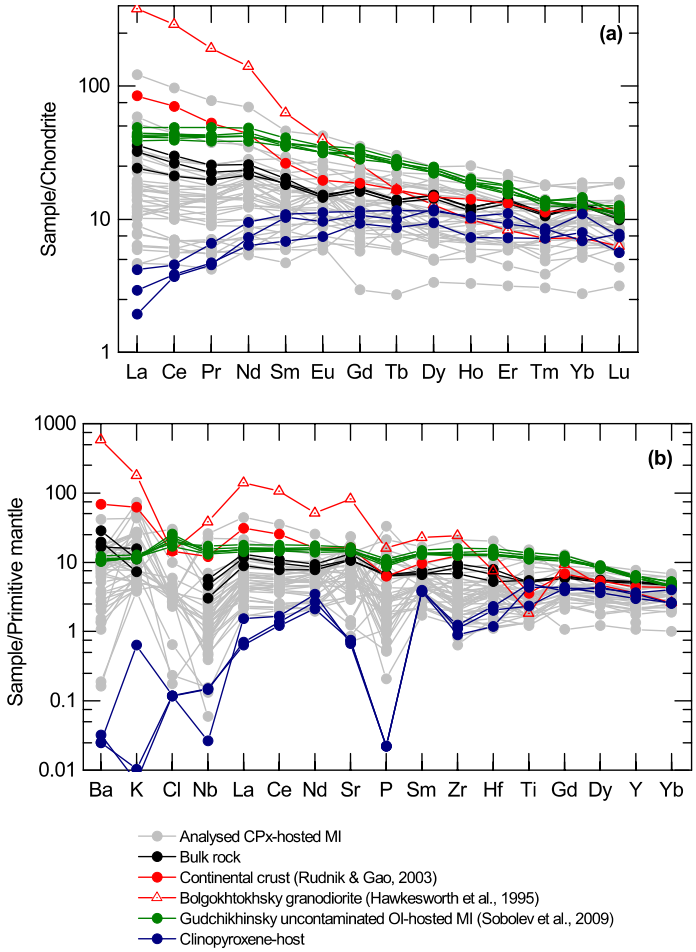

Figure 2. Rare earth (a) and multi-element (b) patterns of analysed clinopyroxene-hosted melt inclusions from lava flows south from Norilsk (grey), host clinopyroxenes (blue), basalt where the clinopyroxene crystals were picked from, bulk rock (black), continental crust [4] (red), Bolgokhtokhsky granodiorite [5] (dotted red with empty triangles), most primitive uncontaminated melt inclusions from Gudchikhinsky formation [3] (green). Concentrations are normalised to the C1-chondrite values [6] and Primitive mantle [7] correspondingly.

References

[1] Malich et al. (1974). Map of geological formations of the Siberian platform cover
[2] Sobolev et al. (2009) Petrology **17**, 253-286.
[3] Black et al. (2012) EPSL, **317-318**, 363-373.
[4] Rudnick, R. L. & Gao, S. (2003) *Treatise on Geochemistry* **3**, 1-64
[5] Hawkesworth, et al. (1995). Lithos **34**, 61-88.
[6] Sun, S. & McDonough, W. F. (1989). In: Magmatism in the Ocean Basins. Geological Society, London, Special Publications, pp 313-345.
[7] McDonough, W. F. & Sun, S. (1995). Chemical Geology **120**, 223-253.

Selecting samples as potential microanalysis reference materials: glass from naturally hydrated rhyolitic tephras

N.J.G Pearce[1], J.A Westgate[2]

[1] Department of Geography and Earth Sciences, Aberystwyth University, SY23 3DB, Wales, United Kingdom.
[2] Department of Earth Sciences, University of Toronto, Toronto, Ontario, M5S 3B1, Canada.

Introduction

The quality of geochemical analyses is only as good as the reference materials (RMs) used to monitor accuracy and reproducibility. In trace element microanalysis, where appropriate RMs are often not available, this is a significant obstacle to the production of high quality data and to inter-laboratory and inter-method comparisons. In recent years trace element analyses of single grains (shards) of hydrated volcanic glass from tephra deposits have become an essential part of tephra characterisation and a necessary component of many Quaternary tephrochronological studies. These analyses are commonly performed by laser ablation (LA) ICP-MS [1], however there are no natural hydrated rhyolite glass reference materials against which to check analytical accuracy.

The use of tephra in Quaternary studies is important for stratigraphic correlation, as it provides an isochronous marker which can be used to link different archives of palaeoclimate data such as ice cores, marine sediment cores or terrestrial records such as lake cores, peat bogs, loess sequences etc. Tracing these minute quantities of volcanic glass preserved within archives such as the Greenland ice-cores and North Atlantic marine records can significantly strengthen chronological models by incorporation of independent tephra age estimates as well as permitting the precise correlation of such sequences [2]. However, at present, because of a lack of appropriate reference materials for trace element analyses of glass shards at small spot sizes, it can be difficult to compare with any degree of certainty analyses performed under different conditions or in different laboratories. Additionally, with tephra deposits being recorded from ever more distal locations, there is a need for better analytical data on ever smaller shards of glass.

Micro-analytical trace element studies of glass from tephra deposits build on and compliment the widespread use of major element analyses from these materials which started in the late 1960s, and these types of tephra compositional studies have been at the centre of several large research programmes (INTIMATE, RESET, SMART, TRACE). In these studies trace element analyses can be vital in making the correct correlation, with the distal records often preserving a more complete record of volcanism than the proximal record, which contributes valuable data to volcanic evolution and hazard studies. The rapid improvements in LA-ICP-MS methods over the last 10-15 years have seen the technique become the most widely used method for the determination of trace elements in glass shards from tephra deposits, but in common with other microbeam analytical methods, this is not without issue. While it is possible to determine the major element composition of these small fragments by electron probe microanalysis, the practical limit for trace element analyses by LA-ICP-MS is probably between 6-10 μm with many routine analyses being performed at 20 μm to 50 μm. However, at the highest analytical resolutions (<20 μm) elemental fractionation becomes apparent, becoming more severe as crater diameters decrease, but at present it is difficult to define the extent of this fractionation without appropriate reference samples.

Results

In an attempt to address the lack of reference materials for the microanalysis of individual glass shards, ten candidate tephra samples have been selected from the collection of Westgate held at the University of Toronto. These 10 samples show good homogeneity for their major element compositions determined by EPMA, and are relatively coarse-grained, with shards in some cases up to 350 to 400 μm in diameter. All ten samples were analysed by LA-ICP-MS and ion microprobe at Aberystwyth University and University of Edinburgh respectively, to assess the trace element homogeneity (see example of data from one sample in Table). From these 10 candidate glasses, four samples showed relative standard deviations on the trace element determinations by ion probe which were better than 5% for the abundant trace elements (about 8 analyses per sample), or better than 10% by LA-ICP-MS (which has lower analytical precision, about 25 analyses per sample). We consider these four samples to have suitable homogeneous to make them useful as hydrated rhyolitic glass

reference samples. These are the Old Crow tephra (OCt), Alaska ~130 ka, the Rangitawa Tephra (RT), New Zealand ~340 ka, Huckleberry Ridge tephra (HRt), USA ~2.00 Ma and the Maninjau Ignimbrite, Sumatra ~52 ka.

The Old Crow tephra is already widely used by the EPMA community to monitor major element analyses. The reproducibility of multiple analyses of glass shards from these deposits includes both analytical errors and any sample heterogeneity, and is generally in the ±5-10% range, or less (see Table), and this compares favourably with the quoted uncertainty for the MPI-DING reference rhyolitic glass ATHO-G. The glass from these four tephra deposits thus has the potential to make a suite of natural microanalysis reference samples, materials which are not represented in the current set of available microanalysis reference materials. We are currently seeking funds to support the collection and distribution of large volumes of the four most homogeneous of these samples in a round-robin exercise to produce agreed concentrations for each sample. Once these have been characterised by as many labs as we can interest, we will then make these available as glasses to be used as reference samples in tephra (and other glass) microanalysis.

In addition characterisation of these materials will allow the behaviour of these hydrated glass shards (between 2-6 wt% H_2O) during laser ablation analyses to be better understood, and thus quantified, and this will improve the analyses of the smallest, most distal glass shards using small (<20 μm) ablation craters. Thus, the production of these reference materials will facilitate better inter-laboratory comparisons of glass microanalysis, and will improve the quantification and understanding of element fractionation during LA-ICP-MS (and other microbeam) analyses of hydrated rhyolitic glasses, improving data quality in (in particular) tephra studies.

Trace element analyses , Huckleberry Ridge tephra, Yellowstone Nat Park, USA							
	LA-ICP-MS Aberystwth			Ion probe, Edinburgh		Ratio	ATHO-G 1 s.d
	UT1039 avg (1 s.d.)	RSD		UT1039 avg (1 s.d.)	RSD	LA/Ion probe	Uncert'ty
Rb	262 (10.61)	4.1%		315 (7.91)	2.5%	0.83	4.6%
Sr	1.83 (0.75)	41%		2.06 (0.57)	27%	0.89	2.9%
Y	105 (7.45)	7.1%		86.4 (6.7)	7.7%	1.21	3.7%
Zr	176 (12.25)	6.9%		158 (8.66)	5.5%	1.12	3.9%
Nb	86.4 (2.8)	3.2%		76.9 (7.97)	10%	1.12	4.2%
Cs	5.94 (0.47)	7.9%		4.95 (0.18)	3.7%	1.20	10.2%
Ba	14.4 (2.61)	18%		21.5 (6.93)	32%	0.67	2.9%
La	41.4 (4.46)	10%		45.8 (7.98)	17%	0.90	2.7%
Ce	85.1 (4.05)	4.8%		99 (12.91)	13%	0.86	3.3%
Pr	10.1 (0.64)	6.3%		11 (1.04)	9.5%	0.92	2.7%
Nd	40.2 (3.86)	9.6%		41.2 (3.54)	8.6%	0.98	3.3%
Sm	12.2 (1.17)	9.6%		11.1 (0.37)	3.3%	1.10	2.8%
Eu	0.24 (0.09)	37%		0.18 (0.07)	36%	1.31	3.6%
Gd	13.5 (1.25)	9.2%		12 (0.4)	3.3%	1.13	4.6%
Tb	2.49 (0.22)	8.7%		2.22 (0.16)	7.3%	1.12	3.2%
Dy	17.7 (1.69)	9.5%		14.3 (0.92)	6.4%	1.24	4.3%
Ho	3.73 (0.3)	8.1%		2.79 (0.17)	6.2%	1.34	3.2%
Er	11.1 (0.91)	8.2%		9.01 (1.05)	11%	1.23	4.9%
Tm	1.7 (0.19)	11%					4.6%
Yb	11.1 (0.86)	7.7%		9.07 (0.79)	8.7%	1.22	3.8%
Lu	1.59 (0.14)	9.0%					3.2%
Hf	9.04 (0.78)	8.6%		7.54 (0.58)	7.6%	1.20	3.6%
Ta	6.64 (0.44)	6.6%		4.84 (0.43)	8.8%	1.37	5.1%
Pb	49 (3.63)	7.4%					10.9%
Th	34.2 (2.22)	6.5%		32.5 (1.51)	4.6%	1.05	3.6%
U	9.45 (0.38)	4.0%		10.4 (0.35)	3.3%	0.91	5.1%

References

[1] N.J.G. Pearce et al. (2011) Quaternary International, **246,** 57-81.
[2] D.J. Lowe (2011) Quaternary Geochronology **6,** 107-153.

Impact of iron biological availability on the deglacial release of CO_2 from the Southern Ocean

L. E. Pichevin, W. Geibert, R. S. Ganeshram
School of GeoSciences, University of Edinburgh, Edinburgh EH9 3JW, UK

Background and Objectives

Dust input to the ocean has been shown to increase by an order of magnitude on average during the last glacial period in tandem with declines in CO_2; suggesting a causal link between the efficiency of the biological pump and micronutrient (Fe, Zn) supply[1]. However, only a very small but highly variable proportion of dust-borne Fe is solubilised on deposition in sea water. Solubilisation is affected by a range of factors such as the size and nature of the mineral aerosols as well as the presence of ligands in the water[2]. In addition, there are clear evidences that dust is not the only source of Fe to the surface ocean[3]. Therefore paleo-reconstructions of micronutrient biological availability cannot be solely based on sedimentary dust accumulation. So far the lack of a suitable proxy to evaluate changes in micronutrient availability has limited our understanding of the role of micronutrient supply in modulating carbon cycling. Reconstructing past micronutrient availability in areas like the Southern Ocean is crucial to understand the role of dust supply on biological productivity and to assess whether the biological carbon pump was invigorated during glacial time, hence contributing to atmospheric CO2 draw-down.

Recent laboratory studies have demonstrated that diatoms incorporate trace metals such as Fe and Zn, in proportion to their biological availability in sea water[4]. More recently, I have used the ion microprobe technique (Grant IMF396/0510) on settling and sedimentary diatoms to further investigate the incorporation of trace-metals in diatom frustules in natural seawater and the subsequent preservation of the diatom-bound signal in sediments[5]. Our results demonstrate that trace metal concentrations in sedimentary diatom frustules can be used to track past changes in micronutrient availability in the surface ocean. The advantage of using this method in sediment cores is that it would provide for the first time a direct measure of past changes in micronutrient bioavailability rather than indirect inferences from dust fluxes as it has been the case so far[1].

The close synchronicity between atmospheric CO_2 variations and Antarctic temperature history suggests a tight coupling between carbon dioxide levels and climate in the southern hemisphere high latitudes. In the Southern Ocean (SO) deep upwelling of CO_2- and nutrient-rich waters at the Polar Front Zone facilitates the efflux of CO_2 from the ocean to the atmosphere[6]. This release of CO_2 to the atmosphere is dampened by surface biological carbon fixation utilising the macronutrients (nitrate, phosphate and silicic acid) in the upwelled waters. However, biological productivity and nutrient utilisation in the SO appear to be severely hampered by the limited availability of micronutrients (mainly Fe) partly supplied through dust[7].

The overarching objective of the project was to apply a new proxy (diatom-bound trace metals) for past micronutrient availability in the surface SO in order to document the role of micronutrients on marine productivity and atmospheric CO_2 levels in the past. We have measured micronutrient availability in a sediment core from the Indian sector of the SO (Core S2, 42° 0.258' S; 48° 0600' E, 3305 m water depth) during the last glacial cycle when dramatic changes in dust input, biological productivity, ice cover and atmospheric CO_2 are known to have happened in order to explore the relationship between micronutrient availability, dust supply, macronutrient utilisation/inventory and productivity.

Results

1) Diatom-bound Fe record in Core S2

The following isotopes were measured in the sedimentary diatom samples and in a NIST standard for comparison: ^{23}Na, ^{26}Mg, ^{27}Al, ^{30}Si, ^{54}Fe. A total of 359 analyses were conducted on the cleaned diatom frustules. Each measurement focussed on a single or a couple of isolated diatom frustules. It was therefore important to analyse several diatoms in each sample in order to account for the variability in the sample and to obtain statistically significant average values. The Fe:SiO_2 (ppm) values plotted in Figure 1 represent an average of the 10-12 measurements made for each sample.

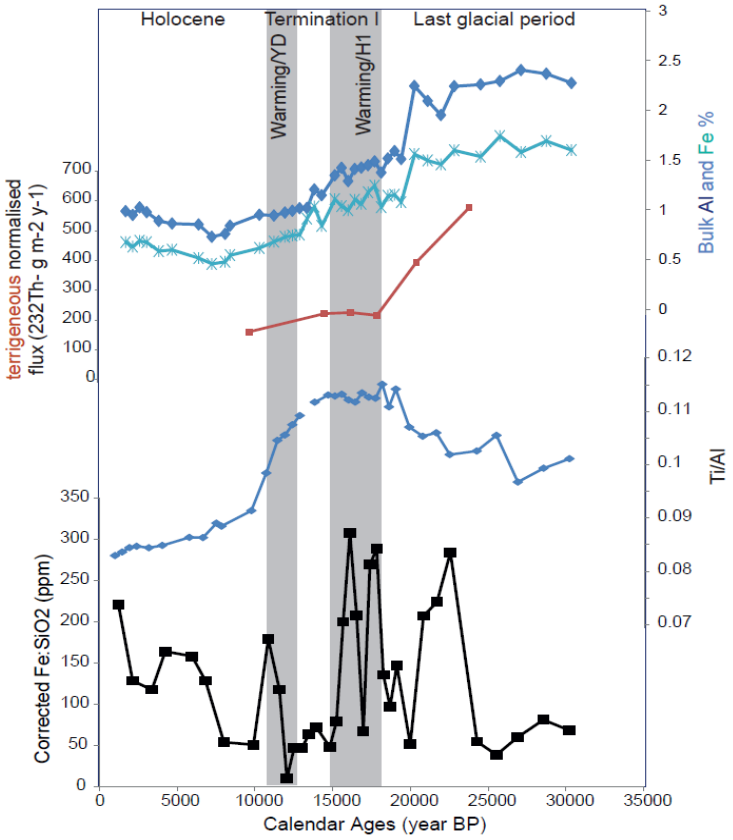

Figure 1: (from bottom to top) Diatom-bound iron concentrations (ppm), Ti/Al ratio in the bulk sediment, terrigenous fluxes based on ^{232}Th measurements and Al and Fe concentration in the bulk sediment (terrigenous inputs) versus time in sediment core S2. YD and H1 stand for Younger Dryas and Heinrich event 1, respectively.

Potential terrigenous (clay) contamination and signs of early diagenesis were assessed by measuring ^{27}Al in the diatoms frustules. Al has been shown to replace Si in the biogenic silica matrix during synthesis of the frustule and even more so during diagenesis after the organism's death and post deposition [8]. Therefore, Al content in diatom frustules is expected to be in the region of 3000 ppm (0.3%) with values much higher if the frustules have been altered during diagenesis. We obtained Al values of 3000 ppm on average with maximal accepted values of 6000 ppm [8].

Contamination or diagenetic incorporation of metals would result in high levels of Al:SiO_2 (>6000) at the surface of the frustules during the first couple of measurement cycles, rapidly decreasing as the ion beam penetrates inside the opal matrix. This trend was only rarely observed in our samples (if it was, the analysis was aborted or disregarded) which mostly showed very constant metal levels throughout the analyses. This demonstrates the cleanliness of the diatom frustules and that the metal contents determined were associated with the matrix of the frustules. Moreover, Fe/Al ratios measured in the frustules are highly variable and different from the upper crustal values hence further ruling out terrigenous contamination of the Fe concentration measured. The lack of correlation between Al:SiO_2 and Fe:SiO2 in the frustules further indicates that the iron measured is incorporated in the diatom frustule and cannot be attributed to contamination by clay.

2) Comparison between Diatom-bound Fe concentration and dust accumulation records

In this region remote from continental masses, most terrigenous supply is brought by the winds as dust. We reconstructed past changes in dust supply to the core site by measuring bulk Al, Fe and Ti concentrations in the sediment cores (Fig. 1). In addition, we measured ^{232}Th isotopes (dust proxy) in few bulk sediment samples selected during the deglaciation. Both sets of data show that dust supply to the core site starts to decrease sharply prior to the deglaciation at the end of the LGM, continues to decrease progressively during the deglaciation and reaches low level during the Holocene, akin to global dust records. Ti/Al ratio of the bulk sediment can be used to track changes in the provenance and/or in the distance of the dust source. Ti/Al ratio displays different values during the Holocene, the deglaciation and the Last glacial period, suggesting progressive changes in the origin of the dust during the last glacial cycle.

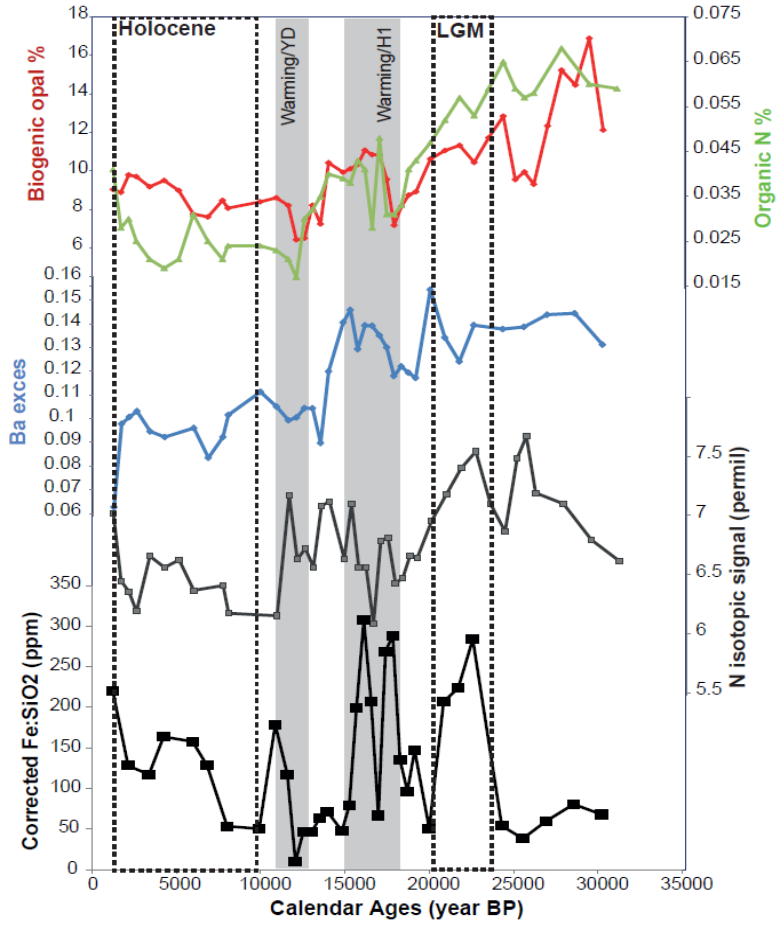

Figure 2: (from bottom to top) Diatom-bound iron concentrations (ppm), N isotopic composition of the organic matter (proxy for nitrate relative utilisation in the sea surface), excess Barium (biogenic barium) and biogenic opal and organic nitrogen concentration in the bulk sediment (biogenic inputs) versus time in sediment core S2. YD and H1 stand for Younger Drya and Heinrich event 1, respectively. All proxies show high dust supply, Fe availability, efficient nitrate utilisation and productivity during the last glacial maximum (LGM) compared to the Holocene. This relationship does not hold for the rest of the Glacial period and the termination.

Diatom-bound Fe concentrations show a very different pattern compared to the dust records and display high frequency variations that cannot be explained by changes in the dust supply. In particular, the very high levels of diatom-bound Fe during H1 and to a lesser extent, the YD occur when dust delivery to the surface ocean was already low but at times when important oceanic circulation changes in the southern ocean caused the upwelling of deep water to the surface of the subantarctic ocean[6]. This suggests that 1) dust inputs are not the main source of bioavailable Fe in the region and/or 2) dissolved iron from a deep ocean source might have reached the sea surface during the millennial scale events of the last deglaciation in the study area. In the next section we explore whether biological productivity at the core site responded to dust inputs and/or Fe availability as records by the diatoms.

3) Impact of iron biological availability on macronutrient utilisation and productivity

Paleo-productivity records (Barium excess, Biogenic opal and organic nitrogen, fig. 2) and biogenic fluxes (not shown) point to a progressive decrease in biological production and nitrate relative utilisation from the last glacial period to the Holocene and suggests an overall reduction of the efficiency of the biological carbon pump in the study area. This long term trend in paleo-productivity matches the decrease in dust input to the core site over the last 30 kyrs (fig. 1). However, in the details, and in particular during the millennial scale events recognizable during the deglaciation (H1), increases in productivity (high opal, N and Ba excess % and accumulation rates) cannot be explained by higher dust supply to the core site but match the millennial scale increases in diatom-bound Fe (H1 and YD), indicating a potential increase in soluble iron availability at times of low dust supply. This suggests an alternative source of iron to the surface ocean at these times either from deep upwelling of old water [6] or surface water. During these events, N isotopic signal is light, pointing to low relative Nitrate utilisation while biological productivity is high. Together these point to high nitrate availability in the sea surface and confirm the occurrence of vigorous upwelling of CO_2-, Fe- and nitrate-rich deep water

concomitant with the deglacial CO_2 increases as proposed in the literature. During the LGM and Holocene, N isotopes and diatom-bound Fe concentration display similar trends, indicating that relative nitrate utilisation (the efficiency of the biological pump of carbon) at these times increases/decreases with enhanced/reduced iron availability for the biota (Fig. 2).
It is unclear to us why we observe low diatom-bound Fe values during the early part of the Last glacial period (31-24 kyrs) when global and local dust input to the ocean was high and more work is needed to understand whether changes in ocean chemistry, ligand concentration or diatom assemblages could explain this counter-intuitive relationship.

Implications of the findings

While the clear discrepancy between the dust records and the new Fe biological availability reconstruction (diatom-bound metal) cannot always be straightforwardly explained (for instance from 31 to 24 kyrs BP), it confirms that dust accumulation records cannot be used to reconstruct past changes in micronutrient availability. For instance productivity variations during the deglaciations are better explained by changes in Fe biological availability (diatom-bound Fe) from a deep source than by the dust inputs. Similarly, variations in nitrate relative utilisation (limited by Fe availability in the Southern ocean today) during the Holocene and the LGM match changes in diatom-bound Fe rather than changes in dust supply. This confirms that, while more work is needed to better understand metal incorporation in diatom frustules, diatom-bound metal concentration is a much more suitable and accurate proxy for micronutrient biological availability than dust accumulation.

Appendix

The clean diatom samples were pressed into an indium foil and analysed several (10-12) times for up to 10 cycles with the iron microprobe. We used a 10nA primary beam, 25 micron image field and energy filtering (75eV).

References

[1] Martinez-Garcia, A. et al. (2011) Nature **476**, 312-U141.
[2] Baker, A. R. & Croot, P. L. (2010) Marine Chemistry **120**, 4-13.
[3] Henderson, G. M. et al. (2007) Chemie Der Erde-Geochemistry **67**, 85-131.
[4] Ellwood, M. J. & Hunter, K. A. (2000) Limnology and Oceanography **45**, 1517-1524.
[5] Pichevin, L. E., et al. (2014) Nature Geoscience **7**, 541-546.
[6] Anderson, R. F. et al. (2009) Science **323**, 1443-1448.
[7] Martin, J. H., Fitzwater, S. E. & Gordon, R. M. (1990) Global Biogeochemical Cycles **4**, 5-12.
[8] Lal, D. et al. (2006) Geochimica et Cosmochimica Acta **70**, 3275-3289.

The influence of volatiles on the interaction of mafic and felsic hydrous magmas

M. Pistone [1,2], J. D. Blundy [1], R. A. Brooker [1]

[1]School of Earth Sciences, University of Bristol, BS8 1RJ, Bristol

[2]Department of Mineral Sciences, National Museum of Natural History, Washington DC, U.S.A.

Mantle-derived mafic magmas are often invoked as a mechanism to transfer heat, mass and volatiles to felsic plutons that reside in the Earth's crust. This process has been suggested as a means of sustaining shallow magmatic bodies and triggering volcanic eruptions. Various field observations suggest that mafic, H_2O-rich magmas often intrude viscous felsic crystal-rich mushes. This scenario might be expected to produce H_2O advection from the crystallising mafic magma to the felsic magma, leading to an increase of melt fraction in the felsic mush, and subsequent mobilisation, at the same time as the mafic magma becomes quenched through a combination of thermal equilibration and H_2O loss.

The primary objectives of the proposed project is to address the following questions:

- How are processes affected by the movement of H_2O when a hydrous mafic intrusion interacts with a H_2O-undersaturated felsic crystal mush?
- What types of textures are produced by thermal quenching? What types are produced by chemical quenching? Can we discriminate the different types of mafic enclaves in the field?
- Can we develop a quantitative relationship between chemical transfer processes and crystal textures for wider application to natural igneous rocks?

The principal motivation of the present project is to interpret the natural textures and structures of felsic-mafic magma interaction observed in the field. Based on observed field relationships (e.g. Adamello Massif, Italy [1]), we wish to hypothesise the following plausible scenario whereby: (i) a felsic pluton formed in the crust (4-15 km depth) comprises a crystal mush close to its rheological lock-up point and at or close to H_2O-saturation for the interstitial melt; (ii) this is then intruded by a H_2O-rich mafic magma; (iii) during the subsequent interaction the two magmas act as a closed-system (i.e. no net loss of volatiles). This scenario might be expected to produce: a) advection of H_2O from the crystallising mafic magma to the felsic magma; b) increase of melt fraction in the felsic mush; iii) quenching of the mafic magma and remobilisation of the felsic system.

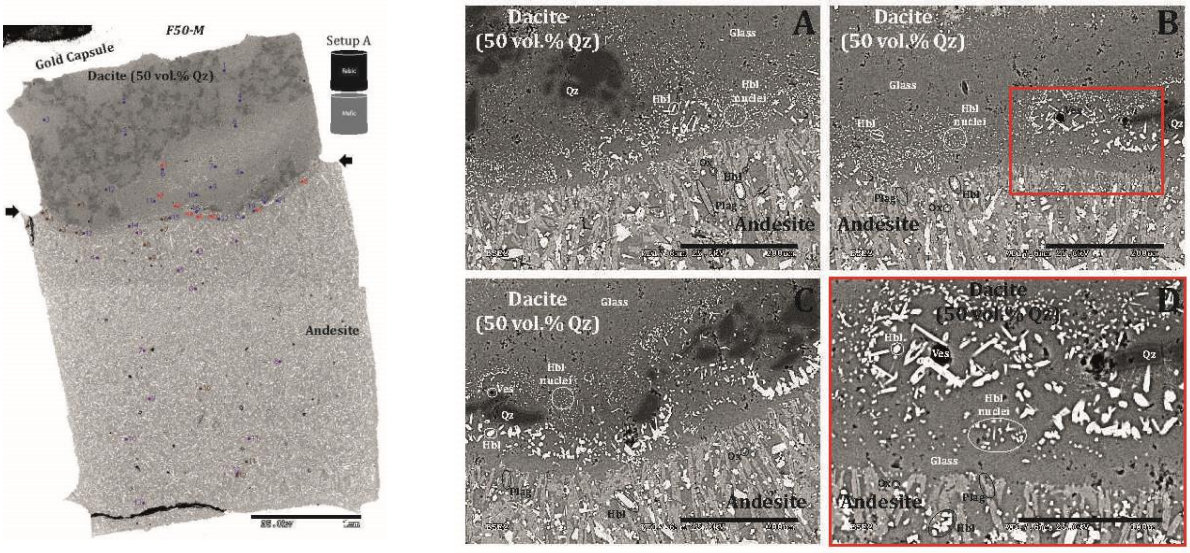

Figure 1: BSE images (25 kV; 1 nA) of the representative run product F50-M (950 °C; 5 kbar; 24 hours). The phases in the sample are: vesicles (Ves; black circles), quartz (Qz; very dark grey objects), hornblende (Hbl; very light grey objects in M and white objects close to Qz crystals in F50), plagioclase (Plag; light grey objects), oxides (Ox; white objects), and silicic glass (Glass; dark grey matrix). Red and brown dots *and* blue and purple dots indicate EPMA and SIMS analysis spots respectively. Black arrows indicate the location of the interaction interface between the two samples. The black scale bar is 1 mm in the BSE image on the left. The black scale bar is 200 µm in ***A-B-C*** and 100 µm in ***D***, which is a zoomed BSE image in ***B***.

To test this interaction scenario we conducted piston cylinder experiments to establish the petrological and mechanical evolution of H_2O-saturated (4 wt.% H_2O in the interstitial melt) dacitic crystal mush (50-80 vol.% quartz crystals) subject to a volatile supply released from a H_2O-saturated (6 wt.% H_2O) andesite magma at 500 MPa (15 km depth) and 950 °C. Experiments were run for 24 hours and run products were characterised by FEG-EPMA (not reported here), SEM, EPMA, and SIMS (Figure 1). Microstructural results for the run products display the following features 1) a reduction of crystal size in the mafic end-member towards to the interface of the two samples; 2) hornblende and plagioclase comb layering in the mafic end-member in which crystal grow from the interface towards the interior of the mafic melt; 3) formation of a crystal-free, super-liquidus melt as well as a hornblende-bearing "hybrid front" in the dacitic domain close the interface (Figure 1). The experimental and analytical results clearly demonstrate both the movement of H_2O into the felsic end-member from the mafic end-member ("H_2O uphill diffusion"; Figure 2A,B) as well as the effect of undercooling that results from a change in liquidus temperatures of the interacting magmas with changing H_2O concentrations. This has produced chemical and microstructural features that are strikingly similar textures to those observed for natural enclaves within felsic host rocks. In particular, the "quench" textures found in the run products can be explained by enhanced crystal nucleation rates driven by H_2O diffusion, rather than rapid cooling as is normally expected. For the first time to our knowledge we have generated experimentally comb layering or unidirectional solidification textures (USTs) in which crystal nucleate at the mafic-felsic interface and grow into the mafic end-member (Figure 1).

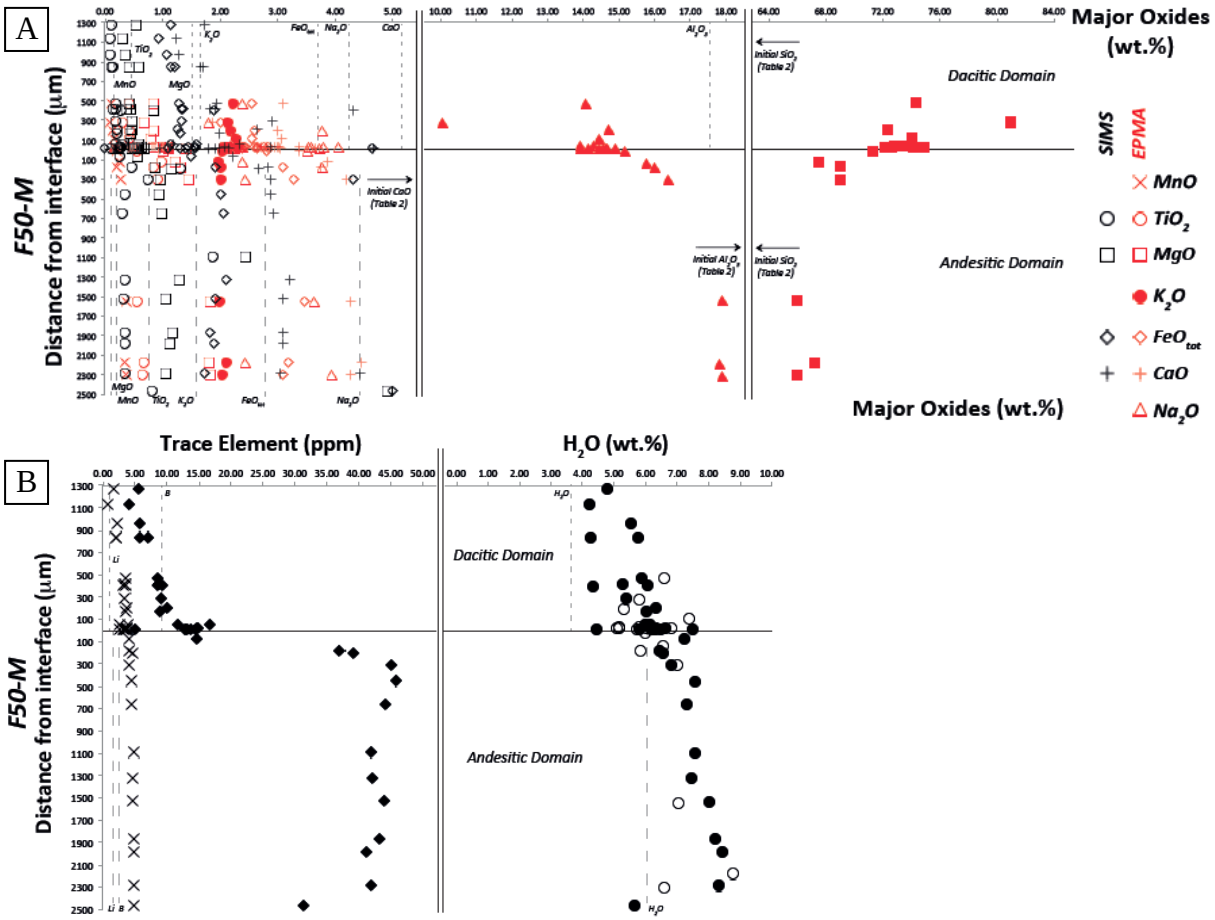

Figure 2: ***A)*** EPMA- and SIMS-based concentration profiles of major element oxides along the run product F50-M. SIMS data display larger accuracy than that of EPMA data. ***B)*** SIMS-based concentration profiles of trace elements and SIMS- and EPMA-based H_2O contents in the residual glass along the run product F50-M. Note that the bulk H_2O content (depending on the volumetric crystal fraction of the single sample) increases from the mafic to the felsic sample. Data are displayed according to the distance of the analysis spots from the interaction interface between the two samples (see Figure 1A).

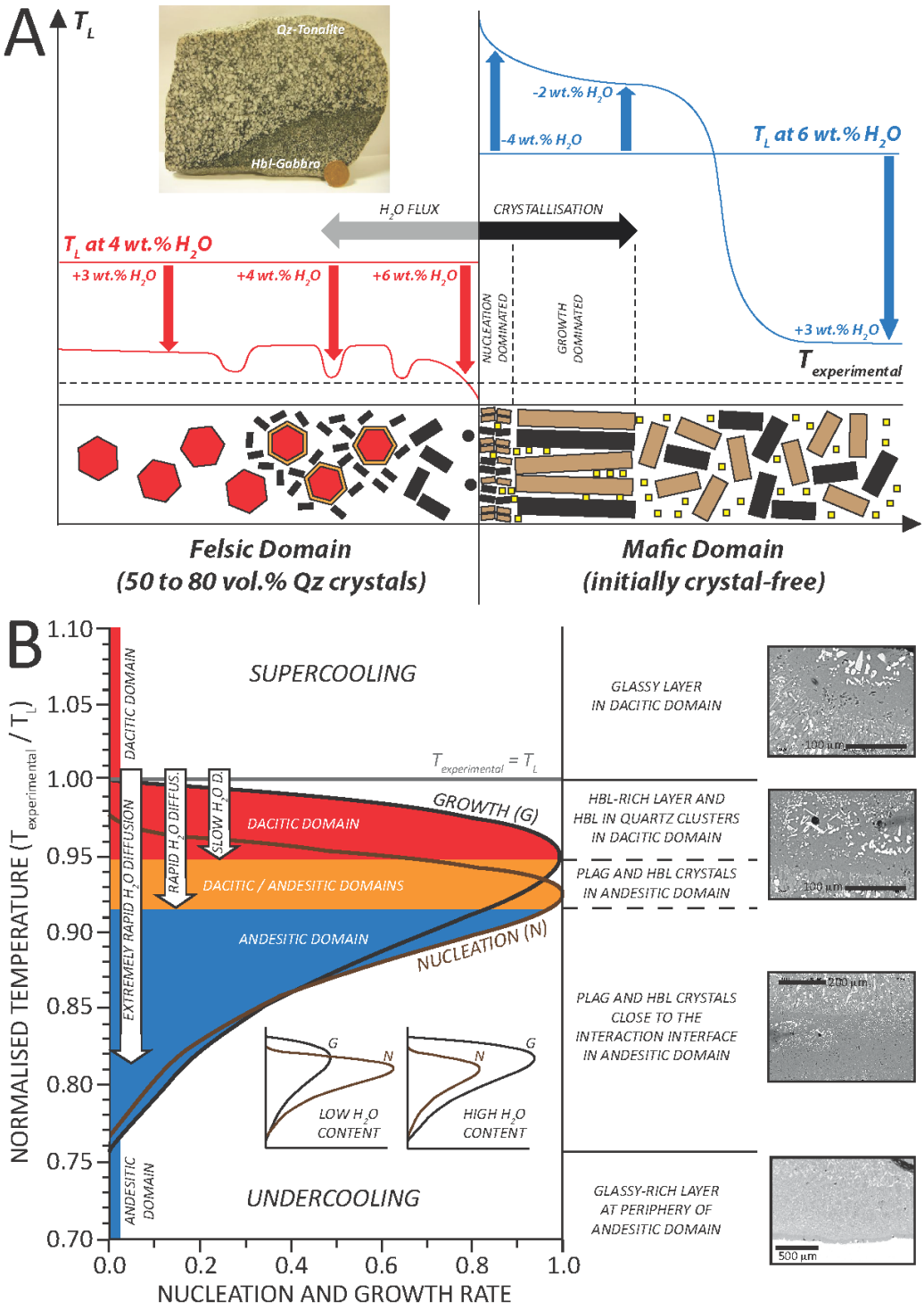

Figure 3: ***A)*** Conceptual diagram showing the effect of undercooling (i.e. change of liquidus temperature, T_L) driven by flux of H_2O during interaction between mafic (blue) and felsic (red) magmas. The diagram shows the schematics of textures generated during the experiments: quartz (red hexagons) with orange SiO_2-dissolution rims, hornblende (black rectangles), plagioclase (light brown rectangles) and Fe-Ti oxides (yellow squares). ***B)*** Normalised temperature (experimental temperature of 950 °C / liquidus temperature, $T_{experimental}$ / T_L) vs. dimensionless crystal nucleation and growth rate (after [2]). The grey line (at $T_{experimental} = T_L$, thereby $T_{experimental}$ / T_L = 1.0) separates the field of supercooling ($T_{experimental}$ / T_L > 1.0) from that of undercooling ($T_{experimental}$ / T_L < 1.0). Black and brown lines are the Gaussian trends of crystal growth and nucleation rate respectively. Red and blue areas indicate the nucleation and growth of crystals in the dacitic and andesitic domain respectively. The orange area indicates common conditions of crystal nucleation and growth in the two domains. Two inset schematics indicate that low H_2O content favours crystal nucleation rate and high H_2O content promotes crystal growth rate. On the right hand side SEM-based BSE images highlight the main microstructural features.

We propose that the interaction of mafic and felsic magmas leads to an initial flux of H_2O from the mafic to the felsic magma. The loss of H_2O raises the liquidus temperature of the mafic magma at the interface, which drives nucleation. As further H_2O diffuses out of the mafic magma, an undercooling front propagates into the mafic magma. This undercooling is less than that at the interface, hence crystal growth is favoured over nucleation and crystals grow away from the interface and increase in size. Conversely, in the felsic host the addition of H_2O reduces the liquidus temperature such that close to the interface the felsic melt is super-liquidus and a crystal-free glass forms (**Figure 3A**). Based on the distribution of H_2O in the two interacting samples of the run products, and how the liquidus temperature for the glass varies across the charge, we have determined the relationship between dissolved H_2O and textures by constructing a map of liquidus temperature and H_2O-undercooling across the run products (**Figure 3B**). The experimental and analytical results here summarised allow us to explore some fundamental concepts for understanding the origin of mafic enclaves, how volatiles contribute to crystal mush remobilisation within the Earth's crust and can trigger explosive volcanic eruptions during recharge of mafic inputs into felsic magma reservoirs, and how degassing processes may be manifest texturally. This is the first study exploring felsic-mafic magma interaction under conditions that approximate those observed in the field and shows that textures associated with mafic-felsic interactions are not simply cooling-driven in origin.

References

[1] Blundy, J.D., R.S.J. Sparks (1992) Journal of Petrology **33**, 1039-1104.
[2] Hort, M. (1998) Journal of Petrology **39**, 1063-1076.

Apatite as a tool for tracking magmatic volatile abundances: Experimental determination of H_2O and CO_2 partitioning between apatite and silicate melts

J.M. Riker[1,2], M.C.S. Humphreys[1] & R.A. Brooker[2]

[1]Department of Earth Sciences, Durham University, Durham DH1 3LE, UK
[2]School of Earth Sciences, University of Bristol, Bristol BS8 1RJ, UK

Motivation

Reliable estimates of magmatic volatile contents are crucial to our understanding of everything from to subduction zone fluxes to eruption styles and triggers. Unfortunately, the low solubilities of volcanic gases – in particular the deep-degassing CO_2 – means that they are often poorly-preserved in erupted products, and few direct measures of pre-eruptive magmatic volatile contents exist. The calcium phosphate mineral apatite can accommodate all major magmatic volatile components (H_2O, CO_2, F, Cl, S) within its crystal structure; it is also a common accessory phase in igneous rocks. As such, it has tremendous potential as a tool for tracking magmatic volatile budgets and degassing behaviour. However, a major hurdle to the development of apatite as a quantitative tool for tracking magmatic volatile contents is the absence of suitable apatite-melt partition coefficients for the key volatile species H_2O and CO_2. This project aims to generate high-quality partitioning data for H, C, F, and Cl between apatite and silicate melts through a series of high-temperature, high-pressure experiments. The specific objective of SIMS analysis was to quantify the OH^- and CO_3^{2-} contents of experimentally-generated apatite crystals and the dissolved H_2O and CO_2 contents of surrounding glasses. These data enable the direct calculation of apatite–melt partition coefficients and will elucidate the underlying mechanisms that govern partitioning systematics.

Results

We have run a suite of 16 experiments investigating the partitioning behaviour of volatiles between apatite and haplo-basaltic melt. Experiments were run in piston cylinder apparatus at 1 GPa and 1250 °C, with a slow initial cooling ramp employed to facilitate crystal growth. Each charge contained the starting basaltic powder doped with Ca-phosphate and variable proportions of H_2O, CO_2, F, and Cl. Run products are glass-rich charges containing 5–25 vol% large, euhedral apatite crystals (± minor clinopyroxene). Experimental apatites and glasses have been characterised by BSE imaging, electron microprobe, and secondary ion mass spectrometry. Apatite compositions range from near-endmember fluorapatite (3.0 wt% F), to chlorine-rich (1.8 wt% Cl), water-rich (0.8 wt% H_2O), and carbon-rich (1.8 wt% CO_2) solid solutions. Associated experimental glasses contain 0.7–11.0 wt% H_2O, <0.1–1.7 wt% CO_2, 0.0–2.4 wt% F, and 0.0–0.8 wt% Cl. Nernst partition coefficients ($D_X^{ap-melt}$ = $X_{apatite}$ (wt%)/X_{melt} (wt%)) calculated from these data indicate that both

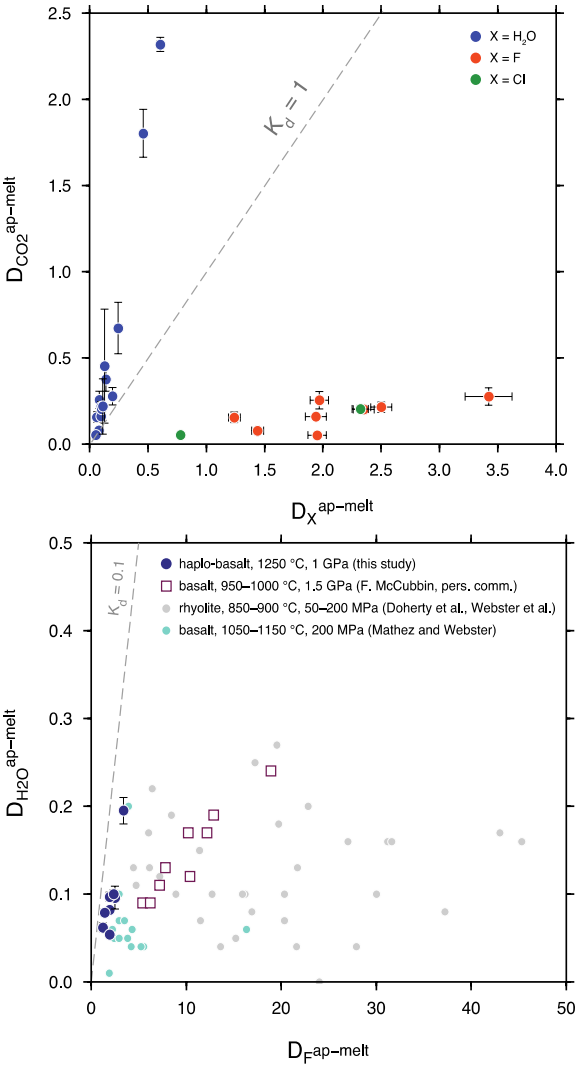

Figure 1. Apatite–melt Nernst partition coefficients (D) for H_2O, CO_2, F, and Cl calculated from the data measured in this study. Exchange coefficients, K_D, are given by the ratios (slopes) of two partition coefficients. CO_2 is incompatible in apatite compared to F and Cl but more compatible than H_2O. H_2O is highly incompatible compared to F, in agreement with data from the experimental literature.

F and Cl are highly compatible in apatite compared to melt (D almost always >1; Fig. 1), water is incompatible (D always <0.6 and typically <0.1), and CO_2 may behave compatibly or incompatibly (D = 0.1–2.3), depending on the concentrations of other volatile components in the system. Partitioning data are however better expressed in terms of exchange coefficients ($K_D^{X–Y} = D_Y^{ap–melt}/D_X^{ap–melt}$) or the ratio of the partition coefficients of two components; Fig. 1), which describe the relative compatibilities of required (rather than trace) components competing for the same structural site. Calculated $K_D^{F–H2O}$, $K_D^{Cl–H2O}$, and $K_D^{CO2–H2O}$ are consistently much less than 1 (0.04–0.13), indicating incompatible behaviour of H_2O compared to other components. Calculated $K_D^{F–CO2}$ and $K_D^{Cl–CO2}$ are also low (0.03–0.13). In contrast, $K_D^{H2O–CO2}$ are consistently greater than 1 (1.0–3.9), as also indicated by the steep slope of D_{CO2} versus D_{H2O} in Fig 1.

Discussion

Data obtained at the IMF establish three key findings. First, H_2O is highly incompatible in apatite compared to melt, in keeping with the results of previous experimental studies, which are largely based on indirect measurements of apatite and/or glass H_2O contents [1–3, F. McCubbin, pers. comm.]. Second, CO_2 can partition readily into apatite at crustal temperatures and pressures. Finally, CO_2 is significantly *more* compatible than H_2O in apatite at our run conditions. Apatite therefore has the potential to be a sensitive tracer of magmatic CO_2 contents, much in the way it is currently used as a melt hygrometer. Importantly, our findings indicate that in magmatic systems with H_2O–CO_2-rich fluids (i.e. halogen-poor systems), apatite can preserve higher absolute CO_2 concentrations than surrounding melt. In this way, apatite could represent a substantial improvement on existing tools for tracking pre-eruptive magmatic CO_2 contents, such as phenocryst-hosted melt inclusions. Our partitioning data also provide insight into the mechanisms of CO_2 substitution in apatite at our run conditions. The data suggest that CO_2 exchanges primarily for other volatile components sitting on the mineral's central channel site ("Type-A" substitution, i.e. $CO_3^{2-} + [] = 2X^-$, where X is another channel anion and [ ] is a vacancy [4]), as opposed to coupled substitution for a phosphate group ("Type-B" substitution). This inference is based on a lack of stoichiometric correlation between carbonate and phosphate groups. It cautions against the calculation of apatite H_2O contents "by-difference" assuming simple, ternary (F+Cl+OH) occupation of the channel site.

Future Work

To ensure the broadest possible application of experimental partitioning data, it is important to extend our experiments to a range of compositions, pressures, and temperatures. To this end, we are currently running experiments on a more evolved, trachytic Campi Flegrei composition at both lower crustal (1 GPa, 1250 °C) and upper crustal conditions (0.2 GPa, 900 °C). We will analyse these experiments during remaining facility time in April 2015. Experimentally-determined partitioning data will ultimately be used to invert the compositions of natural apatite crystals for pre-eruptive melt H_2O and CO_2 contents, with application to the Campi Flegrei and Laacher See Tuff (Germany) volcanic systems. Analysis of volatiles in natural Laacher See apatites is the subject of a complementary IMF project and will take place in May 2015.

References

[1] E.A. Mathez and J.D. Webster (2005) Geochimica et Cosmochimica Acta **69**, 1275–128
[2] J.D. Webster et al. (2009) Geochimica et Cosmochimica Acta **73**, 559–581
[3] A.L. Doherty (2014) Chemical Geology **384**, 94–111
[4] M.E. Fleet and X. Liu (2004) Journal of Solid State Chemistry **177**, 3174–3182

Volatile content of the south Patagonian subcontinental lithospheric mantle

E. E. Rooks[1], S. A. Gibson[1], C. M. Petrone[2] & P. Leat[3]

[1]Dept of Earth Sciences, University of Cambridge, Downing Street, Cambridge, UK
[2]Dept of Earth Sciences, Natural History Museum, Cromwell Street, London, UK
[3]British Antarctic Survey, Madingley Road, Cambridge, UK

Introduction & Objectives

Water content is known to affect many physical and chemical properties of the upper mantle, including melting temperature and viscosity. It is hosted by hydrous phases, such as amphibole and phlogopite, and also by more dominant, nominally-anhydrous mantle minerals (e.g. olivine and pyroxene). The latter have the potential to incorporate hundreds of ppm of water in point defects, and may explain geophysical observations such as seismic and conductivity anomalies in the upper mantle [1]. However, the significance of the reported concentrations of H_2O in nominally anhydrous minerals in mantle xenoliths is still a subject of debate - primarily due to the effects of post-entrainment loss. Fluorine is thought to be able to produce similar effects, and has been discovered to be slightly more compatible in mantle minerals than H [2]. The main objective of this research was to measure water contents in olivines and pyroxenes from alkali basalt-hosted mantle xenoliths sourced from south Patagonia (Pali Aike) and the Antarctic Peninsula. It is thought that the fluid liberated from a subducting slab hydrates the overlying mantle wedge above a long-lived subduction zone may be enriched in volatiles from the subducting slab. This study aimed to test the hypothesis that the mantle beneath Pali Aike and the West Antarctic Peninsula has been hydrated due to the long-lived subduction zone beneath this region. We measured H (calculated to ppm H_2O), F, B and Li, and combined these with existing REE and trace element data in an attempt to trace any subduction influence in these samples.

Results

The SIMS data show that the amples are relatively dry: H_2O contents of olivine span 0-49 ppm, orthopyroxene 150-235 ppm and clinopyroxene 100-395 ppm. On average, West Antarctic samples are slightly more hydrated than those from Pali Aike. Moreover, there is no evidence of any strong partitioning effect between the two pyroxenes (Fig. 1). These H_2O concentrations fall within the global measured range for off-craton mantle minerals[3]. F is most highly concentrated in clinopyroxenes, concentrations are around three times higher in than in orthopyroxene. F contents of olivine are low in all samples, but, as with H_2O, are slightly higher in samples containing garnet. Concentrations of both H_2O and F do not appear to have any relationship with lithology. One Antarctic sample contains up to 200 ppm F in clinopyroxenes, which is significantly higher than other samples. This correlates with higher than average H_2O, howeve,r the highest concentrations are not found in this sample. Li ranges from 0.5-3 ppm in pyroxenes, and 1.3-4.8 ppm in olivines. B was below detection in all samples.

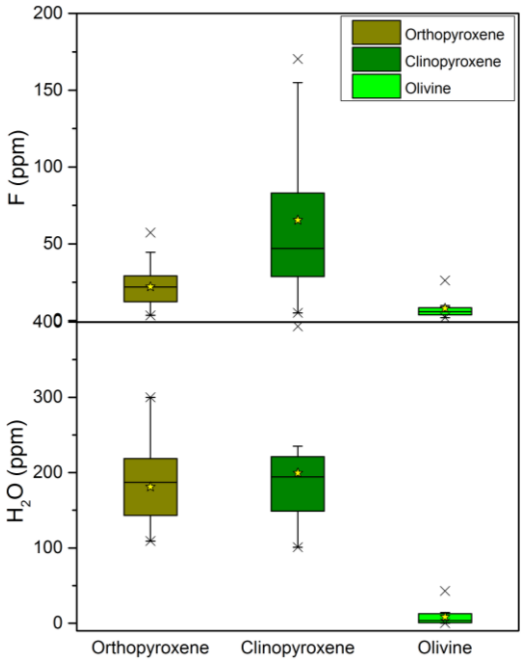

Figure 1: Concentrations of Fluorine (top) and H_2O (bottom) in mantle minerals. Star shows the mean average. Concentrations of H_2O in both pyroxenes are similar – however clinopyroxene is noticeably more fluorine rich than orthopyroxene.

Discussion

We attribute low H_2O concentrations in olivine to diffusive loss, either by exchange with the host magma, shallow level degassing or during cooling. F/Nd ratios of MORB are around 20.5, with arc magmas displaying higher ratios and while some clinopyroxenes have similar or lower values than

MORB, others show F/Nd >> 20.5, implying potential interaction with subduction-related melts. F appears to be approximately three times more compatible in clinopyroxene than orthopyroxene (Fig 1).That H does not appear to show partitioning between the pyroxenes indicates that F may be slightly decoupled from H, or that it has simply undergone less diffusive loss during ascent. F correlates well with TiO_2 in clinopyroxenes. Since higher TiO_2 may be attributed to interaction with a basaltic melt, this points towards the potential of F addition through basaltic metasomatism. The highest F contents in Pali Aike samples were found in a garnet-spinel lherzolite. This sample displays petrographic evidence of melt-rock reaction, which adds weight to the theory of F addition by metasomatism. This theory raises the question of where the F is sourced from: is it from the deeper mantle or subduction zone related fluids? Calculated bulk F contents range from 14 ppm in Pali Aike (similar to the estimated 12 ppm of SCLM [2]) up to ~ 40 ppm in West Antarctica, which exceeds even that calculated for OIB source (up to 34 ppm). Positive correlation between F content and TiO_2 in clinopyroxenes is indicative of metasomatism by basaltic fluids (Fig.3). However, the highest concentrations of F, found in one Antarctic sample, do not correlate with the highest TiO_2. It is unclear what has caused the higher F contents in this sample, but it also displays elevated F/Nd (~45). This potentially points towards a subduction-related fluid source, however further data is required to confirm this.

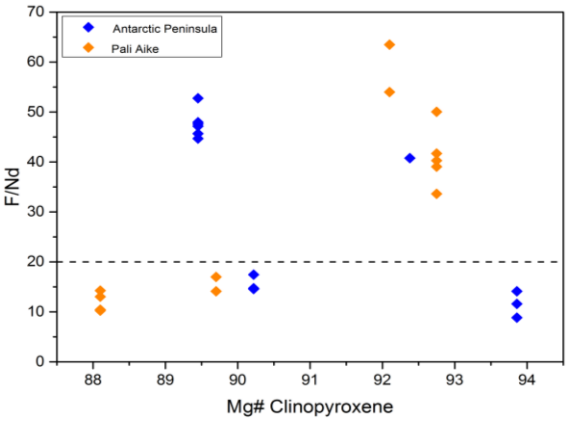

Figure 2: F/Nd of clinopyroxenes in both localities, plotting against Mg#. MORB has F/Nd of 20.5

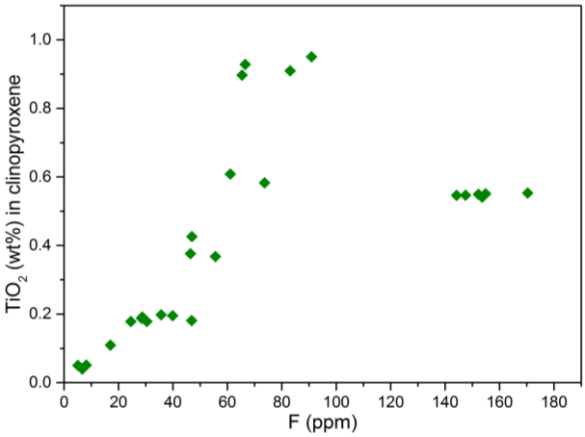

Figure 3 shows the correlation between F concentration and TiO_2 content in clinopyroxenes

Conclusions & Further Work

We attribute low water content in olivines to diffusive loss-post entrainment. Water has also likely been lost from pyroxenes, suggested by their lack of strong correlation with other components. F may be used to investigate covariations between volatile elements and other components, assuming that F and H have the same source. No significant enrichment appears to have taken place in either locality. Principal component analysis (PCA) indicates that the Antarctic Peninsula and Pali Aike may display different primary controls on volatile distribution. At this stage, we attribute the trends in Pali Aike to be mainly melt-depletion related, and trends in the Antarctic Peninsula to be slightly different. In order to form better conclusions and stronger interpretations, we will be collecting more data from both regions, with the addition of Cl, since F/Cl has been shown to be enriched in the mantle wedge above subduction zones. We will also correlate volatile data with oxidation state of the mantle, calcuated from the ferric iron contents of spinels and garnets, measured by XANES.

References

[1] Karato, S., 2010, Tectonophysics, **481**(1-4), 82–88
[2] Koga, K., et al., 2003, Geochem., Geophys, Geosys., **4**(2)
[3] Beyer, C. et al., 2012, EPSL, **337-338**, 1-9
[4] Bonadiman et al. 2009., Eur. J. Mineral. **21**, 637–64

Mixing between degassed and supersaturated, contaminated melts control volatile systematics of the 1669 eruption, Mt Etna, Italy

L. Salem[1], M. Edmonds[1], J. Maclennan[1], R. A. Corsaro[2]

[1]Department of Earth Sciences, University of Cambridge, Cambridge CB2 3EQ, UK
[2]National Institute of Geophysics and Volcanology, Rome, Italy

Abstract
The melts feeding Mt Etna, Italy, are rich in volatiles and drive long-lasting powerful eruptions of basaltic magma in both effusive and explosive styles of activity. The continual influx of mantle-derived volatile-rich magma controls the major compositional and eruptive features of Mount Etna [1] but magma mixing has been recognised as an important process driving large eruptions [2]. We have analysed two eruptions at Mt Etna, the largest effusive eruption in 1669, and a recent explosive eruption in 2000. We aim to understand the source of melts feeding the plumbing system, the processes affecting the melts during storage and ascent, such as mixing, crystallisation, degassing and assimilation, and how their geochemical evolution controls eruption dynamics and style.

Methodology
We collected samples from the main 1669 cinder cone at Monti Rossi, SE Etna flank and received tephra samples from our collaborator at INGV for the 2000 eruption. We crushed tephra, picked olivine crystals, and polished. We analysed olivine-hosted glassy melt inclusions with no visible shrinkage bubbles for volatiles and a full suite of trace elements using 4f-ion probe (SIMS) in Edinburgh, and major elements using electron microprobe (EPMA) in Cambridge.

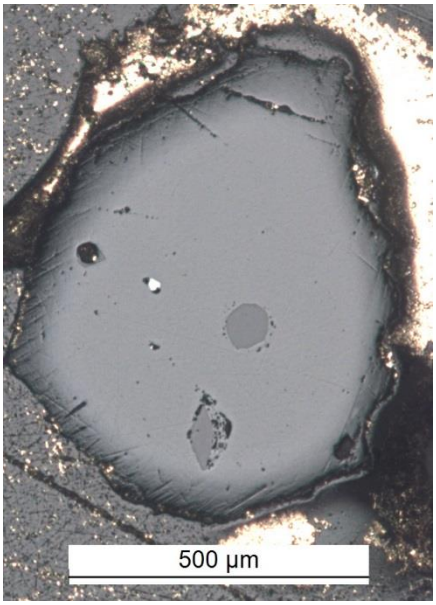

Figure 1. Reflected light microscope image of an olivine crystal with hosted melt inclusions picked and polished from 1669 tephra.

Results
We observe considerable heterogeneity in terms of both trace and volatile elements in the melt inclusions for both eruptions. There is a strong positive correlation between Sr and CO_2 and between CO_2 and S in the 1669 MIs, which has not been observed previously, and a similar but less strongly positive correlation between CO_2 and Sr in the 2000 MIs. H_2O appears to be re-set to ~1.6-1.7wt% in almost all 1669 MIs measured, but water concentration is more variable in the 2000 MIs, perhaps suggesting variable degrees of degassing during MI entrapment.
In the 1669 MIs H_2O, CO_2 and sulphur concentrations range up to 2.0 wt%, 1200 ppm and 1900 ppm respectively. H2O/Ce is <150 in MI hosted by olivines with Fo_{73-75} mol%. CO_2/Nb is low, suggesting CO_2 has been subject to extensive degassing or sequestration into a shrinkage bubble. There is a relationship between "degree of enrichment" (LREE/HREE, Ce/Y) and volatile content, which may indicate mixing. There is a strong negative correlation between CO_2 and Nb which contrasts with the positive correlations measured in undegassed melt inclusions from the Siqueiros fracture zone on the East Pacific Rise [3] and calculated for undegassed Mid-Atlantic Ridge basalts [4]. Discussion of these results will focus on the 1669 MIs. The 2000 MIs are more degassed in CO_2 and S and there is generally more spread in the data with weaker correlations. Further statistical work is needed to investigate the degree of correlation and comment on the melt evolution.

Discussion
The 'apparent' negative CO_2-Nb correlation could be due to a combination of CO_2 saturation in the MI and sequestration into a shrinkage bubble, reducing the CO_2 measured in the melt, and Nb becoming

more concentrated in the MI after Post-Entrapment Crystallisation (PEC). However, the low degree of PEC (<1%) and analysis of shrinkage-bubble-free MIs negates this reasoning and so another mechanism is required to explain the relationship. MIs with low Nb and high CO_2 are also lower in LREE-enrichment compared to the high Nb, low CO_2 MIs. This is evidence for mixing between two different melt sources with different degrees of LREE-enrichment and CO_2 exsolution. CO_2 rich MIs show Sr enrichment and degassed MIs have lower Sr, due to fractional crystallisation of plagioclase, removing Sr from the melt. Sulfur is also strong positively correlated with CO_2. MIs with high CO_2 have high S, suggesting the melt is supersaturated in both C and S. The LREE-enriched melt is more degassed in CO_2 and S and so is supersaturated at shallower depths. These observations confirm that two sources of melt, at different pressures within the crust, are involved in the final MI mixing array.

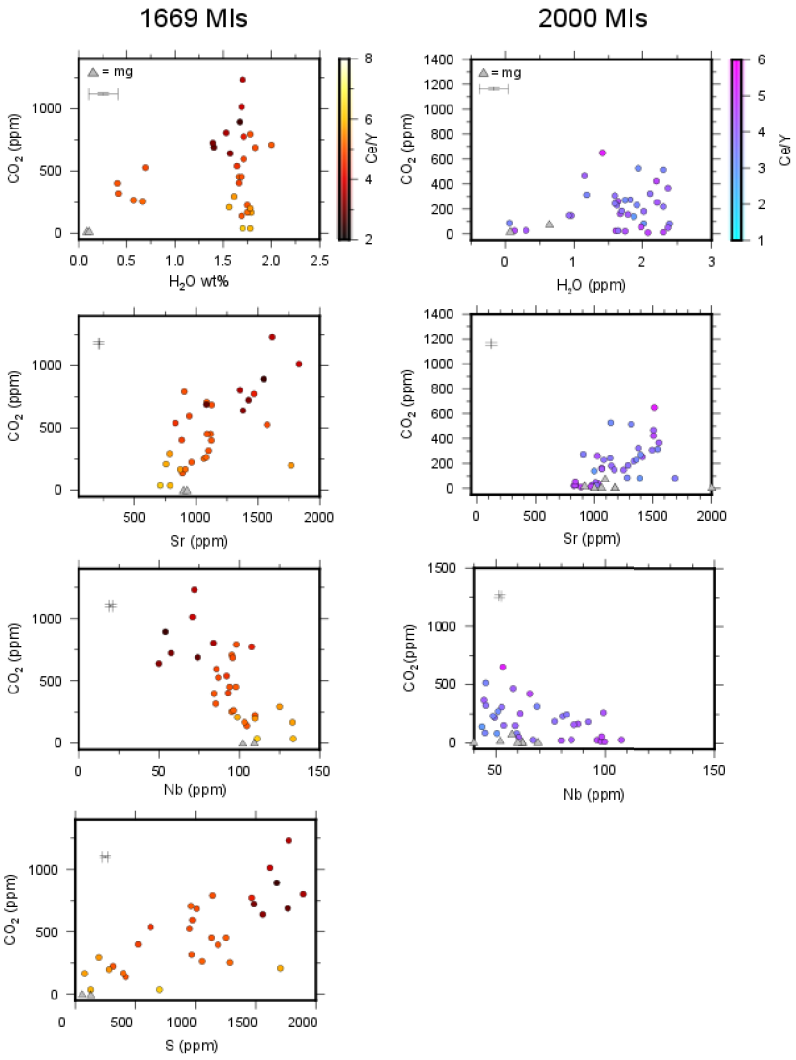

Figure 2. Results from SIMS MIs analysis, 'hot' colours, 1669 MI analyses; 'cool' colours, 2000 MI analyses; grey triangle, matrix glass analyses; error bars marked.

To preserve supersaturation and a positive correlation between CO_2 and S the ascent of the deeper, undegassed melt to shallower pressures must have been rapid to preserve the volatile signature before mixing with the resident, more evolved melt stored at shallower depths. The olivine crystals erupted all have a $Fo_{73\text{-}74}$ wt%, independent of the correlation trends. This suggests that the melts mixed to varying degrees before final olivine crystallisation.

Conclusions and future work

The MI array represents mixing of two different composition melts. A more evolved, LREE-enriched, Sr-poor, degassed melt, and a less LREE-enriched, Sr, S and C enriched melt. Ascent of the deeper melt must have been rapid to preserve S and C supersaturation and mix with the more degassed, evolved shallower melt. Further work includes completing the statistical analysis of the 2000 eruption and analysis of more Etnean MIs from different eruptions to see if the same trends in CO_2, Nb, Sr, and S hold true for the plumbing system at Etna more generally.

References

[1] Metrich, N. & Wallace, P.J. (2008) Reviews in Mineralogy and Geochemistry **69**, 363-402; [2] Kamenetsky et al., (2007) Geology **35**, 255-258; [3] Saal et al., (2002). Nature **419**, 451-455; [4] Cartigny et al., (2008) Earth Planet. Sci. Lett. **265**, 672–685.

Oxygen isotopes in vertebrates: correlating between calcium phosphate and calcium carbonate

I.J. Sansom & J.R. Wheeley

School of Geography, Earth and Environmental Sciences, University of Birmingham, Birmingham B15 2TT

Introduction

The products of biomineralisation in vertebrates are increasing used as archives of past climate change with both calcium phosphate (teeth, scales and bone) and calcium carbonate (otoliths – "ear stones") receiving attention. Surprisingly, despite the co-occurrence of the two mineral phases in individual fish, there have been no prior attempts to examine the isotopic signal from the same specimen and hence correlate between seawater temperature values derived from $CaPO_4$ and $CaCO_3$ tissues. Utilizing teleost fish from constrained and well-characterised water bodies, we propose to rectify this obvious gap in testing $\delta^{18}O$ values through ion microprobe analyses.

Teleost fish (the most diverse and abundant clade of the ray-finned fish which have a fossil record extending back into the Triassic) have multi-component teeth consisting of cap enameloid, dentine and collar enamel [1] that are continually shed and replaced, typically on a two week cycle. Otoliths (literally ear stones) are found within the inner ear of vertebrates and, in teleosts, record the life history of the individual fish due to incremental, centrifugal deposition of calcium carbonate (aragonite) and have experimentally been demonstrated to be stable unless subjected to high temperature [2].

Material and methods

Upon death, a single specimen of barracuda (*Sphyraena* sp.) was collected from the National Sea Life Centre (Birmingham) having been resident in a tropical tank for over three years. The head region of the specimen was defleshed and the jaw dentition (**Fig. 1**) and sagittal otoliths (**Fig. 2**) were dissected out and cleaned. Cut blocks of the dentary, palatine and premaxilla were prepared with a view to analysing the dentition associated with these bones, and a single sagittal otolith were embedded within EpoThin resin blocks, cleaned with dilute H_2O_2 and NaOH, and polished for $\delta^{18}O$ analyses on the NERC Cameca 1270 ion microprobe at the University of Edinburgh. Samples were referenced to Durango apatite (teeth) and calcite (otoliths) standards.

Fig. 1. Premaxilla dentition of barracuda (*Sphyraena* sp.) in external lateral (A) and internal lateral (B) views, posterior to the left and anterior to the right.

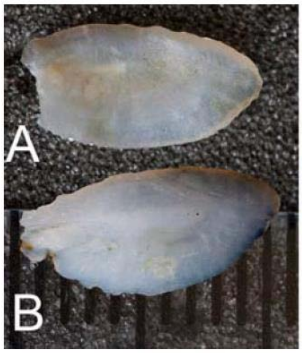

Fig. 2. Saggital otoliths from barracuda (*Sphyraena* sp.) in external lateral (A) and medial lateral views (B).

Results

Analytical tracks were taken across individual teeth of *Sphyraena* sp., with sampling focusing on the tips of the teeth above the cap enameloid/dentine junction to avoid variation inherent within the dentine of vertebrate teeth. There was no statistical difference between the enameloid values across all teeth analysed, irrespective of tooth location. The aggregated values for these phosphate analyses was then compared with two recent phosphate temperature equations [3,4], with those predicted by the former falling closer to the actual tank temperature of 24.5°C (**Table 1**). Analytical tracks were taken across the otolith to determine a robust average value and to counteract varying signals from aragonite precipitated in the initial growth phase with that 'grown' in the Birmingham tanks. Values obtained for the otolith showed a range 30.3‰ – 33.4‰ with the average temperature estimate (24.6°C) equating to the actual (24.5°C) tank temperatures with a remarkable degree of fidelity; variation within the otolith may result from short-term fluctuations in the water composition of the Birmingham

tank due to evaporation and recharge. This contrasts with a lower temperature derived from otolith $\delta^{18}O$ from the same specimen of *Sphyraena* sp. by TC/EA (Table 1); we suspect the deviation between these two methods is a consequence of the bulk sampling undertaken by micromilling with inclusion of a 'pre-Birmingham' water geochemistry from the otolith core as a result of the 'bulk' approach and, potentially, vaterised components of the otolith prepared for TC/EA.

	Average $\delta^{18}O$ (‰, SMOW)	Temperature (T°C) estimate based on equation of Pucéat et al. [3] $T(°C) = 118.7(\pm4.9) - 4.22(\pm0.2)* (\delta_{18}O_{PO_4} - \delta_{18}O_{H_2O})$	Temperature (T°C) estimate based on equation of Lecuyer et al. [4] $T(°C) = 117.4(\pm9.5) - 4.50(\pm0.43)*(\delta_{18}O_{PO_4} - \delta_{18}O_{H_2O})$	Temperature (T°C) estimate based on aragonite equation used by Kobashi et al. [5] $T(°C) = 19.7-4.34*(\delta_{18}O_{arag} - \delta_{18}O_{H_2O})$
Sphyraena sp. teeth	25.3 (n=22 analyses)	23.7 #(20.5–26.8)	16.1 #(12.7–19.4)	
Sphyraena sp. otolith (ion microprobe)	Overall: 31.6 (n=89 analyses)			24.6 #(21.4–27.9)
Sphyraena sp. otolith (TC/EA)	32.6 (n=two otoliths samples)			20.4 #(17.2–23.7)

Table 1. Seawater temperature estimates from phosphate and aragonite *Sphyraena* sp. biomineralised tissues. #Range of temperatures taking into account documented 1.5‰ annual variation in oxygen isotopic composition from the National Sea Life Centre tanks.

Future work

Our results indicate a degree of congruence in the derived temperatures from the phosphate and carbonate mineral phases based upon the equations of Pucéat et al. [3] and Kobashi et al. [5]. Future work will seek to: extend this study using teleosts from a range of host temperatures and across tanks of different water compositions in order to refine the existing temperature equations; develop discrete analyses of all of the tissues *viz* cap enameloid, collar enamel, dentine in the teleost teeth and also the different mineral phases in the allied the otoliths (sagittae, lapilli and asterisci); correlate between teleost fish phosphate and chondrichthyan phosphate (initial work conducted during IMF470/1012); and understand the offset in values obtained via ion microprobe and TC/EA (this is also evident in fossil phosphate tissues JRW pers obs).

Acknowledgements

IMF497/1013 to IJS. The National Sea Life Centre are thanked for allowing this research to be conducted and assisting with sampling. We are indebted to Mike Hall (Edinburgh) and Paul Hands (Birmingham) for their advice and help in sample preparation, and notably to John Craven (Edinburgh) for his advice and assistance in analyses.

References

1. M.M. Smith 1992. Microstructure and evolution of enamel amongst osteichthyan fishes and early tetrapods, in *Structure, Function and Evolution of Teeth* (ed. P. Smith).
2. C.F.T Andrus and D.E. Crowe, 2002 Journal of Archaeological Science **29**, 291–299.
3. E. Pucéat et al. 2010. Earth Planetary Science Letters **298**, 135-142.
4. C. Lécuyer et al. 2013 Chemical Geology **347**, 217–226.
5. T. Kobashi et al. 2004. Paleoceanography **19**, 1-16.

An experimental calibration of the Al-in-olivine geothermometer in the CMAS system

G. Fitton & D. Schaub

School of GeoSciences, University of Edinburgh, Edinburgh EH9 3FE, UK

Background

There is evidence from mantle xenoliths [1] that Al solubility in olivine is temperature dependant. This has led to a new and very useful technique for measuring eruption temperature of primitive basaltic magmas by measuring the Al content of olivine phenocrysts [2]. The objective of Douglas Schaub's MSc project was to calibrate the solubility of aluminium in pure forsterite in part of the CaO-MgO-Al_2O_3-SiO_2 system. The concentration of Al was likely to be ~0.05% and so difficult to measure accurately by electron microprobe, hence an application for an ion probe pilot study was submitted. The intention was to analyse a suite of forsterite crystals synthesised at 1 atmosphere pressure and various temperatures in the synthetic anorthite-forsterite-diopside (An-Fo-Di) system.

Results

Three gels were prepared with different compositions within the An-Fo-Di system and heated to various temperatures for periods of about 72 hours in order to achieve equilibrium. A muffle furnace was used and temperature was monitored with a Re-W thermocouple. The experimental charges were removed from the furnace at the end of each run and cooled quickly to ambient temperature, resulting in glass with forsterite ± anorthite and diopside crystals. The charges were mounted in epoxy resin and polished prior to ion-probe analysis. The results are shown below.

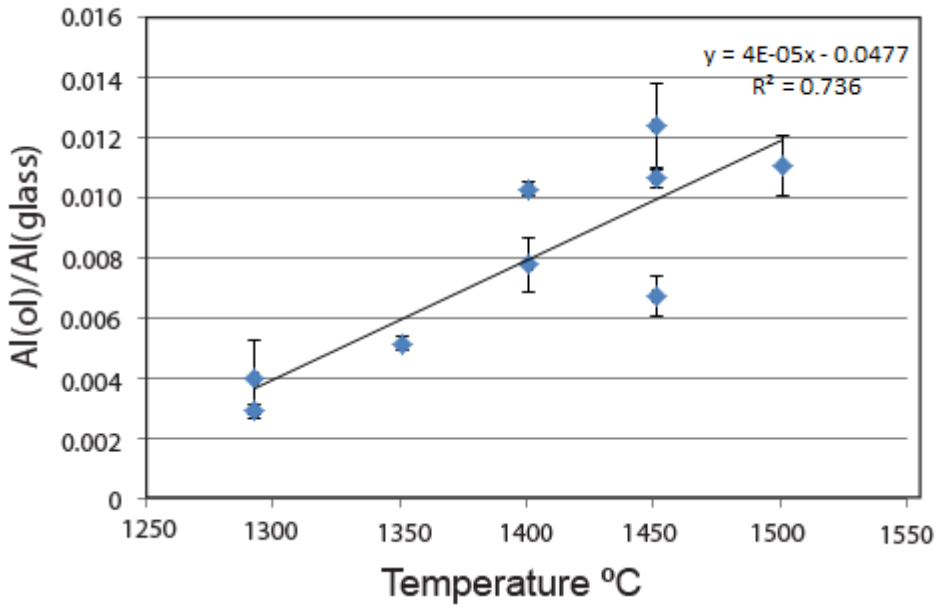

Although there is a correlation between temperature and the olivine-glass distribution coefficient, the relationship is not a simple one. Al concentration is clearly not proportional to Al activity even in such a simple system. Further work is needed in order to calibrate the method.

References

[1] J.C.M. De Hoog, L. Gall & D.H. Cornell (2010). Chemical Geology **270**, 196-215.
[2] L.A. Coogan, A.D. Saunders and R.N. Wilson (2014). Chemical Geology **368**, 1-10.

(PAGE INTENTIONALLY LEFT BLANK)

Understanding the role of degassing in setting the redox state of mid-ocean basalts

O. Shorttle[1], M. Edmonds[1] & B. Murton[2]

[1]Department of Earth Sciences, University of Cambridge, CB1 3BX, UK
[2]National Oceanography Centre, University of Southampton, Southampton, SO14 3ZH, UK

Aim

Recent work has suggested that the recycling of material from Earth's surface back into its interior creates domains of locally reduced mantle that are sampled today along Earth's mid-ocean ridges [1]. This is a surprising result given that for the last ~600 Myr conditions in Earth's oceans and atmosphere have been highly oxidising, and that the upper mantle sampled by mid-ocean ridges is believed to have been contaminated by recycling during this period [2]. In this project we test the hypothesis put forward by [1] that enriched domains are reducing. The key strength of our study is the coupling of ion probe measurements of volatile concentrations (H, C, F, Cl, B) with x-ray absorption near edge structure (XANES) spectroscopy determinations of ferric iron proportions on a suite of samples from the Reykjanes Ridge south of Iceland. By combining these two measurements on the same suite of samples we will have the potential to understand how magmatic processes such as crystallisation and degassing affect the oxidation state of magma. This will enable us to resolve any mantle signal of changing oxidation state present in the dataset from the influence of the enriched Iceland plume on the northern Reykjanes Ridge.

Results

Ion probe data was collected in March 2014, followed by XANES data at Diamond Light Source in August of the same year. Figure 1 reports our XANES results, presented as the proportion of ferric iron to total iron in each sample ($Fe^{3+}/\sum Fe$) as a function of distance from the Iceland plume. This dataset contains two striking features: 1. Basalts become more oxidised (higher $Fe^{3+}/\sum Fe$) towards Iceland; 2. As well as long wavelength changes in geochemistry as Iceland is approached, there is also variability on the scale of single eruptions, in particular with the enriched seamount 14D which is as oxidised as basalts erupting 700 km to closer to the centre of the Iceland plume. Colouring the points in Figure 1 by Zr/Y (a proxy for source enrichment) indicates that this change in oxidation towards Iceland correlates with increasing enrichment of the source. This result is the opposite of that found by [1], making it critical to include volatile element data in order to understand how primary mantle derived $Fe^{3+}/\sum Fe$ could have been altered by degassing.

Our new ion probe volatile data is presented in Figure 2 along with ridge axial depth, the shallowing of which is the main driver of degassing towards Iceland (the major element chemistry of the lavas remains approximately constant). Of the volatile elements carbon is degassing over the whole ridge length, with concentrations systematically decreasing towards Iceland. However, the more soluble elements H, Cl and F actually show in increase in concentrations towards Iceland, whilst B remains roughly constant. It is important to note that whilst CO_2 decreases over much of the ridge length up to 1000 km, it is only in the final 600 km that basalts become more oxidised, at which point the CO_2, concentrations in the melt are nearly constant. These results indicate that degassing of H, C, Cl or F cannot be controlling the along-ridge changes in $Fe^{3+}/\sum Fe$ and that instead changes in $Fe^{3+}/\sum Fe$ are likely to be a mantle derived signal.

Further work

A key volatile element to add into the interpretation of our XANES data is S, which potentially has a large effect on magmatic redox and will exsolve from the melt at a similar point to water. With existing low precision data we can resolve that for most samples S degassing has not occurred, however, for the three samples erupted at <500 m water depth an extra correction for degassing is likely required.

References

[1] E. Cottrell & K.A. Kelley (2013) Science **340**, 1314-1317; [2] M.B. Anderson et al. (2015) Nature **517,** 356-359; [3] B. Murton et al. (2002) Journal of Petrology **43:11**, 1987-2012; [4] V.C. Kress & I.S.E Carmichael (1991) Contributions to Mineralogy and Petrology **43:11**, 1987-2012

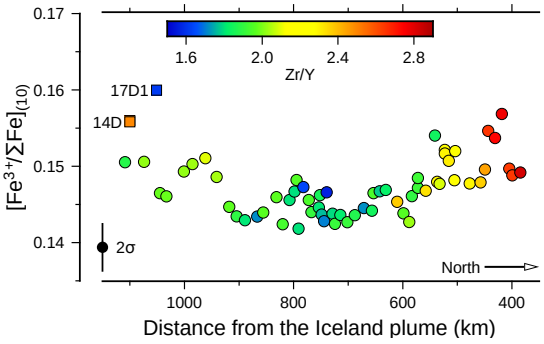

Figure 1 (above): The results of our XANES analyses of the Reykjanes Ridge glasses at Diamond Light Source. The ferric iron proportions ($Fe^{3+}/\sum Fe$) of the glasses are plotted against distance from the Iceland plume centre. Ferric iron proportions have been corrected for fractional crystallisation to MgO = 10wt% and samples are coloured by Zr/Y, a proxy for source enrichment. The key result is that as Iceland is approached basalts become both more enriched (higher Zr/Y) and more oxidised (higher $Fe^{3+}/\sum Fe$). In addition to this long wavelength signal of increasing oxidation towards Iceland, the enriched seamount 14D (square symbol) is also relatively oxidised. Trace element data from [3].

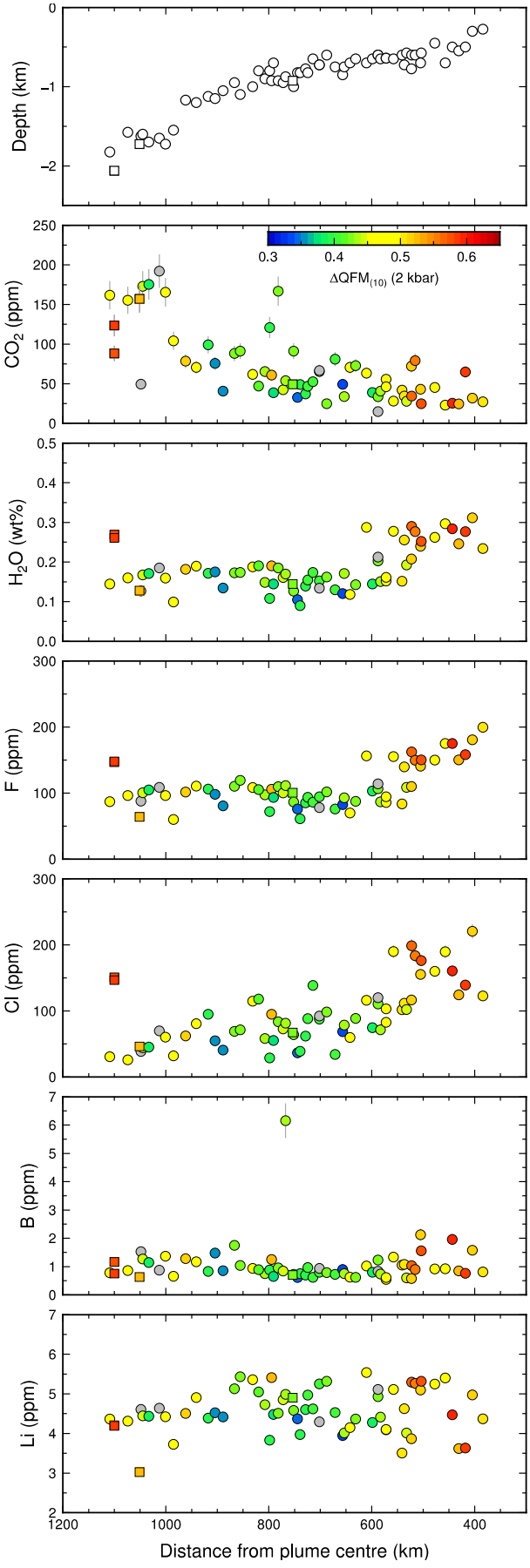

Figure 2 (right): The results of our ion probe analyses of the Reykjanes Ridge glasses. Each point represents an average of at least two repeat analyses and the external reproducibility of reference glass BIR1 over the analytical session has been used to determine relative precision (plotted as grey 1 sigma error bars). Square symbols represent the enriched seamount 14D (furthest from Iceland) and a sample with anomalous chemistry [3], 17D1 (at 1050km). Samples have been coloured by their oxygen fugacity with respect to the quartz-faylaite-magnetite buffer ($\Delta QFM_{(10)}$) calculated from the XANES determinations of $Fe^{3+}/\sum Fe$ and using the calibration of [4].

Resolving the origin of volatiles in the Icelandic mantle using boron isotopes

O. Shorttle[1], M. Edmonds[1], B. Murton[2] & R. Tanaka[3]

[1]Department of Earth Sciences, University of Cambridge, CB1 3BX, UK

[2]National Oceanography Centre, University of Southampton, Southampton, SO14 3ZH, UK

[3]Institute for the Study of the Earth's Interior, Okayama University, Japan

Aim

Geochemical evidence from the trace element, isotopic and major element chemistries of Icelandic basalts indicates that in addition to the ambient upper mantle sampled by most mid-ocean ridges, there are (at least) two other distinct components present in the Icelandic mantle: a recycled basaltic component present in the Iceland plume source [1] and primordial material that has been identified from its noble gas geochemistry and which must have remained un-mixed since early in Earth's history [2]. However, whilst these 'enriched' components are well characterised for many of their lithophile element characteristics, it remains uncertain how they contribute to the volatile (H, C, Cl, Fl, B, S) budget of Icelandic magmas. In particular it is unclear whether the high water contents observed in some Icelandic basalts [3] are due to the presence of hydrated recycled material in the source, primordial volatile rich material, or from an increase in brine/crustal assimilation along-ridge being driven by the increased crustal thickness. Distinguishing between these different models has important implications for the transfer of volatiles between the solid Earth and surface environment and whether volatile elements can experience long-term storage in the mantle. To answer these questions this project will collect new boron isotope data from a suite of basalts along the Reykjanes Ridge south of Iceland, sampling enriched seamounts, ambient depleted mantle and enriched mantle close to the Iceland plume centre. By coupling these new boron isotope observations with our recently acquired volatile element dataset on the same samples (IMF495-1013) we will be able identify the key processes controlling volatile chemistry in these basalts and so fingerprint their origin.

Results

The volatile element chemistry from these samples is shown in Figure 1 with the aim of resolving how assimilation of altered oceanic crust, seawater or hydrothermal brines could have affected the dataset.

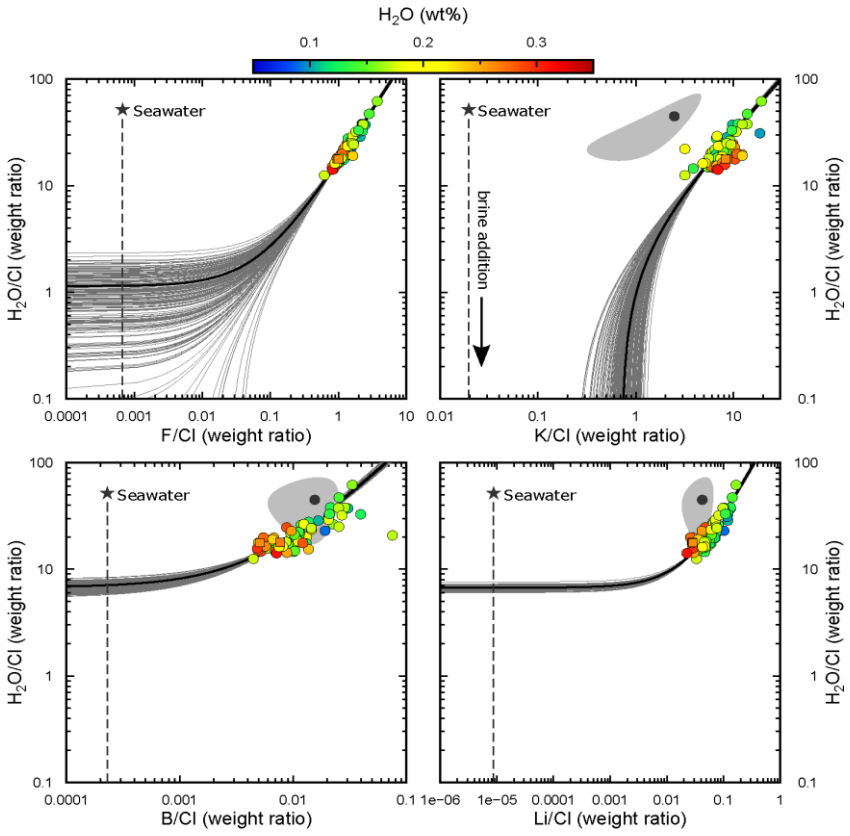

Figure 1 (left): Volatile concentrations in the Reykjanes Ridge basalts ratioed to Cl. Solid black lines are error weighted regressions through the data, whilst grey lines are Monte Carlo simulations recalculating the regressions for randomly resampled datasets. The star represents average seawater chemistry, the vertical vector heading away from this is the trajectory of brine formation and the black circle and grey region represent typical compositions of altered oceanic crust [4]. Points are coloured according to their water concentration. Volatile data collected under NERC ion probe grant IMF495-1013.

Neither direct addition of seawater nor altered oceanic crust is a viable mechanism for explaining the high Cl contents of some Icelandic basalts, however brines are more difficult to rule out. What the regressions through the data do show is that for the simplest model of brine chemistry no single brine composition is consistent with the trends, suggesting that the variability is mantle derived. The new boron isotope data (presented as deviation from a reference composition as $\delta^{11}B$, Figure 2) is a powerful discriminator of contamination processes, as both the boron concentration and isotopic composition of seawater are significantly higher than the mantle. Although there is a slightly greater scatter in boron concentrations at low MgO, possibly consistent with seawater addition correlating with the progressive differentiation of basalts, the mixing line in B-$\delta^{11}B$ space indicates that sweater is unlikely to be controlling the boron or volatile element chemistry of these basalts. Figure 3 plots the new $\delta^{11}B$ data as a function of distance from the Iceland plume. There is no clear signal of changing $\delta^{11}B$ towards Iceland, despite the systematic variation in concentration and isotopic composition present in many other volatile and lithophile elements. Partly this may be due to the low precision (~1‰) attainable in such low B concentration samples and only limited solid-Earth $\delta^{11}B$ variability.

Figure 2 (right): B versus MgO records how boron concentrations in Reykjanes Ridge glasses evolve during differentiation. The increased scatter at low MgO could be due to contamination from altered oceanic crust or brines. B versus $\delta^{11}B$ is plotted to test mixing with seawater (black line). All error bars are 1s.e. (n=5).

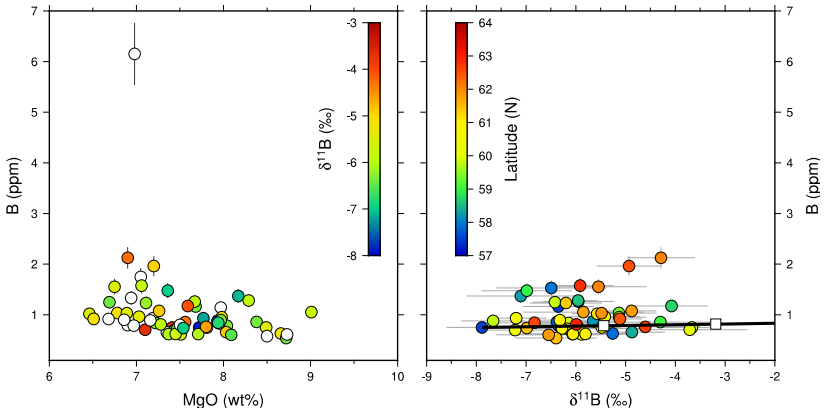

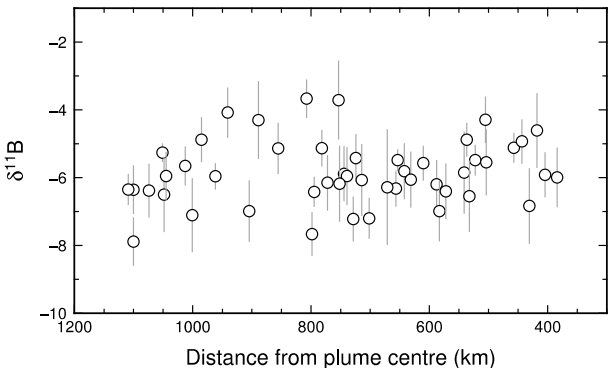

Figure 3 (left): Along-ridge trend of boron isotopes ($\delta^{11}B$) in Reykjanes Ridge glasses. Error bars are 1s.e. (n=5).

Further work

The assessment of brine assimilation in Figure 1 takes the simple scenario whereby all volatile elements are concentrated equally (vertical dashed lines). However, it is likely that some fractionation of volatile species occurs during brine formation from their interaction with hydrous mineral phases and precipitates. To rigorously assess the role of brines in controlling the halogen concentrations of Reykjanes Ridge basalts we are beginning to model the brine formation process. The outcome of this modelling work will be valuable for many future studies of halogen chemistry in basalts.

References

[1] O. Shorttle & J. Maclennan (2011) Geochemistry Geophysics Geosystems **12:11.**

[2] S. Mukhopadhyay (2012) Nature **486**, 101-104.

[3] A.R.L. Nichols et al. (2002) Earth and Planetary Science Letters **202**, 77-87.

[4] M.A. Kendrick et al. (2013) Geochimica et Cosmochimica Acta **123**, 150-165.

Assessing the use of apatite as a new magmatic volatile probe: applications for understanding the eruptive behaviour of Campi Flegrei

M.J. Stock[1], V.C. Smith[2], M.C.S. Humphreys[3], R. Isaia[4] & D.M. Pyle[1]

[1]Department of Earth Sciences, University of Oxford, Oxford OX1 3AN, UK
[2]Research Labs for Archaeology and the History of Arts, University of Oxford, Oxford OX1 3QY, UK
[3]Deparement of Earth Sciences, Durham University, Durham DH1 3LE, UK
[4]Istituto Nazionale di Geofisica e Vulcanologia, Osservatorio Vesuviano, Napoli 80154, Italy

High-resolution Late Ordovician (Hirnantian) $\delta^{18}O$ records from conodont apatite

J. R. Wheeley[1], M. Elrick[2] & A. Desrochers[3]

[1]School of Geography, Earth and Environmental Sciences, University of Birmingham, B15 2TT, UK
[2]Earth and Planetary Sciences, University of New Mexico, Albuquerque, USA
[3]Département des sciences de la Terre, Université d'Ottawa, Ontario, Canada

Background

Despite elevated atmospheric pCO_2, the latest part of the Ordovician (Hirnantian; 447-445 Ma) was a time of extensive south polar glaciation[1]. Coincident with the glaciation was a major mass extinction which decimated >85% of the world's marine species and a major perturbation in the global carbon cycle[2]. The growth and decay of Ordovician southern hemisphere ice is hypothesized to have driven glacio-eustatic sea-level oscillations resulting in the development of transgressive-regressive sedimentary sequences (Myr-scale) and cycles (<100 Kyr) and changing the extent of available shallow-marine shelf habitats for benthic marine organisms[2,3].

In 'far-field' carbonate systems of low-latitude Laurentia, a detailed picture of latest Ordovician glaciation is revealed through repeated stratigraphic sequences, each composed of higher frequency cycles[3]. The late Hirnantian-earliest Silurian Latest Ordovician Glacial Cycle (LOGC3)[3] exposed on Anticosti Island, Quebec, Canada **(Fig 1.)** was the focus of this study because it encompasses the glacial maxima and the second phase of the mass extinction[2,3]. Long-period orbital forcing (~1.2 Myr) is hypothesized as controlling sequence formation with sea-level changes on the order of 50–100 m based on various stratigraphic relationships[3]. Previously, no high-resolution oxygen isotope profile existed through LOGC3 to test for a glacio-eustatic origin or to more quantitatively evaluate the magnitude of glacio-eustatic and seawater temperature changes. The latter are particularly important as they have inferences for magnitudes of Hirnantian climate change and its effect on mass extinction models.

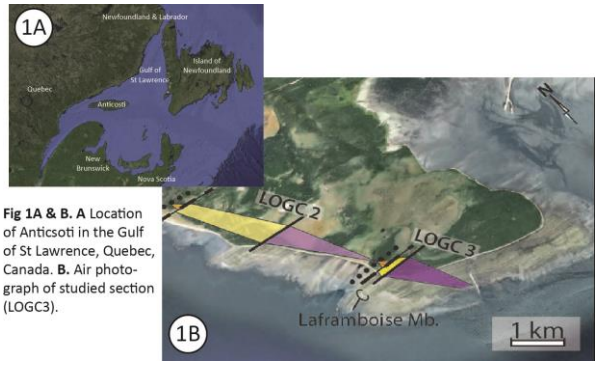

Fig 1A & B. A Location of Anticosti in the Gulf of St Lawrence, Quebec, Canada. **B.** Air photo-graph of studied section (LOGC3).

Oxygen isotopes ($\delta^{18}O$) offer insight into seawater temperature change, global ice-volume effects, and magnitude of sea-level changes[4], but have largely been accrued from diagenetically vulnerable Ordovician skeletal calcites and fine grained bulk limestone[5]. For the Hirnantian, only one low-resolution study (4 data points in ~1–2 Myr) utilised apatite of conodonts, the small (~0.2–2 mm) teeth-like feeding apparatus ('elements') of primitive, jawless, marine vertebrates **(Fig. 2)**[6]. These microfossils are interpreted as holding a more robust archive of seawater oxygen isotopes than carbonates as the phosphate component (PO_4) of bioapatite is chemically very stable in low temperature diagenesis[7].

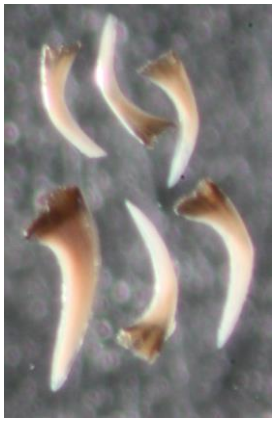

Fig 2 Well-preserved conodonts from LOGC3 Anticosti Canada, which were analysed on the Cameca 1270.

Our aim was to gain a better overview of not only how the low-latitude palaeoceanograhic system responded to high-latitude glacial dynamics, but to deduce at high resolution the behaviour of the Ordovician hydrosphere-cryosphere-isotope system at a critical time in Earth history. The key objective of this project was to establish a conodont oxygen isotope profile at ~20 Kyr intervals for the latter part of the Hirnantian and earliest Silurian (LOGC3) to evaluate the timing, magnitude, and patterns of glacio-eustasy.

Our original proposal set out to test three hypotheses that were dependent on concentrating sufficient conodont yields across the extinction and glacial maxima interval; these include 1) ion microprobe and bulk conodont methods produce similar isotopic trends (and values) across the sampled interval, 2) measured $\delta^{18}O$ trends match sequence stratigraphic trends supporting glacio-eustasy as the primary driver of observed water-depth changes, and 3) the magnitude of sea-level changes detected by oxygen isotopes are consistent with estimates from the independent methods using the stratigraphic record (50–100 m).

Results

Sample preparation processes yielded 19 out of 22 samples with sufficient conodonts for isotopic analysis. Of these, only 3 samples had sufficient conodont element abundances to split the conodonts between traditional bulk (TC/EA) and ion microprobe analysis and compare values. Two of these samples had sufficient abundances to compare ion microprobe isotopic analysis among different taxa occurring within the same sample.

Ion microprobe isotopic analysis values range from 17.5‰ to 19.2‰ whereas TC/EA bulk analysis isotopic values range from 18.5‰ to 19.7‰; the standard deviation between both methods is the same (1 sigma = 0.23‰). These isotopic values are similar to those reported in previous studies[6]. Isotopic values from different taxa within the same sample record similar values (Appendix 1). The microprobe oxygen isotope values of 2 of the 3 comparison samples record lower values compared to the bulk value (lower by an average of ~0.8‰); whereas the values of the remaining sample records similar isotopic values between the two analytical methods. Because so few samples contained sufficient conodonts for the comparison, the results of hypothesis #1 are inconclusive and require further study. Taxa with similar isotopic values within the same sample suggest that there are no vital effects or biologic fractionation between taxa[cf.8,9].

These inconclusive results have important implications for testing hypotheses #2 and #3. Figure 3 illustrates stratigraphic trends across the sampled interval assuming no offset between analytical methods (uncorrected) and trends assuming a ~0.8‰ offset between methods (corrected). In either interpretation, two isotopic excursions are observed with the first spanning from the base of the section to about 12 meters, and second from about 12 meters to the top of the section. The magnitude of isotopic shift across the two excursions range from 1.8‰ to 2.0‰ (corrected) and 1‰ to 1.5‰ (uncorrected). These magnitudes of isotopic change lie within the range observed for Neogene glacial-interglacial stages (1–3‰[10]) and suggest major climatic shifts occurred during the Hirnantian. We assume that similar to the Neogene, these isotopic shifts are the result of seawater temperature changes and ice-volume effects; however, we do not have deep-time proxies that permit us to independently determine the relative portion each of these effect have on the observed isotopic shifts. If we assume Neogene portions of ~70% of the isotopic shift due to ice-volume effects (and 30% due to seawater temperature change), then this equates to glacio-eustatic changes across the two excursion of between 70-140 meters (assuming a 0.1‰/10 meter sea-level change[11]). These preliminary results support hypothesis #3.

Figure 3 illustrates isotopic trends versus the Upper Ordovician (late Hirnantian) stratigraphy and interpreted water-depth curve. Preliminary interpretations support hypothesis #2 as the highest isotopic values signalling the largest ice sheets and coolest seawater temperatures coincide with the major sea-level fall/lowstand and development of an unconformity between the Ellis Bay and Becscie Formations (~12 m). Due to the interplay between eustasy, sedimentation rates, and subsidence, the lowest oxygen isotopic values (signalling maximum deglaciation and warmer seawater) do not coincide with the deepest water facies.

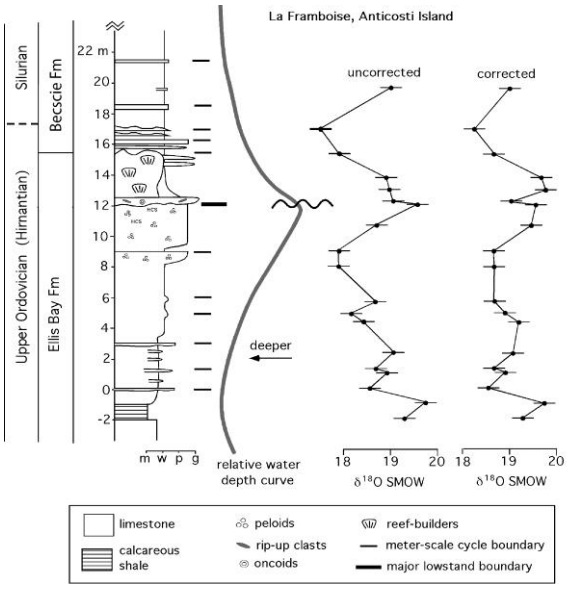

Fig 3. Preliminary results showing oxygen isotope trends (combined ion microprobe and TC/EA), general stratigraphy, and interpreted water-depth curve from studied Anticosti Island section.

References

[1] Le Heron & Dowdeswell 2009. J Geol Soc **166**, 277-281. [2] Sheehan 2001. Ann Rev Earth Planet Sci **29**, 331-364. [3] Ghienne et al. 2014. Nature Comm 5, Art 4485 [4] Elrick et al. 2013. Geol **41**, 775-778. [5] Armstrong 2007. Spec Publ Micropal Assoc 101-121. [6] Trotter et al. 2008. Science **321**, 550-554. [7] Joachimski et al. 2009. Earth Planet Sci Lett **284**, 599–609. [8] Wheeley et al. 2012. J Geoll Soc, **169**, 239-250. [9] Herrmann et al. 2010. Palaios, **25**, 831-836. [10] Lisiecki, & Raymo 2005. Paleocean **20**. [11] Fairbanks 1989. Nature, **342**, 637-642.